DEVELOPMENT OF NANO-BASED DRUG-DELIVERING CARRIERS FOR
COLORECTAL AND BREAST CANCER TARGETING

By
Ms. Yin Yin MYAT

A Thesis Submitted in Partial Fulfillment of the Requirements
for Doctor of Philosophy PHARMACEUTICAL TECHNOLOGY
(INTERNATIONAL PROGRAM)
Department of PHARMACEUTICAL TECHNOLOGY
Silpakorn University
Academic Year 2022
Copyright of Silpakorn University

-

โดย
Ms.Yin Yin Myat

วิทยานิพนธ์นี้เป็นส่วนหนึ่งของการศึกษาตามหลักสูตรปรัชญาดุษฎีบัณฑิต
สาขาวิชาเทคโนโลยีเภสัชกรรม (หลักสูตรนานาชาติ) แบบ 1.2 ปรัชญาดุษฎีบัณฑิต
ภาควิชาเทคโนโลยีเภสัชกรรม
มหาวิทยาลัยศิลปากร
ปีการศึกษา 2565

DEVELOPMENT OF NANO-BASED DRUG-DELIVERING CARRIERS FOR COLORECTAL AND BREAST CANCER TARGETING

By

Ms. Yin Yin MYAT

A Thesis Submitted in Partial Fulfillment of the Requirements
for Doctor of Philosophy PHARMACEUTICAL TECHNOLOGY
(INTERNATIONAL PROGRAM)
Department of PHARMACEUTICAL TECHNOLOGY
Silpakorn University
Academic Year 2022
Copyright of Silpakorn University

Title   Development of nano-based drug-delivering carriers for colorectal and breast cancer targeting
By   Ms. Yin Yin MYAT
Field of Study   PHARMACEUTICAL TECHNOLOGY (INTERNATIONAL PROGRAM)
Advisor   Associate Professor Prasopchai Patrojanasophon, Ph.D.
Co advisor   Professor Praneet Opanasopit, Ph.D.
             Chaiyakarn Pornpitchanarong, Ph.D.

Faculty of Pharmacy, Silpakorn University in Partial Fulfillment of the Requirements for the Doctor of Philosophy

.... Dean of Faculty of
(Assistant Professor Surasit Lochidamnuay, Ph.D.)   Pharmacy

Approved by

.... Chair person
(Assistant Professor Wipada Samprasit, Ph.D.)

.... Advisor
(Associate Professor Prasopchai Patrojanasophon, Ph.D.)

.... Co advisor
(Professor Praneet Opanasopit, Ph.D.)

.... Co advisor
(Chaiyakarn Pornpitchanarong, Ph.D.)

.... Committee
(Assistant Professor Boonnada Pamornpathomkul, Ph.D.)

620830007 : Major PHARMACEUTICAL TECHNOLOGY (INTERNATIONAL PROGRAM)
Keyword : Colorectal cancer, Breast cancer, Nanocarriers, Targeted Drug Delivery, Polyethylene glycol diacrylate, Acrylic acid, Chitosan, Iodoacetamide, Alginate, Maleimide, Cysteine

Ms. Yin Yin MYAT : Development of nano-based drug-delivering carriers for colorectal and breast cancer targeting Thesis advisor : Associate Professor Prasopchai Patrojanasophon, Ph.D.

This study aimed to develop three types of nanocarriers for targeted delivery of chemotherapeutic drugs to colorectal and breast cancers: Polyethylene glycol diacrylate/polyacrylic acid nanoparticles (PEGDA/AA NPs), trastuzumab (Tras)-decorated liposomes (Tras-Lip), and Tras-decorated maleimide-conjugated chitosan/cysteine-conjugated alginate nanoparticles (Tras-CHI-Mal/Alg-Cys NPs). Doxorubicin (Dox) and curcumin were selected as model compounds. PEGDA/AA NPs were prepared by surfactant-free emulsion polymerization using V50 azo initiator and bisacrylamide crosslinker. Tras-Lip formulations were prepared by thin-film hydration method followed by coating with iodoacetamide grafted chitosan (CHI-IA) and conjugated with Tras. Tras-CHI-Mal/Alg-Cys NPs were prepared by ionic gelation and click reaction between the polymers and followed by conjugation with Tras by the thiol-maleimide reaction. The structural characterization was performed using proton nuclear magnetic resonance (^{1}H-NMR), attenuated total reflection Fourier transform infrared (ATR-FTIR) and inductively coupled plasma mass spectrometers (ICP-MS). Their physicochemical properties, morphology, drug content/release, antibody content, and cytotoxicity on normal and cancer cells were investigated. The cellular uptake and apoptosis mechanism of the nanocarriers on colorectal and HER2-positive breast cancer cells were also determined. All nanocarriers were successfully developed with desirable sizes, good polydispersity index, and presented a spherical shape. The zeta potential of PEGDA/AA NPs and CHI-Mal/Alg-Cys NPs were negative charges, while that of Tras-Lip was positive. Dox was encapsulated in the nanocarriers with a % loading efficiency (%LE) of 45.8 ± 0.23 % in PEGDA/AA NPs and 84.6 ± 5.2 % in Tras-CHI-IA coated liposome. Dox was released completely from PEGDA/AA NPs and 78.0 ± 1.8 % from Tras-CHI-IA coated liposome within 24 h at tumor pH. Curcumin was incorporated with a high %LE of 74 ± 3.2% in CHI-Mal/Alg-Cys NPs and released completely within 7 days in tumor pH. The nanocarriers showed potent cytotoxic effects with relatively low IC50 values against HT-29 and SK-BR-3 cells while being non-toxic to Caco-2 and HGF cells . Dox-PEGDA/AA NPs were able to be accumulated passively inside colorectal cancer cells and induce apoptosis, while Tras-CHI-IA coated liposomes and curcumin-CHI-Mal/Alg-Cys NPs demonstrated greater cell toxicity towards breast cancer cells via ligand-receptor mediated endocytosis. Our findings suggest that these nanocarriers could be promising carriers for delivering therapeutic anti-cancer drugs by both passive and active targeting strategies.

ACKNOWLEDGEMENTS

I would like to convey my heartfelt gratitude to everyone who contributed to completing this thesis and helped me to accomplish my Ph.D. First and foremost, I would like to express my greatest gratitude to my supervisors, Associate Professor Dr. Prasopchai Patrojanasophon and Professor Dr. Praneet Opanasopit for the continuous support and tremendous advice to my study and all stages of my thesis research. The valuable motivation, understanding, enthusiasm, and immense knowledge of my supervisors make me a better and stronger person related to my study. Moreover, my supervisors offered me many opportunities to have memorable experiences in Thailand which improve not only my skills and competence but also my self-confidence and social relations. I feel that I have always been surrounded by all the support and faith and I am also delighted for the finest Ph.D. years at Silpakorn University, Thailand.

Next, my special appreciation goes to Dr. Chaiyakarn Pornpitchanarong who is my co-supervisor for his invaluable supervision and support in my laboratory experiments, and for helping me with writing up my research article and thesis. His brilliant teaching and advice improve my skills and critical thinking. Again, I would like to express my gratitude to Dr. Nitjawan Sahatsapan and Dr. Supusson Pengnam who help me and assist me to progress my laboratory skills and problem-solving skills.

Moreover, I would also like to acknowledge Professor Dr. Tanasait Ngawhirunpat for accepting and heartfelt welcoming me to join the Ph.D. program at the Faculty of Pharmacy, Silpakorn University and Associate Professor Dr. Suwanee Panomsuk for providing me with valuable emotional and mental support during my study.

Again, my gratitude belongs to my thesis committees, Assistant Professor Wipada Samprasit, and Assistant Professor Dr. Boonnada Pamornpathomkul for giving valuable time and incisive comments that give me a broad perception of my thesis research.

Also, I would like to thank my friends, seniors and colleagues from the Pharmaceutical Development of Green Innovation Group (PDGIG) and especially Mrs. Areerut Sripattanaporn for their heartfelt welcoming and encouragement and also for supporting laboratory techniques. I have learned and inspired many technical and social

skills, outstanding laboratory skills and moral support from each of the PDGIG members.

Most importantly, I also would like to show my profound appreciation to my dearest family for their unconditional love, encouragement and precious mental and physical support which teach me to live with compassion, gratitude and mindfulness abroad.
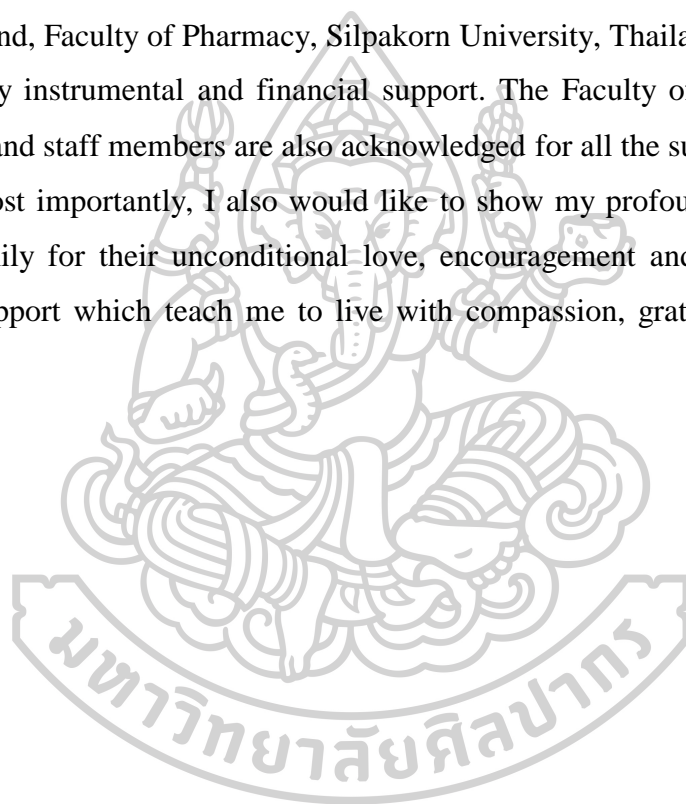
Ms. Yin Yin MYAT

TABLE OF CONTENTS

LIST OF TABLES

Page

LIST OF FIGURES

Page

LIST OF ABBREVIATIONS

®	Registered trademark
TM	Trademark
µg	Microgram
µL	Microliter
µM	Micromolar
%	Percent
%CI	Percent confidence interval
%EE	Percent entrapment efficiency
%LE	Percent loading efficiency
% v/v	Percent volume by volume
ºC	Degree Celsius
AA	Acrylic acid
Alg-Cys	Alginate conjugated with cysteine
ATR-FTIR	Attenuated total reflection Fourier-transformed infrared
BCA	Bicinchoninic acid assay
Caco-2	Human colorectal adenocarcinoma cells (Cancer coli-2)
CHI	Chitosan
CHI-IA	Chitosan conjugated with iodoacetamide
CHI-Mal	Chitosan conjugated with maleimide
D_2O	Deuterated water
DI	Deionized water
DLS	Dynamic light scattering
DMEM	Dulbecco's Modified Eagle Medium
DMF	Dimethyl formamide

DMSO	Dimethyl sulfoxide
Dox	Doxorubicin
EDAC	1-Ethyl-3-(3-dimethylaminopropyl) carbodiimide
EGFR	Epidermal Growth Factor Receptor
EPR	Enhanced permeation and retention
ER	Estrogen receptor
et.al	And others
FBS	Fetal bovine serum
FGER	Fibroblast growth factor receptor
^{1}H-NMR	Proton nuclear magnetic resonance spectroscopy
HEPES	(4-(2-hydroxyethyl)-1-piperazineethanesulfonic acid)
HER2	Human Epidermal Growth Factor Receptor 2
HGF	Human gingival fibroblast cells
HNO$_3$	Nitric acid
HPLC	High-performance liquid chromatography
HT-29	Human Colorectal Adenocarcinoma Cell Line
IA	Iodoacetic acid
IC50	The half maximal inhibitory concentration
ICP-MS	Inductively coupled plasma mass spectrometry
kDa	Kilodalton
LC	Loading capacity
Lip	Liposome
M	Molar
mAb	Monoclonal antibody
MBA	*N, N′*-methylene bisacrylamide

mL	Milliliter
mM	Micromolar
MPS	Mononuclear phagocytic system
MW	Molecular weight
MWCO	Molecular weight cut off
NaOH	Sodium hydroxide
NHS	*N*-hydroxysuccinimide
NPs	Nanoparticles
PBS	Phosphate buffer saline
PC	Phosphatidylcholine
PCS	Proton correlation spectroscopy
PE	Phosphatidylethanolamine
PEG	Polyethylene glycol
PEGDA	Polyethylene glycol diacrylate
PG	Phosphatidylglycerol
PGA	Poly(glycolic acid)
PLA	Poly(lactic acid)
PLGA	Poly(lactic-co-glycolic acid)
PR	Progesterone receptor
PS	Phosphatidylserine
RPM	Round per minute
SEM	Scanning electron microscopy
SK-BR-3	Human breast cancer cell line that overexpresses the HER2
SMCC	Succinimidyl 4-(*N*-aleimidomethyl) cyclohexane-1-carboxylate
	Spectrometer
TEM	Transmission electron microscope

TGF-β	Transforming growth factor beta
Tras	Trastuzumab
Tras-Curcumin-NPs	Trastuzumab-conjugated curcumin-loaded nanoparticles
UA	Uranium acetate
V50	2,2'-Azobis(2-methylpropionamidine) dihydrochloride
VEGF	Vascular endothelial growth factor

CHAPTER 1

INTRODUCTION

1.1 Rational statement and problems of research

Cancer is the second leading cause of death in the world and one type of health concern in public health. It is a genetic disease expressed by a rapid increase in cell differentiation, a decreased cell death, the setup of blood supply to tumor cells, malfunction, and consequent spreading to other organs of the body (1). In 2018, there were around 1.73 million new cases of cancer and more than 609,000 deaths in the United States (2). The etiology of cancer disease is related to smoking (causing lung (3), breast (4), and ovarian cancers (5)), being overweight or obese (associated with breast cancer, kidney, womb, and bowel cancers), intake of processed meat (6), radiation (causes skin cancer) (7), family history, stress, environmental factors, etc. (8). Although, a lot of attempts have been used for cancer therapy, the incidence and mortality rates of cancer remain high in the past 30 years. Therefore, the expedition for more efficient and less toxic cancer treatment strategies is still at the forefront of current research (9).

Even though various treatment approaches, such as immunotherapy, photothermal, photodynamic, gene, and hormone therapy become promising cancer-removing methods in preclinical studies; however, surgery, radiation, and chemotherapy remain the first-line treatment options for most cancers (10). Nevertheless, these treatment strategies are unable to control metastatic tumors. In addition, a highly non-specific targeting of the drugs to the cancer cells causes severe toxicity to the healthy tissues (11). Moreover, poor aqueous solubility, nonspecific biodistribution, inadequate drug concentrations at the tumor or cancerous cells, and the development of multiple drug resistance are the limitations of conventional cancer treatments (12, 13).

Colorectal cancer is the third leading cause of cancer-related mortality in men and women (14). Treatments such as chemotherapy, surgery, and radiotherapy are key current methods used to treat colorectal cancer. Generally, to achieve the desired outcome, two or more treatment modalities are combined (15). Surgery is the first-line strategy for colorectal cancer treatment, especially if it is detected at an early stage.

However, the disadvantage of such a method is a recurrence of the disease, which may lead to metastasis (16, 17). Although chemotherapeutic agents have proved useful in cancer treatment, patients experience severe side effects; for example, hair loss, fatigue, nausea and vomiting, constipation or diarrhea, anemia, immunosuppression, and other organ toxicities (18, 19). Doxorubicin (Dox), an anthracycline derivative, has been applied in various curative drug combinations for the treatment of ovarian, breast, bladder, lung, and colon cancers (14, 20). Its mechanism of action is intercalating the DNA base pairs and inhibiting DNA and RNA replication that causes DNA damage and induces cellular apoptosis (21), and it is a very potent and cost-effective compound compared with other therapeutic agents (22).

Breast cancer is the second most prevalent type of cancer. Moreover, it was the second leading cause of death and most commonly diagnosed in women (2). There are three main steps for the treatment of breast cancer. Chemotherapy is the first-line treatment to reduce the size of the tumor following surgery to cut off the tumor (23, 24). Then, adjuvant treatments such as chemotherapy, radiation, and targeted therapies eliminate the remaining tumor cells and prevent reoccurrence (25, 26). Generally, breast cancer can be categorized as estrogen-receptor-positive type or estrogen-receptor-negative type, and it can be further sub-categorized as luminal A and B, basal-like, and human epidermal growth factor receptor 2 (HER2) positive based on biomarkers such as the presence of progesterone receptor and HER2 receptor (27, 28). Basal-like or triple-negative breast cancer is a unique one being the absence of the biomarkers ER, PR, and HER2 (29). The treatment strategy for breast cancer remains very complex due to its complicated behavior against protein expression, and different types of breast cancer respond differently to treatments. The choice of treatment regime is determined based on the type of tumor, disease stage, and clinical situation of the patients (29, 30). The chances of survival for the patient with breast cancer are still unsatisfactory. Therefore, other forms of treatment for breast cancer should be developed, in the form of therapeutics, adjuvants, chemopreventive agents, or effective cancer-targeted delivery systems (31, 32). Alternative anticancer therapeutic approaches, such as the use of low-toxicity natural sub-products and extracts, are becoming potential modalities (33, 34). In the last few years, phytochemicals have

been studied as innovative approaches for the killing of cancer cells (35). Curcumin, a turmeric-derived phytochemical, possesses advantageous biological activities, such as anticancer, antibacterial, anti-inflammatory, antiviral, and antioxidant properties, and was found to exert preventive and therapeutic effects in various cancers, including breast cancer (34, 36). However, its low water solubility and bioavailability lead to the main hindrance to the use of curcumin (34, 37).

Cancer nanotechnology is potential research owing to its wide application for cancer therapy including imaging, diagnosis, and targeted therapy. Nanoparticles (NPs) are nanoscaled in size, 1 to 1000 nm; a size in the range of 50 to 500 nm is preferable for cancer drug delivery applications for enhanced blood circulation, tissue penetration, and cellular interaction (38-40). Currently, a large number of NPs such as liposomes (41), polymeric NPs (42), micelles (43), solid lipid NPs (44), and other organic and inorganic nanoparticles have been explored to improve the therapeutic efficiency through the design of nanoparticle size, shape and surface charge. It is expected to reach the targeted cancer cells after being administered into circulation via two basic mechanisms including passive and active targeting. Passive targeting is based on the accumulation of drugs in a malignant tissue through highly permeated blood vessels (600 nm gaps). The enhanced permeation and retention (EPR) effect has been regarded as the prime mechanism of passive targeting that underlies the accumulation of drug-containing nanoparticles in cancer tissues (45). The nanoparticles can overcome solubility problems and chemical instability of anti-cancer drugs, and protect anti-cancer drugs from biodegradation or excretion. They can improve distribution, targeting of anti-tumor medication, and decrease drug resistance. Moreover, they can be designed to release the drugs upon a trigger resulting in stimuli-responsive therapeutics. First-generation nanomedicine drugs mainly depend on controlling the pharmacokinetics and biodistribution of a compound by modulating its physicochemical properties (46). For example, PEGylated liposomal Dox (Doxil®/Caelyx®) and nab-paclitaxel (Abraxane®) are first-generation nanomedicine drugs based on passive targeting (47). However, the heterogeneous tumors and their stroma greatly affect the therapeutic effects of passively targeted drugs (48). For this reason, it is important to develop a new generation of functionalized nanosystems. The recent approaches in the development

of nanomedicines are based on decorating the nanoparticle surface with active-targeting ligands including small molecules like carbohydrates and folic acid or macromolecules like peptides, antibodies, oligonucleotides, aptamers, and proteins. This approach is defined as active targeting. Active targeting enhances therapeutic effects and reduces toxic effects by increasing the specificity and improving the uptake of carriers in cancer cells (49).

Most cancer cells frequently show excessive expression of their respective receptors or growth factor ligands on their tumor surfaces which can be effectively targeted using either mono- or polyclonal antibodies for strategic cell killing. Those receptors are the epidermal growth factor receptor (EGFR), fibroblast growth factor receptor (FGFR) family, Human epidermal growth factor receptor 2 (HER2), vascular endothelial growth factor (VEGF), namely VEGFR, transforming growth factor-β (TGF-β), transferrin receptor (TfR) and folate receptors. The most commonly used monoclonal antibodies in clinical practice are bevacizumab, cetuximab, panitumumab, trastuzumab (Tras), and tocilizumab which are covalently linked to a drug delivery system (50). These can be beneficial tools for attracting specific ligands in smart nanomedicine. The specific ligands can be functionalized on the surface of nanocarriers, to get preferable accumulation and uptake at the site of action (51).

As mentioned earlier, various kinds of ligands have been investigated and applied in the field of active targeting industry to improve the cellular uptake of drugs and increase therapeutic effects such as proteins, transferrin, antibodies, nucleic acids, polysaccharides, peptides, and aptamers (52-54). Among these explorations of ligands to target tumors, antibodies (Abs) have attained much attention due to remarkably improved binding specificity and affinity toward their specific antigen targets (55). For example, HER2, a member of the epidermal growth factor receptor family can be characterized and overexpressed in 20%-30% of invasive breast cancers (56, 57). The overexpression of HER2 is usually due to HER2 gene amplification and results in poor prognosis of patients related to these tumors (58). Nowadays, optimal drug delivery systems were a crucial challenge to attain the best pharmacokinetic paradigm (59). Cancer therapeutics with targeting strategies have had significant attention over passive targeting in the last decade (60). Because the accumulation of anticancer drugs in tumor tissue does not get an efficient stage to get powerful therapeutic

outcomes. Hence, the ability of the nanocarrier should be manifested in a more effective strategy to facilitate the therapeutic cargos to reach their molecular targets (61). Tras is a monoclonal antibody used to treat early-stage HER2-positive breast cancer as the first line of treatment. Its proposed mechanisms of action are related to the reduction of PI3K/Akt signaling and augmented the degradation of the HER2 receptor protein through endocytosis, and antibody-induced cellular cytotoxicity (56). Although it is employed in the management of early-stage breast cancer and metastatic breast cancers, it may have the risk of therapeutic resistance and tumor recurrence after a certain period of the treatment. Also, it is further approved in combination formula with other chemotherapeutic drugs (62). Because, the treatment with Tras alone offers 15%-30% response; however, when combined with various kinds of chemotherapeutics, the response can be improved to 50%–75% in HER2-positive breast cancer patients (26).

There are two general approaches to the synthesis of nanomaterials including the top-down approach and the bottom-up approach. The top-down approach involves the breaking down of the bulk material into nano-sized particles to produce the desired structure with appropriate properties in physical and mechanical ways. These methods are solvent evaporation, nanoprecipitation, salting-out, dialysis, supercritical fluid technology, and ionic gelation. The main problem with the top-down approach is the malfunction of the surface structure. The alternative approach, which has the potential of creating less waste and more economical nanomaterials, is the bottom-up approach. Polymeric nanoparticles can be fabricated by the direct polymerization of monomers by applying multiple polymerization techniques such as micro-emulsion, mini-emulsion, surfactant-free emulsion, and interfacial polymerization (63).

In this study, different nanocarriers such as polymeric nanoparticles and liposomes were synthesized and conjugated with antibodies to achieve targeted delivery of drugs for treating colorectal and breast cancers. The polymeric nanocarriers were fabricated by emulsion-polymerization and ionic gelation. Both hydrophobic and hydrophilic polymers and monomers were used for the synthesis of polymeric nanocarriers. The liposomes were prepared by the thin-film hydration method. The physicochemical properties, functional structure confirmation, and cancer-targeting ability of the developed nanocarriers were determined. The

quantitative analysis of the antibody was also performed. Therapeutic anticancer agents such as Dox and the natural compound curcumin were used as model chemotherapeutics to be incorporated into the nanocarriers, and Tras was employed as a model antibody to be conjugated on the nanocarriers. The loading content and the release of the drug were analyzed. In addition, the biocompatibility and in vitro cytotoxicity activities of the drug-incorporated nanocarriers were examined.

1.2 Objectives

1.2.1 To synthesize and prepare polyethylene glycol diacrylate (PEGDA)/acrylic acid (AA) nanoparticles (NPs) incorporated with Dox for colon cancer.

1.2.2 To synthesize the Dox-loaded liposome decorated with Tras for breast cancer.

1.2.3 To develop the chitosan-maleimide/alginate-cysteine (CHI-Mal/Alg-Cys) NPs functionalized with Tras for breast cancer.

1.2.4 To evaluate the size, morphology, drug loading, and drug release properties of drug-loaded nanoparticles and liposomes.

1.2.5 To determine the in vitro cellular activity, cytotoxicity, cell internalization, and cell death mechanism against HT-29 colon cancer cells and HER2-positive SK-BR-3 breast cancer cell lines.

1.3 Hypothesis

1.3.1 PEGDA and AA could be employed to synthesize polymeric NPs by surfactant-free emulsion polymerization with desirable physicochemical properties and can be loaded with Dox for significant cytotoxicity.

1.3.2 The anionic liposomes coated with chitosan-iodoacetamide (CHI-IA) and conjugated with antibody, Tras, can be successfully fabricated and provide excellent anti-cancer activity against breast cancer cells.

1.3.3 The CHI-Mal/Alg-Cys NPs can be synthesized and incorporated with curcumin and conjugated with Tras with desirable physicochemical properties, drug loading efficiency, drug release, and anticancer activities.

1.4 Scope of research

     In the present study, polyethylene glycol diacrylate/acrylic acid nanoparticles, chitosan conjugated with maleimide/alginate conjugated with cysteine nanoparticles, and chitosan-iodoacetamide coated liposomes were developed. The nanocarriers were loaded with a chemotherapeutic agent such as Dox and curcumin and decorated with Tras to improve cancer-targeting ability. The physicochemical properties, morphology, and chemical structure of nanocarriers were investigated. Then, the drug loading content, the antibody contents, and the drug release from the nanocarriers were determined. In addition, the biocompatibility, cytotoxicity, uptake ability, and cell death mechanisms of drug-loaded NPs against the colorectal cancer cell line and HER2-positive breast cancer cell lines were studied.
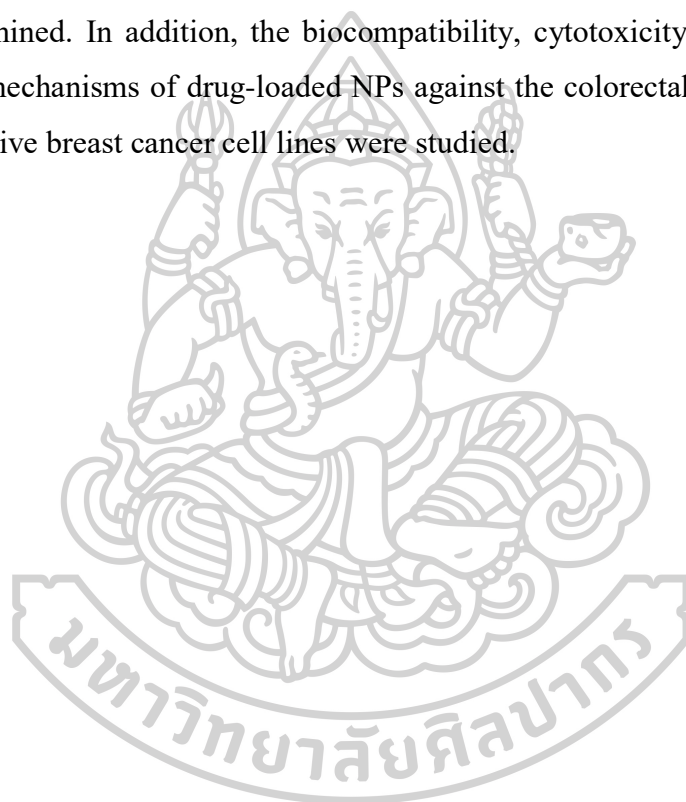
CHAPTER 2

LITERATURE REVIEW

2.1 Cancers

2.1.1 Colon Cancer

Colorectal cancer is a heterogeneous disease (64). It can arise from the gradual progression from normal tissue to the abnormal epithelium and then change to carcinoma due to multiple genetic alterations, the activation and inactivation of tumor suppressor genes, and mismatch repair genes. 2-5% of all colon and rectal cancers can arise from other cancers such as Lynch syndrome, hamartomatous, hyperplastic, and familial juvenile polyposis (65). 1-2% of colorectal cancers can be inherited from inflammatory conditions such as ulcerative colitis and Crohn's disease (66-68). Increased consumption of dietary fat (oxidized form) and red meat, diets with a low intake of fruit and vegetables, protein, alcohol consumption, physical inactivity, and tobacco smoking have been associated with increased risk of colorectal cancer (69).

Colorectal cancer is the third leading cause of cancer-related mortality in men and women (14). Treatments such as chemotherapy, surgery, and radiotherapy are current methods to treat colorectal cancer. To achieve the desired outcome, two or more treatment modules can be combined (15). Surgery is the first-line strategy for colorectal cancer treatment especially once detected at an earlier stage. However, the disadvantage of such a method is a reappearance which may lead to further metastasis stage (16). Many chemotherapeutic agents have been prescribed to treat colorectal cancer commonly oxaliplatin, capecitabine, fluorouracil, and irinotecan (17). Although the combination improved cancer treatment efficacy, general side effects, for example, hair loss, fatigue, nausea and vomiting, constipation or diarrhea, anemia, and immunosuppression are still experienced. Moreover, multi-drug resistance and severe toxicity to healthy organs have become the major drawbacks (18, 19).

2.1.2 Breast Cancer

Breast cancer originates in the breast tissue and then mutates and grows out of control, creating a mass of tissue (tumor). Similar to other cancers, breast cancer can

invade and grow into the tissue surrounding the breast and other parts of the body and form new tumors. When this happens, it's called metastasis. Breast cancer is highly heterogeneous, in some cases showing slow growth with an excellent prognosis, whereas in other cases taking a highly aggressive clinical course (70). The etiology of breast cancer is age, gender (mostly occurring in women), personal history of breast cancer, family history, genetic risk factors, reproductive risk factors, and exogenous hormone use (71).

According to the American Cancer Society, one in every eight women in the United States is diagnosed with breast cancer and approximately 232,340 new cases of invasive breast cancer and 39,620 breast cancer deaths were projected for 2013 among US women (72). The worldwide incidence of female breast cancer will reach almost 3.2 million new cases per year by 2050 (73). Clinically, breast cancer can be classified into different types based on tumor morphological characteristics. Breast tumors have also been recognized into five different subtypes based on the presence of estrogen receptors (ER) and progesterone receptors (PR), and HER2 oncogene (74). Thus, there are two ER/PR-positive subgroups, Luminal A and Luminal B, and three ER-negative subgroups. One of the ER-negative types can be analyzed by high overexpression of HER2 and related genes. The second ER-negative type is associated with high expression of genes normally identified with myoepithelial or basal cells, called the basal-like subtype; and a third ER-negative group that expresses a varied gene expression profile is termed normal-like subtype (75).

HER2 oncogene is associated with the epidermal growth factor receptor family and is overexpressed in approximately 20% of breast tumors (76). Moreover, the breast tumors that do not show either ER, PR, or HER2 are called triple-negative breast cancers and about 15 % of breast cancers are of this type. Also, there is another form of breast cancer known as inflammatory breast cancer that is characterized by breast tenderness (70) and frequently occurred at an advanced stage. Surgery, radiation therapy, chemotherapy, hormone therapy, targeted therapy, and immunotherapy are the basic treatments for various stages of breast cancer. Current therapy involves a multimodal strategy combining surgery, chemotherapy, radiotherapy, adjuvant therapy, and hormonal therapy (77-79). However, long- or

short-term use could result in an economic and psychological burden on patients and, worse, a high chance of multidrug resistance and detrimental side effects (80).

2.2 Chemotherapeutics for colon cancer and breast cancer

2.2.1 Anthracycline derivatives (Dox and epirubicin)

Anthracyclines are among the most exploited antitumor drugs ever developed. The first discovered anthracyclines, such as daunorubicin and Dox, were isolated from pigment-producing *Streptomyces peucetius var. caesius* in the early 1960s and remain in widespread clinical use today (81). Dox, an anthracycline derivative, has been applied in various curative drug combinations for the treatment of different kinds of tumors such as ovarian, breast, bladder, lung cancers, and colon cancer (14, 20). It is considered a very potent and cost-effective compound compared with other therapeutic agents (21). Doxil, Caelyx as PEGylated liposomal formulations, and Myocet as non-PEGylated liposomal forms are available in the clinical market (82-84). The main structure of Dox (Figure 1) is the tetracyclic ring, containing three planar and aromatic hydroxy anthraquinones rings and one nonplanar, nonaromatic ring attached to an aminoglycosidic side chain. There are two proposed mechanisms by which Dox acts in the cancer cell that is the intercalation into DNA and interference of topoisomerase II-mediated DNA repair and generation of free radicals which can damage cellular membranes, DNA, and proteins (85). In brief, Dox is oxidized to an unstable metabolite, semiquinone which is changed back to Dox in a process that generates reactive oxygen species. This reactive oxygen species transform into lipid peroxidation and membrane damage, DNA damage, and oxidative stress, and triggers apoptotic pathways of cell death (86). A major limitation of the use of Dox is cardiotoxicity (87).
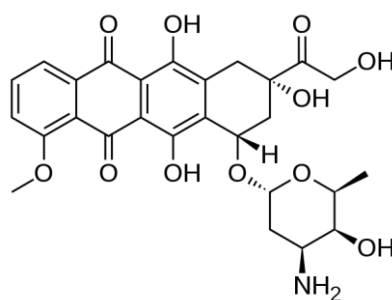
Figure 1. Chemical structure of Dox

2.2.2 5-Fluorouracil

This agent was introduced by Heidelberger et al. during the 1950s (88). It has been progressively used during the last decades and is regarded as the backbone of most chemotherapy regimens. It has also been used in combination with other potent cancer therapies especially targeted therapeutics including vascular endothelial growth factor (VEGF) inhibitors and anti-epidermal growth factor receptor (EGFR) therapies (89, 90). The main cytotoxic activity of 5-fluorouracil (5-FU) is induced through the inhibition of cellular thymidylate synthase (TS) that lead to the disruption of DNA replication (91) and also the prevention of RNA synthesis by the integration of its metabolites into RNA after intracellular activation (92). These mechanisms of action are only applicable when 5-FU is administered as a single-agent chemotherapeutic drug. The platinum-based drugs and/or taxanes are mostly used in combination with 5-FU and also concurrently during radiotherapy, as a radiosensitizer (93). The structure of 5-FU is presented in Figure 2.
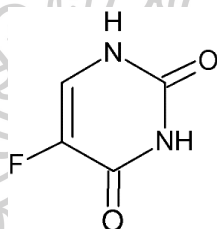
Figure 2. Chemical structure of 5-FU

2.2.3 Taxanes (paclitaxel and docetaxel)

Taxanes derivatives such as paclitaxel and docetaxel, have been well-acknowledged for being the first-line treatment for breast cancer for more than three decades. It is known as a microtubule stabilizer and is also applied as therapeutics for ovarian, prostate, head and neck, and non-small cell lung carcinomas. Even though paclitaxel and docetaxel significantly enhance the overall survival rate of cancer patients, they have poor water solubility and occurrence of severe side effects.

Taxanes are natural diterpenoid substances occurring in yew plants, which received their name from a Latin term for yew, *Taxus sp*. The most clinically used taxane derivative is paclitaxel. Paclitaxel was originally isolated in the 1960s from the stem bark of the western yew, *Taxus brevifolia*, and its structure was characterized in 1971 by Wani et al. Paclitaxel is a tubulin-binding compound, which promotes the

assembly of tubulin dimers to polymerize and stabilize microtubule fibers, and, thereby, arrests the cell cycle in mitosis. Although these properties make paclitaxel an ideal drug for cancer therapy, the mechanism of paclitaxel action is strongly dose-dependent (94). Currently, paclitaxel is marketed as Taxol®, the first medicinal application for ovarian cancer treatment (95). The structures of paclitaxel and docetaxel are presented in Figure 3.
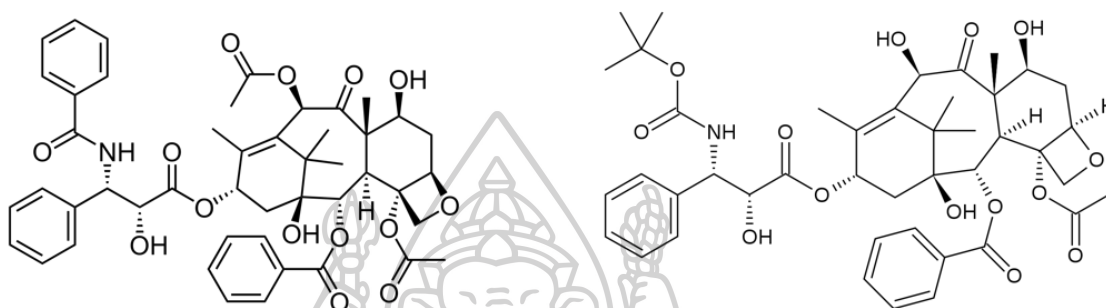
Figure 3. Chemical structures of paclitaxel and docetaxel

2.2.4 Platinum-based chemotherapeutic drugs

A platinum-based anticancer drug is an agent that contains one or more platinum atoms in the oxidation state of II or IV and contains mono- or multidentate non-labile amine carrier ligands and labile chloride or bidentate carboxylate ligands. It undergoes an aquation reaction to form a reactive complex of coordinate bonds with DNA bases. It binds to DNA preventing replication and transcription which causes cell death through apoptosis. Platinum-based anti-cancer drugs, such as cisplatin, carboplatin and oxaliplatin, with obvious therapeutic effects, are extensively applied as the first-line drug for malignant tumors in the clinical (96). Cisplatin, the first generation of the platinum anti-cancer drug, has prominent therapeutic effects on many malignant tumors, such as breast, ovarian, and colorectal (97, 98). It was discovered in the late 1960s and approved for cancer treatment in 1978 (99). The principal mechanism of cisplatin anti-cancer action is platinum binding to the purine base of the DNA by forming intra-stranded and inter-stranded crosslinks (100, 101). Cisplatin plays as adjuvant or neoadjuvant chemotherapy in the treatment mostly in combination with radiation therapy (102). But, the side effects of cisplatin, such as lack of selectivity, high systemic toxicity, and serious damage to normal tissues in long-term use, seriously limit their clinical application. Due to the considerable

therapeutic effect of cisplatin and other first-line clinical platinum drugs on tumor tissues, various strategies have been employed to reduce the damage to normal tissues, such as liposome encapsulation (103, 104), drug delivery by nanomaterial carriers and bioconjunction with antibodies or ligands targeting highly expressed protein moieties on tumors (105, 106). Based on the first-generation platinum drug cisplatin, the second-generation platinum chemotherapy drug carboplatin was developed. Compared with cisplatin, carboplatin exhibits a lower hydration rate and has high biosafety with greatly reduced systemic toxicity, including hepatotoxicity, nephrotoxicity, neurotoxicity, and ototoxicity (107). Cisplatin and carboplatin might have experienced drug resistance during treatment. For that reason, the third generation of platinum clinical drug oxaliplatin was discovered. The mechanism of action of oxaliplatin is similar to cisplatin, without producing cross-resistance with cisplatin or carboplatin. Though, much effort needs to be devoted to discovering new platinum-based anti-cancer drugs (108, 109). The structures of cisplatin carboplatin and oxaliplatin are presented in Figure 4.
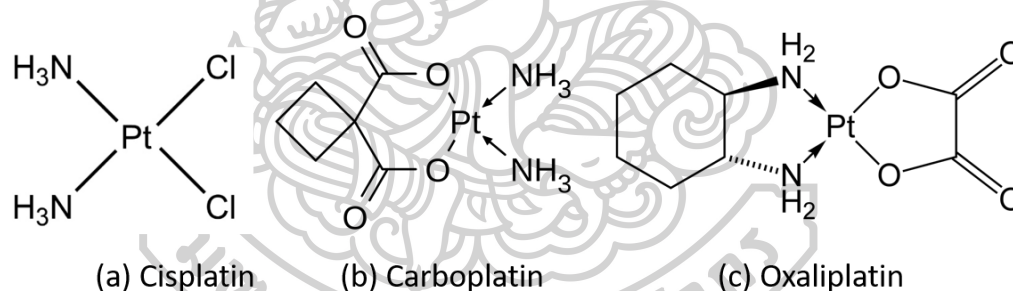
Figure 4. Chemical structure of (a) cisplatin (b) carboplatin and (c) oxaliplatin

2.2.5 Curcumin

Curcumin, the active ingredient of the Curcuma longa plant, and its derivatives had received great attention over the past two decades as an antioxidant, anti-inflammatory, and anti-cancer agent (110). It is the most essential component of the rhizomes of *Curcuma longa L.* (turmeric) (111) and was extracted from the turmeric plant in a pure crystalline form for the first time in 1870 (112). Curcumin exhibits its unique anticancer activity by inducing apoptosis and inhibiting proliferation and invasion of tumors by suppressing a variety of cellular signaling

pathways (113). Curcumin has been studied and shown a potent effect of antitumor activity on breast cancer, lung cancer, head, and neck squamous cell carcinoma, prostate cancer, and brain tumors (114). It can target numerous cancer cell lines. Although curcumin has low water solubility and poor bioavailability, it shows a strong pharmacological effect in clinical applications (115). The chemical structure of curcumin (Figure 5) consists of two phenyl rings substituted with hydroxyl and methoxyl groups and connected via a seven-carbon keto-enol linker (C7). A structure-activity relationship study of curcumin derivatives reveals that the existence of a coplanar hydrogen donor group and a β-diketone moiety is essential for the treatment of prostate cancer (116). Dimethyl curcumin or ASC-J9 (5-hydroxy-1, 7-bis (3, 4-dimethoxyphenyl)-1, 4, 6-heptatrien-3-one) is a newly developed curcumin analog which has shown a significant anti-proliferative effect against estrogen-dependent breast cancer cells (117, 118). Several delivery systems for curcumin have been developed using different nanotechnologies with the aim of improving curcumin properties and targetability (119). The use of PLGA nanospheres encapsulating dimethyl curcumin (ASC-J9) has been studied in breast cancer cells. The PLGA nanospheres were capable to release the curcumin and showed growth inhibition of estrogen-dependent MCF-7 cancer cells (118).
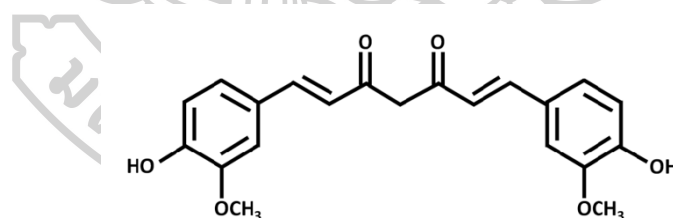
Figure 5. Chemical structure of curcumin

2.3 Tumor-targeted drug delivery approaches

The therapeutic management of cancers by the application of chemical antineoplastic drugs referred to as chemotherapy is the primary therapeutic approach. Even though it was widely used in cancer treatment, chemotherapeutic drugs own many limitations. First, it lacks specificity towards the neoplastic tissue which can damage healthy cells leading to severe side effects such as suppression of bone marrow activity (immuno- and myelosuppression), mucositis, nausea, and infertility

(120). Secondly, the lack of selectivity through the mechanism of action is projecting drawbacks in conventional chemotherapy and susceptibility to induce drug resistance in cancer cells. Third, a relatively high concentration of a drug is required to achieve a therapeutic effect that consequently leads to toxicity (121). Again, conventional chemotherapy encounters certain challenges such as the physicochemical properties of drugs which play a critical role during the transport of the drugs to the tumor. And the acidic environment of tumor tissues can be the reason for the degradation of the acid-labile drugs (122).

To overcome these problems, tumor-targeted drug delivery systems are developed. There are several advantages of targeted drug delivery of nanoparticles for cancer therapy. Those are the cytotoxic drugs that become less harmful to healthy cells due to the selective targeting effect on tumor cells and lead to lower side effects. There are three main targeting mechanisms to improve tumor treatment. These are passive targeting (through the enhanced permeability and retention (EPR) effect), active or ligand-mediated targeting, and stimuli-responsive targeting approaches (123).

2.3.1 Passive Targeting and EPR effect

In cancer treatment, passive targeting (Figure 6) is related to the preferential accumulation of the drug in the targeting tumor sites. In fact, passive targeting is based on the unique properties of the cancer microenvironment and leaky vasculature which can improve fluid retention in the tumor interstitium and can permeate and retain large molecules than the normal tissues. This effect is called the enhanced permeation and retention (EPR) effect (124, 125). The EPR effect in the tumor is the consequence of rapid tumor growth. This effect allows the drug macromolecules larger than 40 kDa to be internalized and retained in the tumors in terms of enhanced accumulation of macromolecules. Because the normal endothelial cells do not allow such extravasation due to having tight junctions. In this manner, the EPR effect offers tumor-targeted drug delivery, which is potentially a promising approach for anticancer drug delivery (126, 127). Usually, NPs less than 400 nm can accumulate in the interstitial space in tumor tissues and deposit anticancer drugs passively after cellular uptake. Therefore, the size and surface charges are critical factors to consider

for drug delivery for tumor accumulation and physiological interactions (128). The clinical example of passive targeted delivery is a Dox-loaded liposomal formulation, Doxil for the treatment of Kaposi sarcoma (129). One of the most prominent limitations of passive targeting is when small molecule drugs are released from nanocarriers in tumor sites, they may diffuse out of the tumor cells and affect surrounding normal tissues (126).
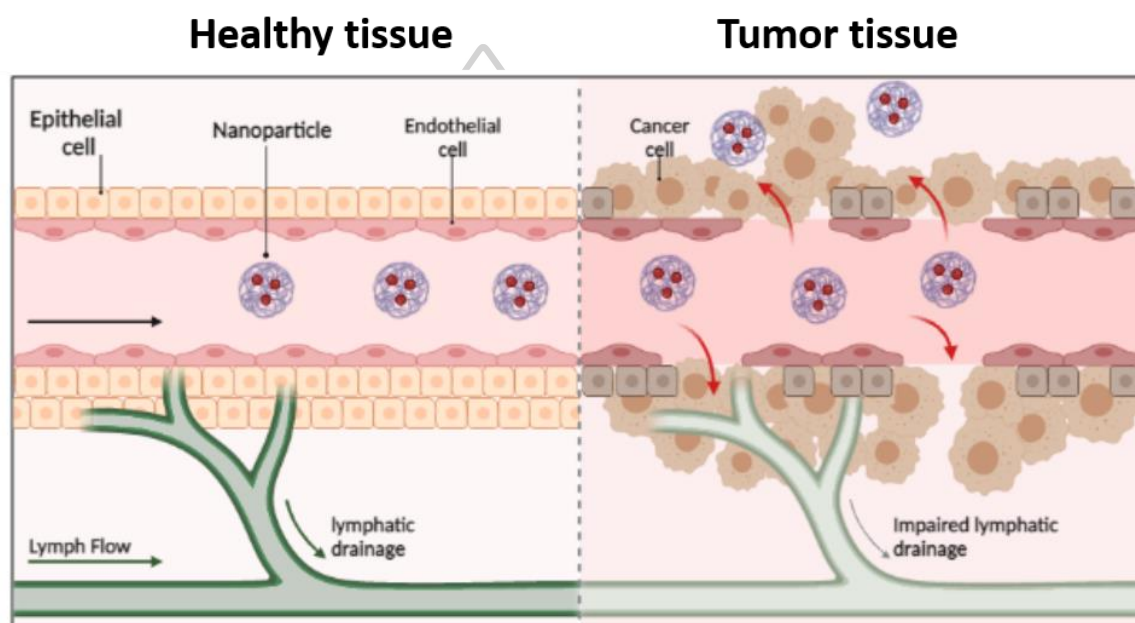
Figure 6. Passive targeting strategies (Image was created with Biorender.com)

2.3.2 Active Targeting

Despite the fact nanocarriers can be passively targeted to the tumor via the EPR effect, there is another potential to improve the tumor targetability of the nanocarriers by implementing various active targeting strategies. After accumulation in the tumor region, the efficacy of the anticancer drug can be even increased by employing active targeting. This is achieved through the decoration of the nanocarrier surfaces with various kinds of ligands (e.g., antibodies, peptides) that can bind to specific receptors that are overexpressed on the tumor cells. This targeting strategy will provide the high affinities of the nanocarriers for the surface of cancer cells and thus leading to enhance drug penetration. The first evidence of this phenomenon was

proposed in 1980 with antibodies grafted on the surface of liposomes followed by other various kinds of ligands (130).

Active tumor targeting gives more specific secondary targeting after primary targeting based on the EPR effect takes place. So, it has been noted that for more effective active targeting, passive targeting must be accomplished first (131). In this approach (Figure 7), nanoparticles will recognize and bind to target cells through ligand-receptor interactions, and the bound nanoparticles are internalized before the drug is released inside the cell, resulting in less off-target drug release compared to passively targeted systems. A variety of ligands have been investigated including folate, transferrin, antibodies, peptides, and aptamers (54). The very effective tumor-targeted drug delivery systems need to have four key elements: retain, evade, target, and release (132). The criteria for ligand selection for the active targeting must be based on the specific cell surface properties that are the membrane overexpressed receptor of the tumor cell. And, the selected targeting moiety (ligands) must favorably bind to the target receptor overexpressed by tumor cells and the target receptor must be homogeneously expressed on all target cells (133).
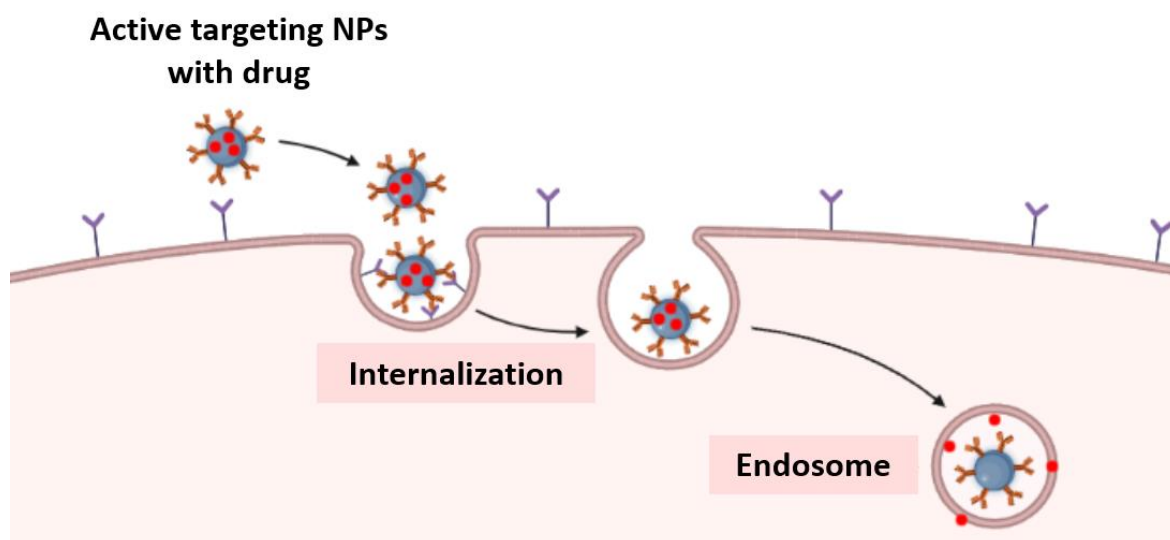
Figure 7. Active targeting strategies (Image was created with Biorender.com)

2.3.3 Stimuli-responsive Targeting

Another smart targeting strategy that takes advantage of specific characteristics of the chemical environments of the tumor interstitium is a stimuli-responsive drug delivery system. This strategy is designed to release or activate the drug only when triggered by specific internal or external stimuli (Figure 8). Those stimuli are pH, proteases, redox potential, heat, ultrasound and light (134).

The concept of stimuli-responsive drug delivery was first suggested in the late 1970s with the use of thermo-sensitive liposomes for the local delivery of drugs through hyperthermia (135). The use of stimuli-responsive nanocarriers offers an interesting opportunity for drug delivery as programmable delivery systems in the optimization of cancer therapy. Stimuli-responsive nanocarriers are assembled of the accurate material composition to construct the nanocarriers that can respond specifically to the pathological "triggers" that occur in the selected targeted site, as the disease establishes and progresses. The existing pH of tumor tissue has been considered an ideal trigger for the selective release of anticancer drugs in tumor tissues and within tumor cells. The variations of pH within cells and in a tumor can be strategies for pH-sensitive drug delivery at local microenvironments (136). This strategy has many advantages of prolonged circulation time, accumulation of the drug in the exact targeted site, improved cellular internalization, and fast intracellular drug release (137).
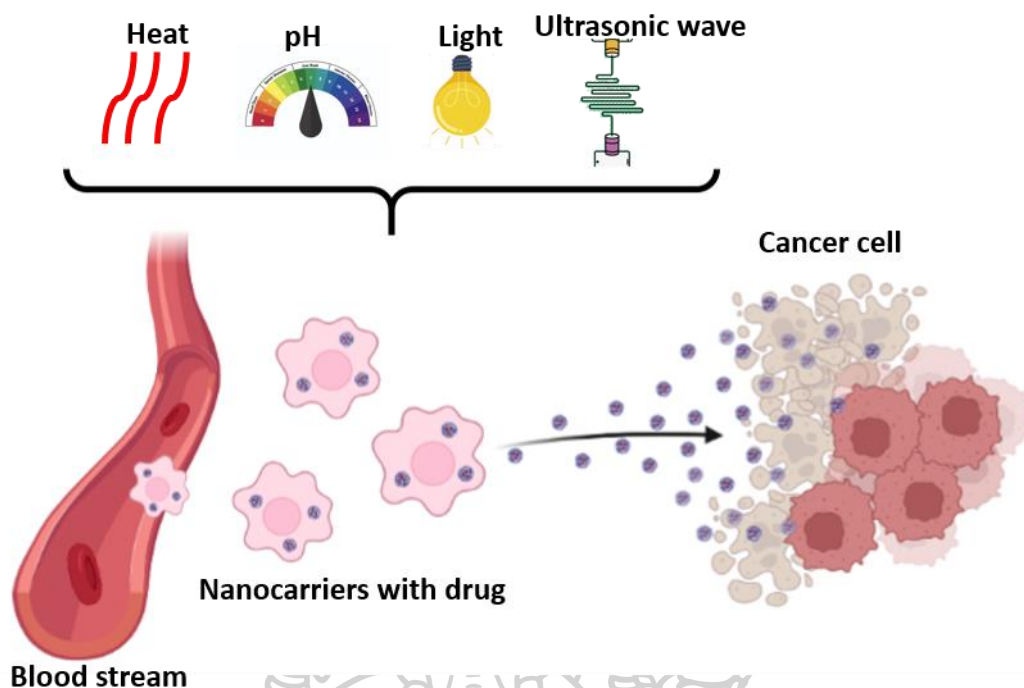
Figure 8. Stimuli-responsive targeting (Image was created with Biorender.com)

2.4 Nanocarriers for cancer treatment

Nanotechnology is an evolving therapeutic platform that involves nanoparticles (NPs) for the diagnosis and treatment of cancer. In the last few decades, nanoparticulate drug delivery systems have revealed enormous applications in many biological, medical and pharmaceutical applications. They can load drugs or biomolecules into their interior structures and conjugate them onto their exterior surfaces. Currently, they have been broadly applied to transport drugs, polypeptides, proteins, vaccines, nucleic acids, and gene (138). NPs are applied in the treatment of cancer owing to their unique size between 1 to 1000 nm, and in the range of 50 to 500 nm is preferable for cancer drug delivery applications (139). These nanometer size ranges are suitable for tumor targeting via the EPR effect. The nano-ranged size, large surface-to-volume ratios and the ability for surface functionalization play an essential role in its biodistribution in vivo. NPs using drug delivery systems offer several advantages for cancer therapy over the application of free drugs. NPs can improve the therapeutic efficacy of the cargo chemotherapeutic agents compared to the drugs delivered via conventional methods. They can increase drug efficacy by achieving

steady-state therapeutic outcomes over a prolonged period. They can lower the toxicity of cargo drugs due to controlled drug release and improve the pharmacokinetics of drugs by increasing the solubility and stability of drugs (140, 141). Moreover, they can easily functionalize by adjusting and modifying the surface functional groups and charges (142). They have the additional benefit of prolonged circulation time in the bloodstream which was favorable for extravasation and passive targeting and avoidance from opsonization (143).

Biodegradable NPs are frequently used to improve the therapeutic effect of various hydrophilic, and hydrophobic drugs and bioactive molecules by improving bioavailability, solubility, and retention time (144). Polysaccharides, lipids, and dendrimers have gained much attention owing to their outstanding physical and biological properties (145). Natural and synthetic polymers have also been well applied in drug delivery (146). In the nanotechnological advanced era, various platforms such as liposomes, polymeric NPs, solid lipid NPs, microspheres, dendrimers, and micelles are developed to attain targeted deliveries (147).

2.4.1 Polymer-based nanoparticles

Polymeric NPs have gained favorable interest over recent years due to their properties resulting from their small size, the ability to control the release of the drug, the ability to protect the drug and other molecules with biological activity from degradation by the environment, improvement of their bioavailability and therapeutic index (148-150). The "NP" involves both nanocapsules and nanospheres, which differ according to their morphology (151). The properties and features, such as size, surface charge, nature of hydrophilic or hydrophobic, and the choice of polymer, govern the potential application of polymeric NPs (152, 153). Polymeric NPs may differ in physical properties, such as size, shape, surface properties, crystallinity, composition and concentration. These properties are usually determined by many methods, such as electron microscopy, Near-infrared spectroscopy, dynamic light scattering (DLS) or photon correlation spectroscopy (PCS), electrophoresis, and chromatography are a few of the most commonly used (154, 155).

Chitosan, dextran, and heparin are natural polymers that have been widely used for drug delivery studies having their biodegradable, biocompatible and

mucoadhesive properties. The most commonly used synthetic polymers are saturated poly (hydroxy esters) such as poly(lactic acid) (PLA), poly(glycolic acid) (PGA), and poly(lactic-co-glycolide) (PLGA) because of their safety profile, confirmed biocompatibility, low levels of immunogenicity and toxicity, as well as their biodegradation during in vivo studies (153). They have been approved by the US Food and Drug Administration (US FDA) and the European Medicine Agency (EMA) (156, 157). Different preparation methods can be used for the production of the particles depending on the type of drug to be loaded in the polymeric NPs and their requirements for a particular route of administration. In general, two main strategies are employed, namely, the dispersion of preformed polymers or the polymerization of monomers and are usually obtained as aqueous colloidal suspensions (Figure 9) (158, 159).

There are four commonly used methods for preparing NPs from preformed polymer dispersions (Figure 9). The first two methods, emulsion solvent evaporation and emulsion solvent diffusion, require the formation of an oil-in-water emulsion. Both methods involve the use of polar organic solvents to dissolve the polymer or drug, and an aqueous phase containing surfactants to facilitate emulsification. The main difference between the two methods is that the first method requires sonication or high-speed homogenization (160, 161). The rest are the salting-out and nanoprecipitation methods. The salting-out method involves separating a hydro-miscible solvent from an aqueous phase by salting out, which can result in the formation of nanospheres without using surfactants or chlorinated solvents (162, 163). The difference is that they are formulated from a water-miscible polymer, and the aqueous phase contains a gel, the salting-out agent (electrolytes, calcium chloride and magnesium chloride) and a colloidal stabilizer without using any high shear forces (164). Nanoprecipitation, also known as the solvent displacement method, is a fast, simple, and reliable method extensively employed for synthesizing both nanospheres and nanocapsules. It involves mixing a miscible solvent with polymer and water with stabilizing agent (165).

In the polymerization of monomers technique, suitable NPs can be obtained by polymerization of monomers which are typically based on micro/ mini emulsion and emulsion polymerization. Emulsion polymerization is the most commonly used

method for the fabrication of a wide range of polymers. It can be categorized as conventional and surfactant-free emulsion polymerization depending on the utilization of surfactant (166, 167).

To prepare NPs via polymerization reaction, the typical components are water, a monomer with poor water solubility, a surfactant, and a water-soluble initiator. In the first step, the monomer is dispersed in the continuous phase and becomes a colloid by adding an initiator, which can be an ion or a free radical (168). An alternative method is surfactant-free emulsion polymerization, which has gained attention as a simple and environmentally friendly process (169) This method does not require surfactants and the associated removal process, and typically involves a water-soluble initiator such as potassium persulfate, deionized water, and vinyl or acrylic monomers (170).
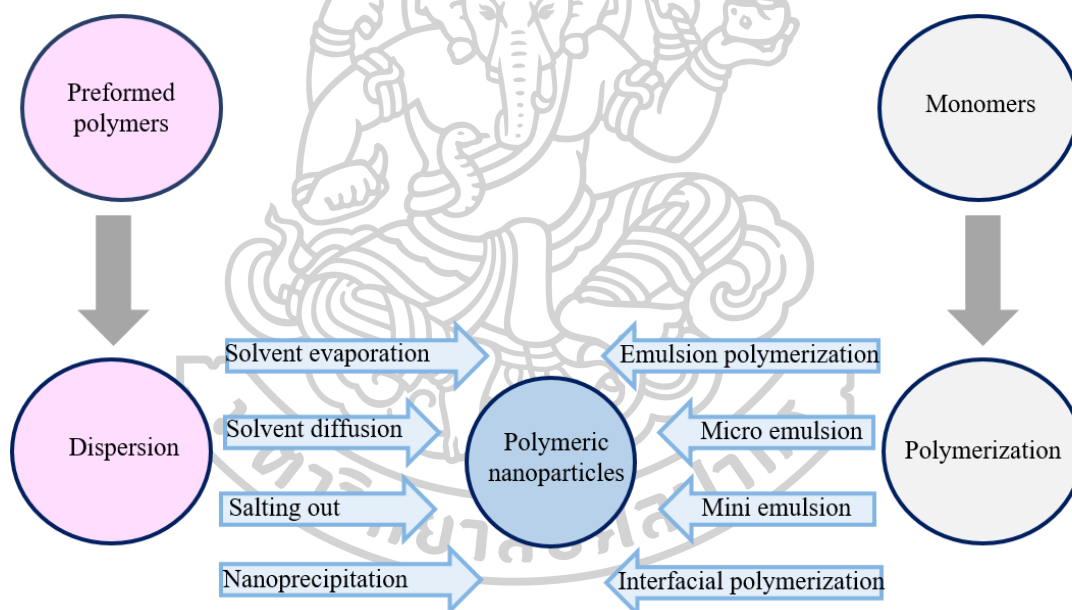
Figure 9. Preparation of polymeric NPs by using various techniques, the dispersion of preformed polymers and the polymerization of monomers

2.4.2 Lipid-based nanoparticles

Liposomes are spherical micro-vesicles and vary in size between 25 nm to 2.5 μm. A liposome consists of a phospholipid bilayer shell and an aqueous core which makes it an ideal carrier for encapsulating both hydrophobic and hydrophilic

compounds (171). In general, the bilayer lipid membrane of liposomes is composed of two essential agents: phospholipid and cholesterol. Phospholipids have polar heads and non-polar tails which allows the formation of a bilayer vesicle above its critical micelle concentration. Liposomes prepared from only phospholipids may give rise to chemical and physical instability and hence the addition of cholesterol becomes popular to provide fluidity and stability. Phosphatidylcholine (PC) is the most widely utilized phospholipid although phosphatidylserine (PS), phosphatidylethanolamine (PE), and phosphatidylglycerol (PG) are also applied. Among the nanocarriers, liposomes have many rewards as they can extensively be used for hydrophilic drugs (entrapped in liposomal inner core), hydrophobic drugs (entrapped in liposomal bilayer) and amphiphilic molecules (lipid-aqueous interface) making them appropriate carriers for therapeutic applications. They are biodegradable, non-toxic and non-immunogenic which could be the ideal carrier for drug delivery and can be modified the external surface of liposomes chemically (172).

The commonly used liposome preparation methods include thin-film hydration, membrane extrusion or freeze-thaw, reverse-phase evaporation, and detergent dialysis. Based on the method applied for the preparation of liposomes, they give different shapes and sizes such as multilamellar vesicles (>500 nm), large unilamellar vesicles (>100 nm) or small unilamellar vesicles (25-100 nm). The size and the number of lamellae in the liposomal structure are the most crucial factors affecting the vesicle half-life and the quantity of active drug that is to be encapsulated. Liposomes are captured by the mononuclear phagocytic system (MPS) after contact with plasma proteins and are cleared from the bloodstream. These stability concerns can be solved through the use of synthetic phospholipids, particles coated with amphipathic polyethylene glycol, and coating liposomes with chitin derivatives (173). It is also possible to use surface functionalization of liposomes by a variety of agents to overcome the limitations of these nanocarriers in terms of biological and physiological barriers. Those are polyethylene glycols (PEGs), aptamers, antibodies, proteins, peptides, ligands, carbohydrates, or small molecules (174).

2.5 Polymers used in the synthesis of nanocarriers

2.5.1 Polyethylene Glycol Derivative

Polyethylene glycol (PEG), a macrogol, is widely utilized in drug delivery and nanotechnology due to its reported "stealth" properties and biocompatibility. It is a polyether consisting of ethoxy units derived from the ring-opening polymerization of ethylene oxide. The traditional PEG is a linear polymer with chemically active hydroxyl groups at both ends, making it easy to conjugate with functional groups. Its significant activity of extending the elimination half-life of a drug has become the gold standard for nanoparticle synthesis (175). PEGDA is a derivative of polyethylene glycol which contains repetitive ethylene oxide units and vinyl ends that can be acquired for polymerization (Figure 10). PEGDA-containing nanoparticles have also been shown to be immunologically inert. Moreover, it is soluble in water and presents very low toxicity (176).
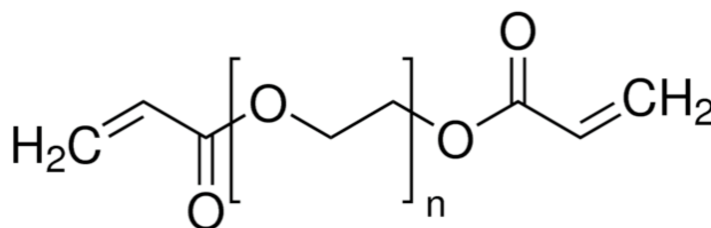
Figure 10. Chemical structure of PEGDA

2.5.2. Chitosan (CHI)

CHI is a polysaccharide composed of *N*-acetyl-D-glucosamine and D-glucosamine and its units are linked by 1-4-β-glycosidic bonds (Figure 11). It can be prepared by deacetylation of chitin in basic media and is the second most abundant natural biopolymer after cellulose (177). It is biodegradable, non-toxic, and can be used for controlled-release formulations (178). It possesses many reactive functional groups such as -NH$_2$ and -OH (179). The solubility issue of CHI can be manipulated by modifying these functional groups. The -NH$_2$ groups can be protonated at acidic pH which makes CHI macromolecules positively charged. Hydrogen bonding and hydrophobic interaction also play important roles in the mucoadhesion of CHI. In addition, these cationic CHI derivatives can target the negative tumor cell membrane

and contribute mucoadhesive effects which improve the uptake of the cargo drug into the cells and enhance the localization of the drugs at the targeted tumor sites (61).

Much research has been made for developing efficient CHI-based NP drug delivery systems. The positive charges target the CHI carriers to the negatively charged cell membrane and have mucoadhesive properties to increase the uptake of nanoparticles and prolong the retention time of CHI in the targeted sites when compared with the other biological polymers (180, 181). Numerous hydrophobic cancer drugs, for example, paclitaxel, docetaxel, Dox, camptothecin, and cisplatin, can be physically entrapped or chemically conjugated to the CHI, and they can precisely distribute the anticancer drugs into tumor sites. The nanocarriers made with CHI for cancer drugs and imaging probes revealed prolonged blood circulation and highly tumor-targeted delivery in cell and animal models as compared to the other NPs (53).
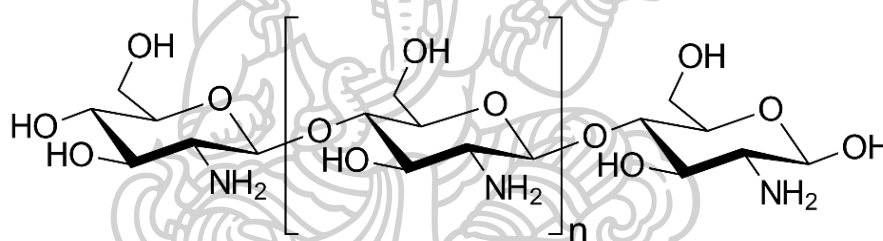
Figure 11. Chemical structure of CHI

2.5.3 Alginate

Polysaccharides-based polymers include alginates, a naturally occurring anionic polymer typically obtained from brown seaweed. Alginate is a linear unbranched polysaccharide that contains varying amounts of 1,40-linked β-d-mannuronic acid and α-l-guluronic acid residues, which, arranged in a pattern of blocks along the chain, may vary widely in composition and sequence (Figure 12) (182). Alginate can form two types of gel dependent on pH: an acid gel and an ionotropic gel; the unique property of gelation by the addition of divalent cations such as Ca^{2+} together with its bioadhesive features has led to a large use of this polymer in the drug delivery field giving the polymer several advantages compared with neutral macromolecules (183).

Alginate is an anionic polymer that is typically obtained from brown marine algae. It is an unbranched polysaccharide copolymer consisting of alternating *D*-mannuronate (M) and *L*-guluronic (G) blocks linked together by 1,4-glycosidic linkages (184). Alginate-based nanocarrier seems to have all the optimal requirements to be a successful drug delivery system due to its biodegradability, biocompatibility, protection of oral drugs against the harsh gastrointestinal environment, controllable release, water solubility, availability and low cost (185). On top of that, the application of alginate nanoparticles in cancer treatment has gained wide attention due to the ability to deliver anti-cancer therapeutics in a sufficient concentration at the target site, promoting the bioavailability as well as reducing drug dosage and its side effects to the normal tissues (186, 187). Alginate NPs have been also used for targeted antibiotic delivery without inducing resistance of bacteria (188, 189).
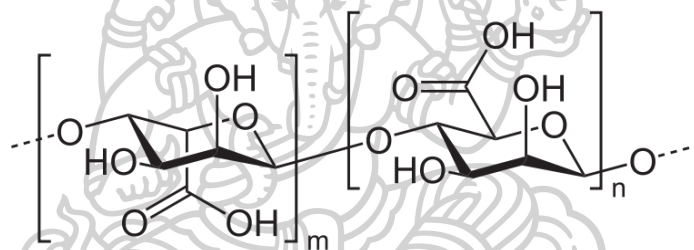
Figure 12. Chemical structure of alginic acid

2.6 Antibodies in cancer therapy

2.6.1 Targeting antibodies

A wide range of targeting ligands have been extensively employed to specifically target nanoparticles to tumor sites. Among these ligands, monoclonal antibody (mAb) ligands and their derivatives have demonstrated significant binding affinity to the receptors on specific tumor targets. The physical properties of nanoparticles can be manipulated for cancer therapy. The use of antibodies and antibody fragments for cancer targeting may overcome many limitations of existing targeted cancer therapies, offering benefits such as smaller size, high potency, and the ability for synthetic production, allowing for scalable production. (190).

Various types of mAbs have been utilized in antitumor targeting therapy. Several nanotherapeutic materials have been approved by the US FDA for clinical

use, specifically targeting tumor tissues, while most are still undergoing preclinical and clinical development. Some FDA-approved therapeutic mAbs for cancer include cetuximab, atezolizumab, bemarituzumab, cemiplimab, and catumaxomab. (191-194).

2.6.2 Advantages of antibody-decorated nanoparticles for cancer therapy

In recent decades, there has been significant interest and development in the use of mAbs for cancer treatment (195). Some mAbs possess acceptable antitumor activity on their own and are utilized as therapeutic agents, while others are used for targeting purposes, such as in the form of antibody-drug conjugates (196). However, concerns exist regarding the chemical conjugation of mAbs with drugs, as it may lead to unfavorable drug inactivation and difficulty in releasing the drug after internalization by cancer cells. To address these issues, Ab-targeted NPs have been developed, as drugs are typically entrapped within NPs. NPs can also carry multiple drugs for combination therapy, which may eliminate the need for complicated multidrug dosing regimens and improve patient compliance (197). Additionally, NPs enable much higher drug-to-Ab ratios, potentially increasing the amount of drug delivery per binding event (198). Furthermore, NPs may overcome drug resistance in cancer therapy, which is often associated with increased drug efflux due to overexpressed protein efflux pumps in cancer cells. Such drug efflux mechanisms can be effectively bypassed by the use of NPs to deliver drugs (119).

2.7 Antibody-nanoparticles conjugation strategies

2.7.1 Physical or adsorption methods

The antibody can be immobilized onto the nanocarriers via a non-covalent method including physical adsorption and ionic interaction (199). Physical adsorption can happen via weak interaction through hydrogen bonds, electrostatic interaction, and hydrophobic and Van der Waals forces (200). Ionic interaction is taken place via the interaction of opposite charges on the nanoparticles and antibodies. Physical adsorption is a favorable method for the rapid binding of antibodies onto NPs, and it is a low-cost approach since it does not require any chemical reagents for conjugation. Despite these advantages, physical adsorption has certain limitations when

conjugating mAbs onto NPs, such as random adsorption, decreased affinity to the receptors on tumor sites, and removal of antibodies by serum proteins during circulation (201).

2.7.2 Chemical or covalent methods

The most commonly used covalent strategies occur via carbodiimide chemistry, maleimide chemistry or "click chemistry" (202). Covalent methods can overcome the limitations of physical methods. Thus, this binding needs prior activation of the NPs before conjugation by using cross-linking reagents such as EDC and NHS (203-205). In carbodiimide chemistry, the binding occurs through the amine functional groups of antibodies. The main disadvantage of this carbodiimide binding is hard to control the orientation of the antibody onto the nanoparticle surfaces but the reaction can be easily occurred (206, 207).

In maleimide chemistry, the binding of antibodies to NPs occurs through the sulfhydryl (–SH) functional group of antibodies which is produced by the reduction of native disulfide bonds of antibodies and attached to the surface of nanoparticles directly or thiol-reactive linkers (208, 209). The most widely used maleimide cross-linking reagents are the NHS/maleimide heterobifunctional linkers, succinimidyl 4-(*N*-aleimidomethyl) cyclohexane-1-carboxylate (SMCC), PEGylated analogs (NHS-PEG-maleimide), and sulfosuccinimidyl 4-(*N*-maleimidomethyl) cyclohexane-1-carboxylate (sulfo-SMCC) (210-212).

2.7.3 Direct conjugation of antibody and nanoparticles

Direct coupling between antibodies and nanoparticles occurs through various reactive functional groups. Antibodies are amino acid polymers that contain primary amine groups, thiol groups, carboxylic groups, and aldehyde groups, which can be readily utilized for conjugation with nanoparticles. However, the major limitations of this direct coupling method include the possibility of random conjugation of antibody orientation and self-cross-linking between antibody molecules (213).

2.7.4 Conjugation of the antibody to nanoparticles through adaptor molecules

One of the non-covalent approaches to overcome the random conjugation of antibodies onto nanoparticles involves the use of adaptor molecules. This approach allows the antigen-binding region of the antibody to freely bind to the receptor site of the tumor. The most widely used adaptor agents are biotin, 'Fc' binding proteins, and DNA nucleic acid (213).

CHAPTER 3

MATERIALS AND METHODS

3.1 Materials and Equipment

3.1.1 Materials

1. 2, 2′-azobis(2-methylpropionamidine) dihydrochloride (V50) (Sigma Aldrich St. Louis, MO, USA)

2. 6-Maleimidohexanoic acid (Sigma-Aldrich St. Louis, MO, USA)

3. AA (Sigma Aldrich St. Louis, MO, USA)

4. Acetonitrile (Merck & Co. Darmstadt, Germany)

5. Acrylic acid (Sigma-Aldrich St. Louis, MO, USA)

6. Alginate (Sigma-Aldrich St. Louis, MO, USA)

7. Annexin V Alexa Fluor™ 647 conjugate (Invitrogen, Carlsbad, CA, USA)

8. Annexin V binding buffer, (Invitrogen, Carlsbad, CA, USA)

9. BCA protein assay kit (EMD Millipore Corp., USA)

10. Caco-2 cells (Faculty of Dentistry, Naresuan University (Phitsanulok), Thailand)

11. Chitosan (CHI) (MW 8000 g/ mol) (OliZac Technologies 88 Co., Ltd., Bangkok, Thailand)

12. Cholesterol (CH) (Nanjing Xinbai Pharmaceutical Co., Ltd., Nanjing, China)

13. Curcumin (Sigma-Aldrich St. Louis, MO, USA)

14. Deuterium oxide (D_2O) (Cambridge Isotope Laboratories Tewksbury, MA, USA)

15. Dimethylformamide (DMF) (QREC Switzerland)

16. Dox hydrochloride (Sigma Aldrich St. Louis, MO, USA)

17. Dulbecco's modified Eagle's medium (DMEM)

18. Ethyl acetate (Merck & Co. Darmstadt, Germany)

19. Fetal bovine serum (FBS) (Gibco BRL, Rockville, MD, USA)

20. HGF cells (Faculty of Dentistry, Naresuan University (Phitsanulok), Thailand)

21. HT-29 cells (Faculty of Dentistry, Naresuan University (Phitsanulok), Thailand)

22. Iodoacetic acid (IA) (Sigma-Aldrich, St. Louis, MO, USA)

23. *L*-cysteine hydrochloride (Sigma-Aldrich, St. Louis, MO, USA)

24. *L*-glutamine, non-essential amino acids, (Gibco BRL, Rockville, MD, USA)

25. Methanol (HPLC grade) (Merck & Co. Darmstadt, Germany)

26. Methylthiazolyldiphenyltetrazolium bromide (MTT) (Sigma Aldrich St. Louis, MO, USA)

27. *N*-Ethyl-*N*′-(3-dimethyl aminopropyl) carbodiimide hydrochloride (EDC) (Sigma-Aldrich, St. Louis, MO, USA)

28. *N*-hydroxysuccinimide (NHS) (Sigma-Aldrich, St. Louis, MO, USA)

29. *N, N*′-methylene bisacrylamide (MBA) (Sigma Aldrich St. Louis, MO, USA)

30. Oleic acid, (Sigma Aldrich, St. Louis, MO, USA)

31. PEGDA (MW = 575) (Sigma Aldrich St. Louis, MO, USA)

32. Penicillin-streptomycin (Gibco BRL, Rockville, MD, USA)

33. Phosphatidylcholine (PC) (Lucas Meyer GmbH, Düsseldorf, Germany)

34. SK-BR-3 cells (Faculty of Dentistry, Naresuan University (Phitsanulok), Thailand)

35. SYTOX™ Green nucleic acid stain (Invitrogen, Carlsbad, CA, USA)

36. Tras (Mylan Institutional Inc., a Viatris Company)

3.1.2 Equipment

1. Analytical balance

2. Attenuated Total Reflectance Fourier transformed infrared spectrophotometer (ATR-FTIR) (Nicolet iS5, Thermo Scientific, USA)

3. Autoclave (LS-2D, Scientific promotion. Co., Ltd.)

4. Bath sonicator

5. CO_2 incubator

6. C18 column (Agilent Technologies, Senta Clara, CA, USA)

7. Filter set

8. Flow Cytometer (The Invitrogen ^{TM} Attune ^{TM} NxT, USA)

9. Freeze dryer (FreeZone2.5, LABCONCO, USA)

10. High-performance liquid chromatography (HPLC; Agilent Technologies, 2100 series, Santa Clara, CA, USA)

11. Incubator shaker

12. Inductively coupled plasma – Mass spectroscopy (ICP-MS; Agilent Technologies, 1100 series, Santa Clara, CA, USA)

13. Inverted fluorescence microscope (Nikon® T-DH, Japan)

14. Magnetic stirrer

15. Microplate fluorometer (Fluoskan Ascent [TM], Thermo Scientific, MA, USA)

16. Microplate reader (VICTOR Nivo [TM], Perkin Elmer, MA, USA)

17. pH meter (HORIBA compact pH meter B-212)

18. Scanning electron microscope (Tescan Mira 3, Czech Republic)

19. Sonicator (Sonic VibraCell [TM])

20. Syringe filter

21. Syringe pump (NE-1000 Programmable Single Syringe Pump, KF Technologies)

22. Transmission electron microscope (Philips® Model TECNAI 20)

23. UV visible spectrophotometer

24. Vortex mixer

25. Zeta sizer (Malvern Instruments, Malvern, UK)
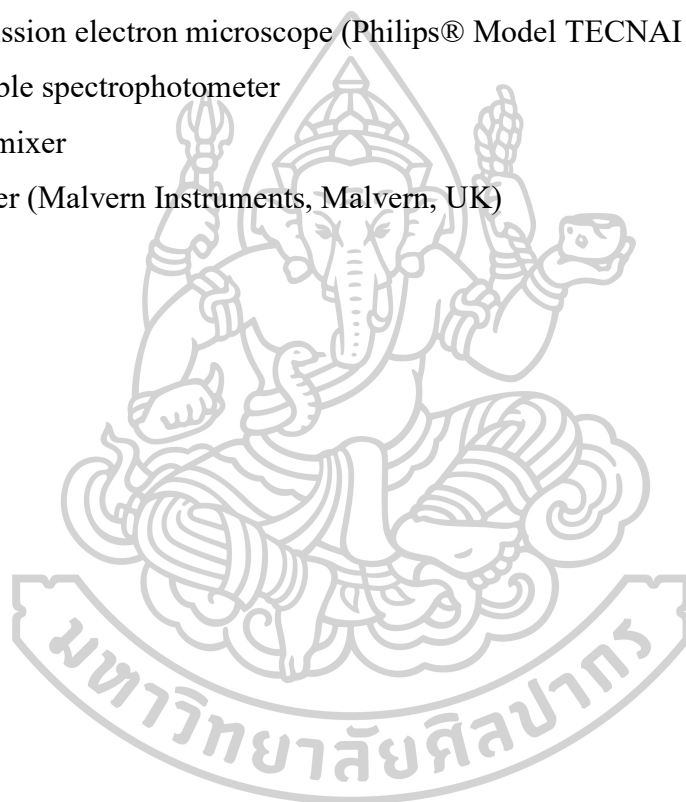
3.2 Development of Dox-loaded PEGDA/AA NPs for colorectal cancer

3.2.1. Synthesis of PEGDA/AA NPs

The synthesis of PEGDA/AA NPs was accomplished by surfactant-free emulsion polymerization consuming different molar ratios of PEGDA and AA (0.5:1, 1:1, and 1:0.5). The procedure was modified from the previous report (214). In brief, 100 mL of deionized water was prepared in a clean round-bottomed flask and warmed to 70 °C with nitrogen flush in an oil bath. To the heated flask, 0.2% of V50 was added and stirred for at least 20 min. Meanwhile, PEGDA, AA, and MBA (10 wt%) were mixed in 5 mL of ethyl acetate before being slowly added into the initiator solution. The mixture was then stirred for 18 h to complete the polymerization reaction. Consequently, the trace reagents and unreacted monomers were removed by dialysis against deionized water. After three consecutive days, the reactant was lyophilized to obtain dried PEGDA/AA NPs.

3.2.2 Characterization of PEGDA/AA NPs

3.2.2.1 Proton Nuclear magnetic resonance spectroscopy

The chemical structure of the synthesized PEGDA/AA NPs was elucidated using proton nuclear magnetic resonance (^{1}H-NMR) spectroscopy. The NPs were homogeneously dispersed in deuterated water (D_2O) and analyzed on an AVANCE III HD (Bruker, Billerica, MA, USA, operated at 300 MHz at 25 °C). The chemical shifts are stated as parts per million (ppm).

3.2.2.2 Attenuated total reflection Fourier-transformed infrared spectroscopy

The structure of NPs was confirmed by an attenuated total reflection Fourier-transformed infrared (ATR-FTIR) spectrometer (Nicolet iS5, Thermo Scientific, USA). The ATR-FTIR spectra were collected from wavenumber 400-4000 cm^{-1} at 16 scans with a resolution of 4.00 cm^{-1}.

3.2.2.3 Determination of particle size and zeta potential

The determination of the particle size, polydispersity index (PDI) and zeta potential of PEGDA/AA NPs was accomplished by the dynamic light scattering (DLS) method using a Zetasizer Nano ZS (Malvern Instruments, Malvern, UK) at 25

°C. The NPs were dispersed in ultrapure water (1 mg/mL) and sonicated with a probe sonicator to disaggregate the particles. The dispersant was diluted with ultrapure water (1:99) and added to the zeta cell through a 0.45-µm syringe filter. Each colloidal sample was measured in triplicate.

3.2.3 Morphology of PEGDA/AA NPs

3.2.3.1 Transmission electron microscopy

The morphology of PDGDA/AA NPs was observed by a transmission electron microscope (TEM) (JEOL JEM-1400Flash, Tokyo, Japan) with 80 kV accelerating voltage. The NPs were suspended in water and stained with 1% uranium acetate being characterized on a support grid.

3.2.3.2 Scanning electron microscopy

The appearance of the NPs was also visualized using scanning electron microscopy (SEM) (Tescan Mira 3, Czech Republic). The lyophilized NPs were coated with a gold layer before the speculation.

3.2.4 Drug loading

Dox was loaded into the PEGDA/AA NPs using the adsorption method. Briefly, 20 mg of lyophilized PEGDA/AA NPs were suspended in 10 mL of ultrapure water containing Dox at different weight ratios of NPs:Dox (1:0.5, 1:1, and 1:2). Thereafter, the mixtures were shaken overnight using a rotary mixer. Dox-NPs were then separated by centrifugation (14,000 rpm for 10 min). The supernatant was discarded and the pellet was washed twice with ultrapure water. The dried Dox-NPs were collected after freeze-drying.

The content of Dox in the NPs was determined by adding 1 mg of Dox-NPs in 1 mL of 0.1 M HCl in ultrapure water (1:49) to instantly elute the drug from the NPs. Then the amount of the drug was determined by using high-performance liquid chromatography (HPLC). The chromatographic condition was adapted from Dharmalingam et.al (2014), with slight modification. The mobile phase was a mixture of acetonitrile and water (pH 3) (30:70) delivered at a flow rate of 1.0 mL/min. The C18 column (250×4.6 mm, 5 µm) was used with a temperature maintained at 30°C,

and the drug content was quantified by a UV-Visible detector (480 nm) (215). The loading capacity (LC) and the percent loading efficiency (%LE) were calculated using Eqs. (1) and (2) respectively.

$$LC = \frac{\text{The amount of Dox quantified (µg)}}{\text{The weight of Dox-NPs (mg)}} \qquad (1)$$

$$\%LE = \frac{\text{The amount of Dox quantified (mg)}}{\text{The amount of Dox added (mg)}} \times 100 \qquad (2)$$

3.2.5 Drug Release

The release of Dox from the PEGDA/AA NPs compared to the Dox solution was carried out by the dialysis technique. The release characteristics were studied in two release media which were the phosphate buffer saline (PBS) solution (pH 5.0) and PBS (pH 7.4). The condition of pH 5.0 was represented the endosomal tumor pH condition in colorectal tumor and pH 7.4 for normal physiological state. Firstly, 10 mg of the Dox-NPs and free Dox (with an equivalent amount of Dox to the Dox-NPs) were dispersed in the release medium (1 mL) and placed in a dialysis bag (molecular weight cut-off = 6000–8000 Da). Then, the bags were submerged in 25 mL of the release medium and agitated at 75 rpm in an incubator shaker controlled at 37°C. At each pre-defined time point (5, 10, 15, 30 min, 1, 2, 4, 8, 12, 24 h), 1 mL of the release medium was sampled and replaced with a fresh medium. Dox content was then analyzed using HPLC.

3.2.6 Cytotoxicity studies

The cytotoxicity of the blank NPs on the model intestinal epithelial cells (Caco-2) was evaluated by using an MTT assay. The cells were cultivated in DMEM supplemented with 10% FBS, 100 mM L-glutamine, 1% non-essential amino acids, 1% sodium pyruvate and 0.1% penicillin-streptomycin. To the 96-well plates, the cells were seeded to a density of 10,000 cells/well and stored in a controlled environment (5% CO2, 95% air, 37°C). Different concentrations (1–5000 µg/mL) of blank PEGDA/AA NPs were prepared in DMEM and used to treat the cells for 24 h. Then, the samples were removed, and the cells were washed with sterile 1x PBS pH 7.4 before the MTT solution in DMEM (0.5 mg/mL) was replaced and further

incubated for 3 h. The resultant formazan crystals were dissolved with dimethyl sulfoxide (DMSO). Then, the absorbance was measured by a microplate reader (Multimode Microplate Reader, VICTOR Nivo™, Perkin Elmer, MA, USA) at 550 nm. The percentage of cell viability was calculated relative to the untreated control cells.

The cytotoxicity of free Dox and Dox-NPs towards Caco-2 cells and human colorectal adenocarcinoma cell line (HT-29) were also assessed using MTT assay. The HT-29 cells were grown in DMEM with 10% FBS, 100 mM L-glutamine, 1% non-essential amino acids and 1% penicillin-streptomycin. Free Dox and Dox-NPs at the concentration range between 0.5–100 μg/mL in serum-free DMEM were used to treat both cell lines for 24 h. The relative cell viability was calculated, and the IC50 values were computed from a constructed dose-response curve of log (concentration) vs relative cell viability using GraphPad Prism v.5.01 software.

3.2.7 Cellular uptake

Flow cytometry analysis was performed to investigate the uptake of Dox-NPs into the HT-29 cells compared to the Dox solution. The HT-29 cells were seeded into a 24-well plate to the density of 50,000 cells/well and incubated for 24 h. The cells were then treated with either free Dox solution or Dox-NPs prepared in serum-free DMEM at the concentration equivalent to the IC50 value of free Dox. At the specified time points (1, 2, 4, and 8 h), the cells were washed with PBS and serum-free DMEM and detached with Accutase®. Once dispersed homogeneously, the cells were fixed with 4% formaldehyde and stored at 4°C until the analysis. The mean fluorescent intensity (MFI) of Dox inside the cells was analyzed using an Attune® NxT Flow Cytometer.

3.2.8 Cell death assay

The apoptosis cell death assay of free Dox and Dox-NPs was determined by the dual staining technique. Briefly, the HT-29 cells were seeded in a 6-well plate to a density of 50,000 cells/well and incubated in a controlled environment until 60–70% confluency was achieved. The cells were then treated with free Dox and Dox-NPs at various concentrations (equivalent to 1, 3, and 5 μM of Dox). After 24 h, the cells

were washed, detached, and incubated with 1× annexin binding buffer in the dark. Consequently, the cell suspensions were stained with annexin V Alexa Fluor™ 647 conjugate and 1 μM SYTOX™ Green. After 15 min incubation in the dark, the samples were analyzed by using a flow cytometer (216).

3.3 Development of Dox-loaded Tras-decorated liposomes for breast cancer

3.3.1 Synthesis of CHI-IA

CHI-IA was synthesized using a published procedure with slight modifications. The synthesis of the CHI-IA was performed by a carbodiimide coupling reaction using a two-step procedure. Firstly, various weight ratios of IA to CHI (1:1, 2:1, 3:1), 0.36 g of NHS, and 0.6 g of EDC were dissolved in 2 mL of DMF in a small vial and stirred with slight warming for a few minutes until the color of the mixture changed into dark brown color. The reaction was continued with stirring for 24 h to get a stable ester intermediate. After that, 0.58 g of low molecular weight CHI was dissolved in 7 mL of 1 M hydrochloric acid in a round bottom flask and mixed for 5 min before 18 mL of DI water was poured. The mixture was mixed using a magnetic stirrer. Then, the mixture of IA, EDC, and NHS was slowly added to the CHI solution with constant stirring. Afterward, the pH was modified to 5 with 1 M NaOH. The reaction was continued for 24 h by continuous stirring to acquire the complete reaction of a reactive ester with a free amino functional group of CHI. After 48 h of the first and second steps, the reactant mixture solution was dialyzed against deionized water for 3 days followed by lyophilization (217). After that, the synthesized CHI-IA was characterized by ATR-FTIR, NMR, and inductively coupled plasma mass spectrometry (ICP-MS).

3.3.2 Characterization of CHI-IA

The chemical structure of CHI-IA was analyzed by ATR-FTIR and NMR. The ATR-FTIR analysis was performed using a Nicolet iS5 attenuated total reflectance Fourier transform infrared (ATR-FTIR) spectrophotometer equipped with a single bounce diamond. The spectra were recorded as an average of 32 scans with 16 cm^{-1} resolution at the wavenumber ranging from 500-4000 cm^{-1}. NMR analysis was

performed using an NMR 300 MHz (AVANCE III HD, Bruker) spectrometer and the spectra were presented as δ in ppm.

3.3.3 Determination of iodine content

To determine the iodine content of CHI-IA, an ICP-MS (Model-Agilent Technologies, 1100 series, Santa Clara, CA, USA) with Mira-Mist (PEEK) nebulizer at 0.1 rpm was exploited. Ten mg of the sample was digested in 5 mL of purified concentrated HNO_3 at 90 °C for 1 h. After cooling, the solutions were transferred to ultrapure water before the analysis by ICP-MS.

3.3.4 Preparation of liposomes

3.3.4.1 Preparation of anionic liposomes

Anionic liposomes were prepared using the thin-film hydration method. Briefly, the 10:1.5 molar ratio of PC and oleic acid were dissolved in chloroform: methanol (2:1). Then the solvent was evaporated under N_2 gas until a thin film was formed. To get complete evaporation of the solvent, the thin film was placed in the desiccator for at least 6 h. Next, the thin film was hydrated with 2 mL of PBS (pH 7.4). To acquire the vesicles, the lipid solution was sonicated for 10 min in a bath sonicator. Then, the particle size of the liposome was reduced by a probe sonicator.

3.3.4.2 Preparation of Tras-conjugated CHI-IA coated liposomes

Firstly, the CHI-IA polymer was dissolved in 1 mL of PBS to obtain a polymer solution with a concentration of 10 mg/mL. Then, Tras was added to the CHI-IA solution and stirred overnight. Afterward, the mixture solution was slowly dropped into the liposome solution and stirred for 3 h to conjugate the Tras- CHI-IA onto the liposome.

3.3.5 Characterization of liposomes

3.3.5.1 Particle size and polydispersity index evaluation

The particle size, PDI and surface charges of the liposomes were measured by DLS method using a Zetasizer Nano ZS (Malvern Instruments, Malvern, UK)

3.3.5.2 Transmission electron microscope

The morphology of the resultant liposomes was viewed by a transmission electron microscope (TEM) (Philips Model TECNAI 20) with 80 kV accelerating voltage. The liposomes were diluted and stained with 1% uranium acetate (UA) and embedded on a supporting copper grid before being characterized.

3.3.6 Determination of Tras-conjugation efficiency to liposomes

The efficiency of Tras conjugation onto the liposomes was determined by a microbicinchoninic acid assay (microBCA assay) compared with unconjugated liposomes. The BCA working reagent was prepared. First, 200 µL of BCA solution was mixed with 4 µL of cupric sulfate. Then, 200 µL of this reagent mixture was pipetted to each well containing the sample. The reaction was accomplished by incubating at 37 ˚C for 30 min. The absorbance at 562 nm was then measured by a microplate reader.

3.3.7 Loading of Dox and determination of drug loading content

Dox was loaded into the liposome by dissolving the drug at different concentrations (1, 2, 3, 4 mM) in PBS before mixing with the liposome thin film followed by probe sonication. The excess Dox was removed by centrifugal-filter unit (Amicon ultra-4, molecular weight cut-off 3 kDa) by centrifugation at 14,000 rpm for 20 min to split up the free drug from liposomes. After washing two times with PBS, the filtrates were mixed with 0.1% Triton™ X-100 in a ratio of 1:1 w/w to break the liposomes. The Dox content was quantified by a microplate fluorescence spectrometer (Fluoskan Ascent^{TM}, Thermo Scientific) at an excitation wavelength of 485 nm and an emission wavelength of 538 nm. The drug loading content (LC) and the percentage of entrapment efficiency (%EE) of Dox in the liposomes were calculated using Eqs (1) and (2), as mentioned in section 3.2.4.

3.3.8 In vitro release study

In vitro release of doxorubicin from liposomes was investigated by dialysis method. One milliliter of free drug, Dox-liposome, Dox-CHI-IA-liposome, and Dox-Tras-CHI-IA-liposome were placed into a dialysis bag (MWCO: 6000-8000 Da). These dialysis bags were immersed into 20 mL of release medium which was PBS (pH 5.0) and PBS (pH 7.4) and incubated at 37 °C in a shaker at 75 rpm. At specific intervals (5, 10, 15, 30 min, 1, 2, 4, 8, 12, 24 h), 1 mL of the drug-containing medium was withdrawn and replenished with the fresh PBS. Then, the content of the doxorubicin was measured by a microplate fluorometer (Fluoskan AscentTM, Thermo Scientific) at an excitation and emission wavelength of 485 and 538 nm, respectively.

3.3.9 In vitro cytotoxicity study

The biocompatibility of the blank liposome, CHI-IA-liposome and Tras-conjugated liposomes were evaluated using an MTT assay to prove their safety on the normal cells. The human gingival fibroblast (HGF) cells were used as the representative of human normal cells. MTT assay was also performed to evaluate the cytotoxicity of free Dox and the liposome formulations toward the HER2-positive breast cancer cell line (SK-BR-3) by measuring cellular mitochondrial metabolic activity at 24 h. The SK-BR-3 cells were cultivated in DMEM with 10% FBS, 100 mM L-glutamine, 1% non-essential amino acids, and 1% penicillin-streptomycin in a controlled atmosphere (95% of air, 5% of CO_2 at 37 °C) in after seeding in a 96-well plate at 10,000 cells per well. The procedure for the MTT assay was similar to Section 3.2.6.

3.3.10 Cellular uptake

The uptake mechanism of the Dox solution and the Dox-loaded liposome formulations was investigated in HER2-positive SK-BR-3 breast cancer cells using a flow cytometer. The SK-BR-3 cells were seeded into a 24-well plate (70,000 cells/well) and incubated for 24 h. The procedure for the uptake analysis by flow cytometry was similar to Section 3.2.7.

3.3.11 Cell death assay

The study of apoptosis cell death assay for the SK-BR-3 cells after being treated with Dox solution and the liposome formulations was determined by flow cytometry by the dual staining method as mentioned in Section 3.2.8. The HER2-positive SK-BR-3 cells were seeded in a 6-well plate with a cell density of 200,000 cells/well before being treated with the samples.

The assay was also conducted using inverted fluorescence microscope. The SK-BR-3 cells were seeded at a density of 10,000 cells/well into a 96-well plate. After being incubated for 1 day in a controlled atmosphere, the cells were treated with free Dox and various Dox-loaded liposomes (equivalent to 3 µM Dox). The Hoechst 33342 and SYTOX™ Green nucleic acid staining were added to the cells, and incubated for 15-30 min. The dead cells were distinguished under an inverted fluorescence microscope.

3.4 Development of Tras-decorated CHI-Mal/Alg-Cys NPs for breast cancer

3.4.1 Synthesis of maleimide-conjugated chitosan (CHI-Mal)

CHI-Mal was synthesized by a coupling reaction between 6-maleimidohexanoic acid and CHI using EDAC and NHS as catalysts (179). First, CHI (5.5 mmol) was dispersed in 1 %v/v acetic acid (20 mL) in a round-bottom flask, and the reaction was undergone under pH 5.5. At the same time, 6-maleimidohexanoic acid (8.25 mmol) was dispersed in DI water before adding EDAC and NHS to activate the carboxylic acid. The reaction was allowed to continue for 1 h. The solution was added to the CHI solution and continued stirring overnight at room temperature. The next day, the mixture was dialyzed and lyophilized. The resultant polymer synthesis was assured by ATR-FTIR and NMR.

3.4.2 Synthesis of alginate-cysteine (Alg-Cys)

Alg-Cys conjugate was obtained by reacting the sodium alginate with *L*-cysteine HCl by the addition of EDAC and NHS. First, 1 g of sodium alginate was hydrated in DI water (100 mL) and then EDAC was added. After stirring for 2 h under pH 6, the cysteine solution in DI water was slowly dropped into the mixture.

The reaction was allowed to stir for at least 6 h before being purified by dialysis and lyophilization. The successful synthesis was evaluated by ATR-FTIR and NMR.

3.4.3. Preparation and characterization of CHI-Mal/Alg-Cys NPs

CHI-Mal/Alg-Cys NPs were prepared by click reaction by reacting the maleimide functional groups on the CHI and the thiol functional groups on the alginate and ionic interaction between the two polymers. CHI-Mal (0.025%) was dissolved in 1% v/v acetic acid (20 mL) and 0.05 % Alg-Cys was dissolved in DI water (20 mL). Then, various amount of curcumin (0.5, 1, 2 mg) solution dispersed in methanol was slowly added to the Alg-Cys solution and stirred for 1 h. After that, the curcumin in Alg-Cys solution was gradually added dropwise to the CHI-Mal solution by ionic gelation method. Then, stirred vigorously for 4 h before centrifugation at 14,000 rpm for 15 min and freeze-dried. Then, the particle size and zeta potential of the NPs were determined by DLS.

3.4.4 Conjugation of the antibody Tras to the CHI-Mal/Alg-Cys NPs

The maleimide functional groups on the backbone of NPs were used to attach the antibody Tras to the NPs. One mg of Tras was added to the 1 mL solution of CHI-Mal/Alg-Cys NPs (2 mg) in HEPES buffer and stirred overnight to take place the binding of Tras. The Tras conjugated CHI-Mal/Alg-Cys NPs were washed with ultrapure water to remove the free antibody. Then, the binding amount of Tras on the NPs was quantified by micro bicinchoninic acid assay (BCA assay kit).

3.4.5 Determination of loading efficiency and loading capacity of curcumin-loaded CHI-Mal/Alg-Cys NPs

The amount of curcumin that was entrapped in the CHI-Mal/Alg-Cys NPs was determined by HPLC. The entrapped curcumin content was estimated by dissolving 1 mg of curcumin-loaded NPs in 1 mL of methanol. The sample was then subjected to centrifuge at 14,000 rpm for 30 min at 25 °C to get a clear supernatant. The concentration of curcumin from the sample was measured by HPLC according to Fonseca-Santos B. et al. with slight modification (218). The supernatant obtained was analyzed using a reverse phase isocratic HPLC system (Agilent, 2100, Agilent

Technologies, Germany). For this, 20 µL of the sample was injected manually in the injection port and analyzed in the mobile phase consisting of a mixture of 60% acetonitrile and 40% water (2% v/v acetic acid), which was delivered at a flow rate of 1 mL/min with a C18 column (C18, 5 µm, 4.6 x 250 mm internal diameter, Agilent, USA). The curcumin levels were quantified by UV detection at 425 nm. The amount of curcumin in the sample was determined from the peak area correlation with the standard curve. Samples were analyzed and the curcumin %EE was calculated from the equation similarly to Dox loading mentioned earlier.

3.4.6 In vitro release study

The release mechanism of curcumin from the Tras-conjugated CHI-Mal/Alg-Cys NPs was investigated by the dialysis method in phosphate buffer saline at pH 7.4 and pH-5.0. The tube containing 20 mL of release medium with 1% Tween 20 was kept shaking at 200 rpm at 37 °C (219) and the dialysis bags containing 1 mL of NPs dispersion (10 mg of curcumin-loaded NPs) were immersed in the medium. Tween 20 was used as an assistance to enhance the solubilizing activity of hydrophobic Cur and Cur-NPs (220). At specific time intervals of 10, 20, 30 min, 1, 2, 4, 8, 12, 24, 48, 72, 96, 120, 144 and 168 h (up to 7 days), 1 mL of medium was withdrawn and replaced with fresh medium. Then, the withdrawn samples were analyzed by HPLC (Agilent, 2100, Agilent Technologies, Germany) to determine the release amount of curcumin from the NPs.

3.4.7 Cytotoxicity studies

The biocompatibility of the blank CHI-Mal/Alg-Cys NPs and Tras-conjugated CHI-Mal/Alg-Cys NPs formulations was evaluated using MTT assay as previously mentioned in Section 3.2.6 and 3.3.9 to prove their safety on the normal cells. The HGF cells were used as the representative of human normal cells. The in vitro cytotoxicity of the blank NPs, curcumin, curcumin-NPs and Tras-curcumin-NPs were also performed toward the HER2-positive breast cancer cell line (SK-BR-3) and normal cells using a colorimetric MTT assay.

3.4.8. Cellular uptake

Flow cytometry analysis was performed to investigate the uptake of Tras-curcumin-CHI-Mal/Alg-Cys NPs into the HER2-positive breast cancer SK-BR-3 cells and compared with free curcumin and curcumin-NPs. The SK-BR-3 cells were seeded into a 24-well plate to the density of 70,000 cells/well and incubated for 24 h. The cells were then treated with either free curcumin solution, curcumin-NPs and Tras-curcumin- NPs prepared in serum-free DMEM at the concentration equivalent to the IC50 value of curcumin. The procedure for the cellular uptake study is similar to Sections 3.2.7 and 3.3.10.

3.4.9 Cell death assay

The study of apoptosis cell death assay for the SK-BR-3 cells after being treated with curcumin solution and the curcumin-loaded NPs formulations was determined by flow cytometry by the dual staining method as mentioned in Section 3.2.8 and 3.3.11. Then the cell death was examined using Annexin V/PI assay, based on the manufacturer's instructions. Then, the levels of necrotic/apoptotic cells were measured by flow cytometer.

3.5 Statistical analysis

All experimental measurements are evaluated in triplicate (n=3). The results are expressed as mean ± standard deviation (SD). P-values of less than 0.05 (two-tailed) were considered as the statistical significance.

CHAPTER 4

RESULTS AND DISCUSSION

4.1 Development of Dox-loaded PEGDA/AA NPs for colorectal cancer

4.1.1 Synthesis of PEGDA/AA NPs

PEGDA/AA-NPs were successfully synthesized by a surfactant-free emulsion polymerization reaction by using the V50 as an initiator, as displayed in Figure 13.
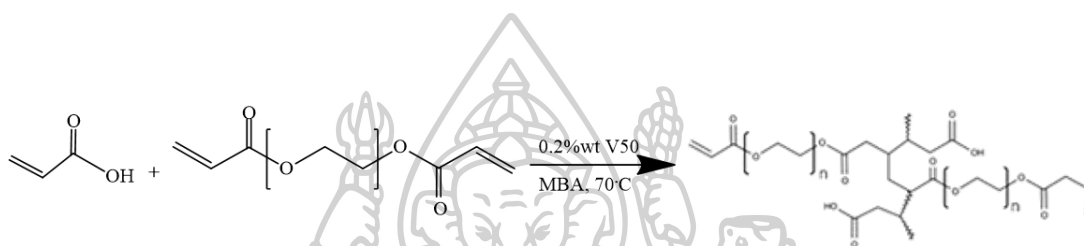
Figure 13. Synthesis pathway of PEGDA/AA-NPs

4.1.2 Characterization of PEGDA/AA NPs

4.1.2.1 Proton Nuclear magnetic resonance spectroscopy (^{1}H-NMR)

The chemical structure of the synthesized NPs was inspected by ^{1}H-NMR and ATR-FTIR. The appeared structure was fully consistent with the proposed structure. The ^{1}H-NMR spectra of PEGDA, AA and PEGDA/AA NPs are presented in Figure 14. The spectra illustrated that the peaks located at 6.6, 6.2 and 5.9 ppm in the PEGDA spectrum were associated with the vinyl groups of the compound, while the signals at 2.7 and 4.4 ppm correspond to the alkyl chain and methylene groups that were adjacent to the ether group, respectively (221, 222). The doublet peaks that appeared at 6.0, 6.3 and 6.7 ppm were responsible for the vinyl group of AA. After the polymerization reaction was completed, the vinyl signals almost completely disappeared. It assured that the reaction was successfully carried out while the small peaks that remain unreacted may be the vinyl group of PEGDA. The multiple peaks that appeared between 1.3-4.7 ppm represent the propagated polymerized chain and side chains of PEG and AA (223).
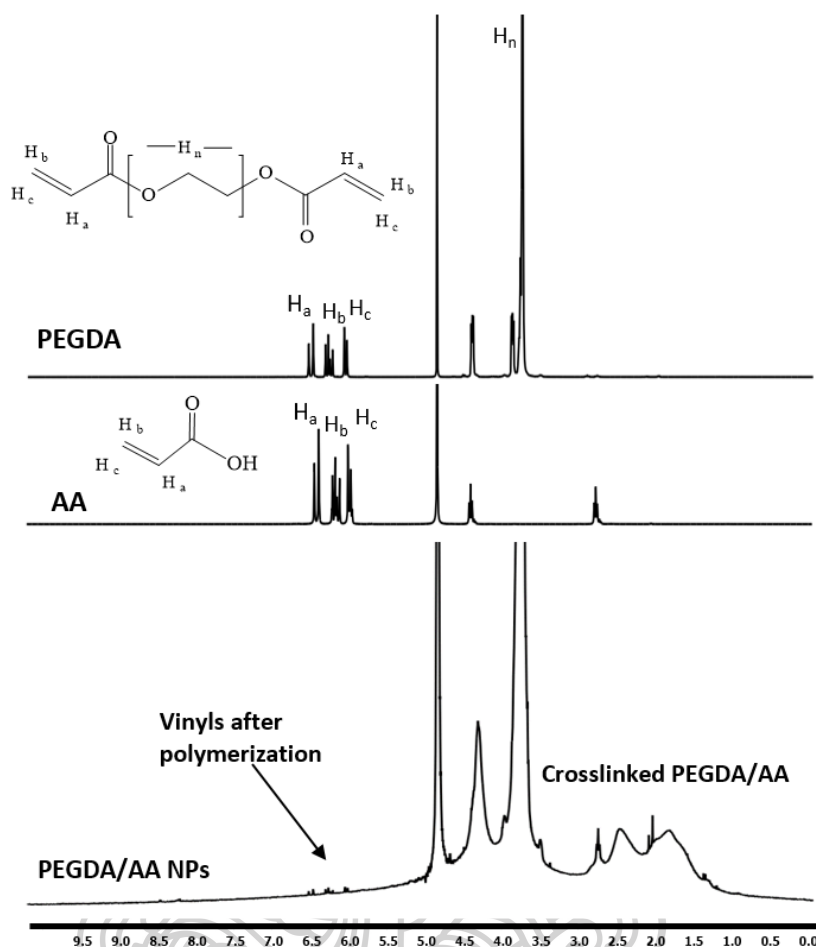
Figure 14. ^{1}H-NMR spectra of PEGDA, AA and PEGDA/AA NPs

4.1.2.2 Attenuated total reflection Fourier-transformed infrared spectroscopy (ATR-FTIR)

The ATR-FTIR spectra of polymerized PEGDA/AA NPs are demonstrated in Figure 15. In the spectrum of PEGDA/AA NPs, the C=O stretching which contained in both monomers are appeared at 1726 cm^{-1}, while asymmetrical and symmetrical bending vibrations of the alkane (C-H) group from the polymerized PEGDA/AA chain and PEGDA alkyl group appeared at 2866 cm^{-1} (224). Furthermore, the sharp band that appeared at 1093 cm^{-1} symbolizes the C-O stretching of the ether group of monomer PEGDA (223). In consideration of the spectroscopic analyses, the consequential PEGDA/AA NPs were successfully obtained according to the described procedure.
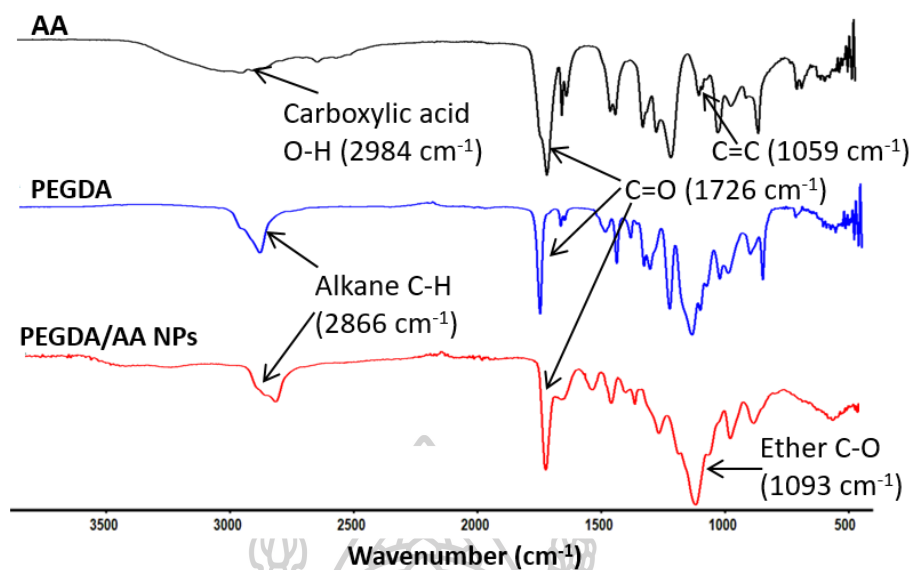
Figure 15. The ATR-FTIR spectra of AA, PEGDA and PEGDA/AA NPs

4.1.3 Determination of particle size and zeta potential

The mean hydrodynamic diameter of particles, particle size distribution in terms of PDI, and zeta potential of the acquired PEGDA/AA NPs with various molar ratios of PEGDA:AA are given in Table 1. The result revealed that all the reaction ratios of monomers provided nano-sized particles with approximately 250 nm in diameter. The zeta potential was also negative for all monomer ratios due to the carboxylic acid group present in AA. The weight variation of the PEGDA and AA did not have an impact on the mean hydrodynamic diameter of the NPs but affected the PDI and the surface zeta potential. According to the size investigation, reactions 1 and 3 (R1 and R3) which use different monomers ratios illustrated higher mean particle size. This consequence may affect the delivery efficiency of the therapeutic cargo to the desired target cell (225, 226). In addition, the alteration of the ratio of the monomers may cause the PDI to be a higher distribution value, because the monomers that remain unreacted after the polymerization process could be colloid and form NPs of homo-monomer, generating different NPs' construction and size. The reduction of AA monomer in R3 reduced the zeta potential, which may cause lesser colloidal stability (227). For R2, PEGDA and AA ratio of 1:1 displayed the narrowest size distribution ($p < 0.05$), with a desirable negative zeta potential value assuring superior colloidal stability. To be able to target passively, the NPs should have a homogenous

size distribution which was a critical parameter to be considered (228). For this reason, R2 was selected for upcoming experiments.

Table 1. Particle size, PDI, and zeta potential of the PEGDA/AA NPs. (* Significant difference from PEGDA:AA (0.5:1)), n = 3.

Reaction	PEGDA:AA	Particle Size (nm)	PDI	ζ potential (mV)
R1	0.5:1	247.6 ± 4.0	0.40 ± 0.02	-29.9 ± 0.5
R2	1:1	$232.0 \pm 4.9*$	$0.25 \pm 0.03*$	$-18.0 \pm 0.1*$
R3	1:0.5	254.0 ± 7.5	0.39 ± 0.02	$-8.0 \pm 0.6*$

4.1.4 Morphology of PEGDA/AA NPs

4.1.4.1 Transmission electron microscopy

The morphology of the PEGDA/AA NPs was observed under TEM, and it is shown in Figure 16(a). As can be seen from the picture, the NPs had a spherical shape with approximately 200 nm in diameter which was similar to the results from dynamic light scattering measurement. The NPs showed slight aggregation on the copper grid.
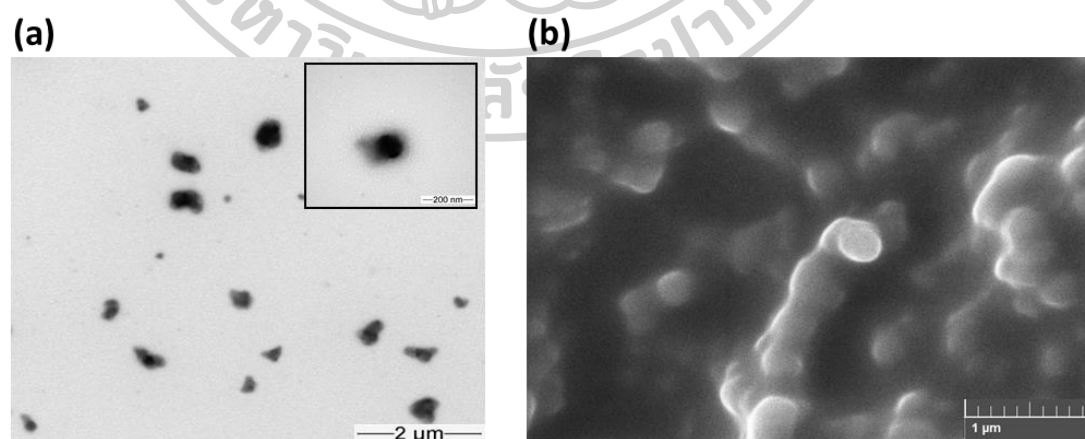
Figure 16. (a) TEM image and (b) SEM image of PEGDA/AA NPs

4.1.4.2 Scanning electron microscopy

Again, the morphology and shape of NPs were confirmed under SEM and shown in Figure 16 (b). When observed under SEM, they seem agglomeration. The possible reason the NPs lyophilized after polymerization and directly observed as a dried form of NPs. This may be due to the hydrophilicity properties of NPs and the possibilities of a large surface area to volume ratio of NPs (128, 229).

4.1.5 Drug loading

The LC and %LE of Dox onto PEGDA/AA NPs were investigated by incorporating various weight ratios of Dox to the NPs using the adsorption technique. The LC and %EE data are shown in Figure 17. It can be observed that as the amount of Dox added to the NPs increased, the values of LC and %LE decreased. The result indicates that the NPs:Dox ratio of 1:0.5 exhibited the highest LC of Dox onto the NPs, with a value of about 152.0 ± 0.77 µg/mg. The reason for the decrease in %LE with higher LC of Dox is that the NPs may become fully loaded with Dox and any excess Dox was removed by washing. The adsorption of Dox onto the NPs occurs through electrostatic interactions between the carboxyl functional groups of the NPs and the protonated amino groups of Dox under normal physiological conditions (230).
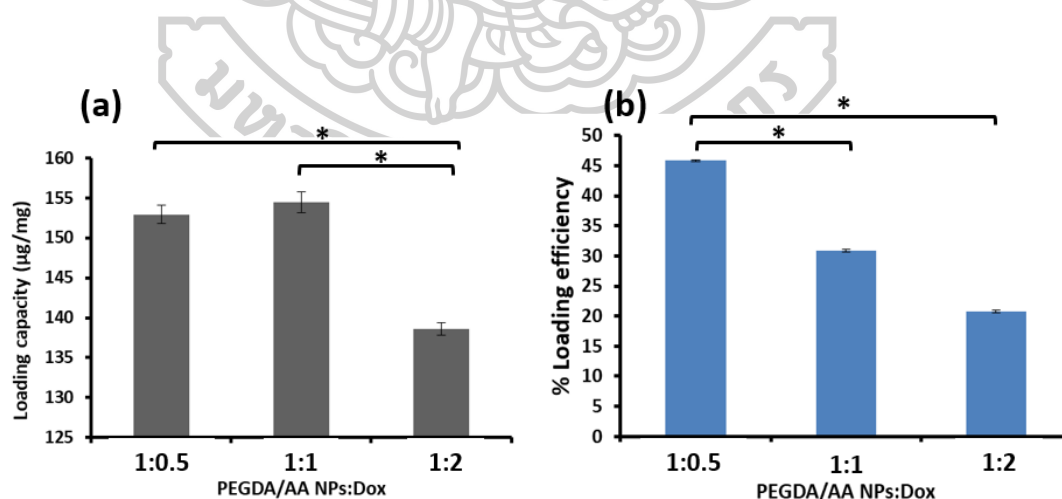
Figure 17. (a) LC and (b) %LE of the Dox-loaded PEGDA/AA NPs. (* Significant difference at 95% CI). The values were determined in triplicate. Each column represents the mean values with the standard deviation.

4.1.6 Drug release

The drug release profile of Dox from the Dox-loaded PEGDA/AA NPs (Dox-NPs) was investigated in PBS at two different pH values using the dialysis method. Dox release profiles from the NPs and free drug are shown in Figure 18. The release study was conducted at pH 7.4 and pH 5.0, which mimic the environments in the bloodstream and tumor, respectively. Figure 18 shows that free Dox was released very rapidly, reaching completion within an hour at pH 5.0, while it exhibited a gradual release with 60% release after 30 min and reached 100% after 4 h at pH 7.4. This may be due to the strong affinity of water and ionization properties of Dox at different pH leading to a different release rate in different environments (216). On the contrary, the release of Dox from Dox-NPs was slower than the free Dox, with only 54% of Dox released in 4 h at pH 5.0. At pH 7.4, the release behavior from the Dox-NPs was more gradual, with less than 50% of Dox released after 12 h. The complete release of Dox occurred in 24 h for pH 5.0, presumably resulting from the protonation of Dox (pKa 8.4) under more acidic environments, which would result in better Dox dissolution (231). The release characteristic of Dox indicated that it can release from the carrier significantly slower at the normal physiological state (pH 7.4) at all time points due to its hydrophilic nature influencing the release mechanism. Another finding at pH 7.4 is that Dox was not completely protonated which may result in the Dox being trapped inside the NPs. However, the release of Dox still increased slowly over time. These factors were associated with the release behavior of Dox-NPs obtained (137, 232). According to the literature review, similar findings of Dox delivery to colorectal cancer were found. For example, Lui et al. (2021) and Abedi et al. (2021) declared a pH-dependent Dox release mechanism observing more rapid drug release at acidic pH value, regardless of the NPs' construction differences (233, 234). Besides, Norouzi et al. (2020) also reported faster Dox release from iron oxide NPs in the acidic tumor environment (pH 5.0) than the physiological pH (235). These previous findings of Dox release profiles are consistent with our research. It can be proposed that targeted drug delivery by passive means should involve the drug residing in the NPs, with the drug discharged upon reaching the targeted tumor area. Thus, the delayed release of Dox under normal physiological conditions was favorable for drug delivery to the

tumor, which was expected to be delivered in the more acidic pH of the tumor area (231).
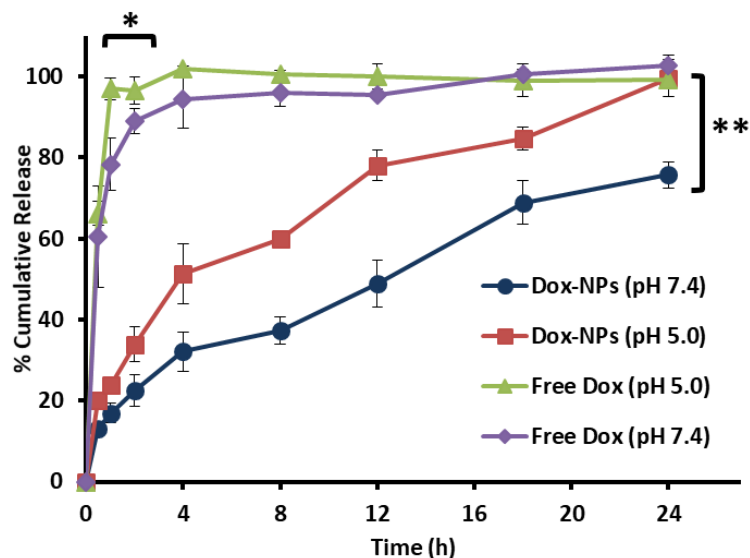
Figure 18. Release profiles of Free Dox at pH 5.0, Free Dox at pH 7.4, Dox-NPs at pH 5.0, and Dox-NPs at pH 7.4. (* Significant difference from free Dox pH 7.4 at 95% CI, ** Significant difference from Dox-NPs pH 7.4 at 95% CI).

4.1.8 Cytotoxicity studies

NPs intended for tumor therapy should not have harmful effects to other tissues. Therefore, the biocompatibility of the blank NPs was assessed on Caco-2 cells, which are used as a model of intestinal epithelial mucosa cells. The results are presented in Figure 19, which shows that cell viability remained over 85% when treated with blank NPs of different concentrations (1-5000 µg/mL). These findings indicate that the synthesized PEGDA/AA NPs did not have any toxic effects on the Caco-2 cells, presumably due to the safety and biocompatibility of PEG and PEGDA (176, 229).
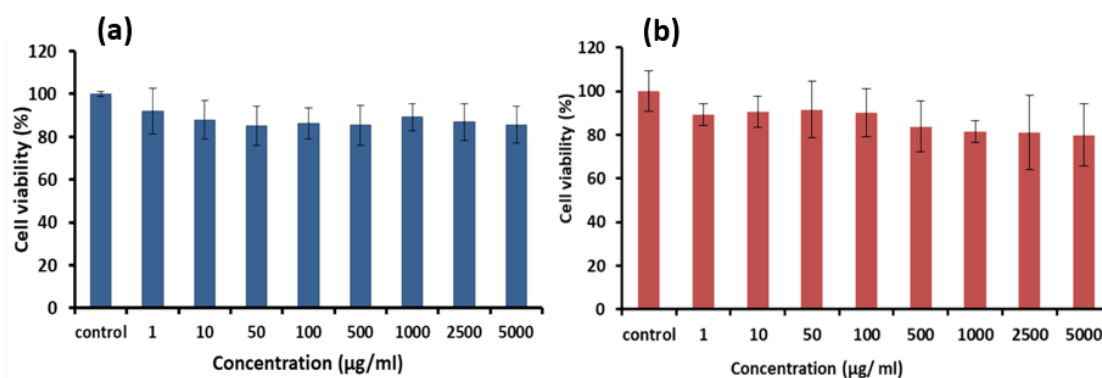
Figure 19. Cytotoxicity study of blank NPs on (a) Caco-2 cells and (b) HT-29 cells

The cytotoxicity of both free Dox and Dox-loaded NPs toward the HT-29 and Caco-2 cell lines was studied. The results are shown in Figures 20 and 21. The free Dox showed potent toxicity towards HT-29 cells, with an IC50 value of 4.3 μg/mL, while the IC50 value of Dox-NPs was 11.8 μg/mL. This observation can be attributed to the direct diffusion of free Dox into the nucleus of HT-29 cells, whereas Dox was steadily released from the NPs. It was found that both free Dox and Dox-NPs exhibited similar effects on the Caco-2 cells. The cell viability of Caco-2 cells treated with free Dox and Dox-NPs was higher than that observed with HT-29 cells. This may be due to the fact that Dox can damage DNA and inhibit cell proliferation, and the doubling time of Caco-2 cells (62 h) is longer than that of HT-29 cells (23 h), which may lead to lesser cell death when analyzed. At the highest concentration of Dox, free Dox kill 50% cell on Caco-2 cells as shown in Figure 21.
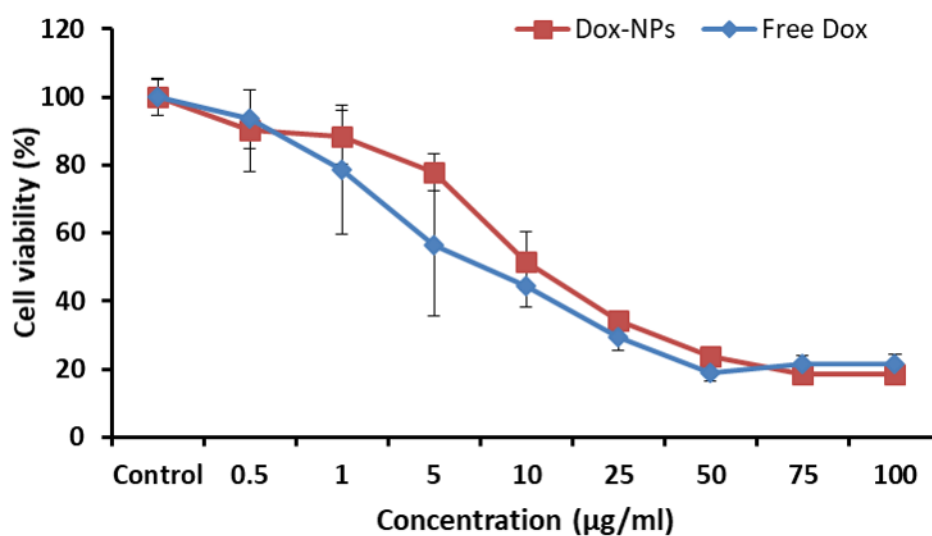
Figure 20. Percentage of cell viability of HT-29 cells after treatment with free Dox and Dox-NPs.
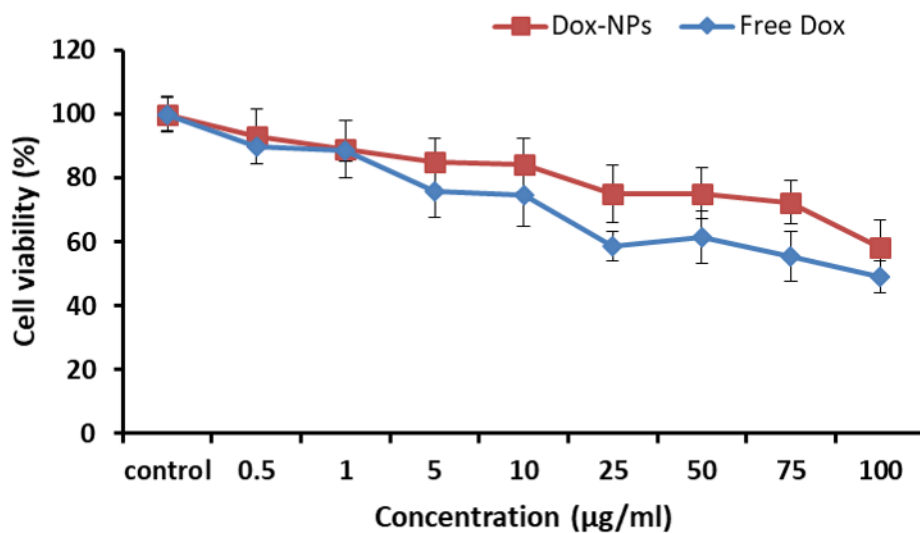
Figure 21. Percentage of cell viability of Caco-2 cells after treatment with free Dox and Dox-NPs.

4.1.9 Cellular uptake

Studying the cellular uptake of cancer cells is crucial to demonstrate the effectiveness of drug-loaded nanocarriers in targeted tumor drug delivery. The detailed results of MFI obtained from the flow cytometer are presented in Figure 22, and it was found to be higher than that of free Dox between 2-8 h ($p < 0.05$). This indicates that Dox from Dox-NPs accumulated inside the colorectal cancer cells more than free Dox. Unlike free Dox, which can rapidly penetrate the cells and inhibit cell proliferation, the Dox-NPs were attached to and taken up by the cells, gradually releasing the cargo drug and leading to a higher fluorescence intensity. Thus, the gradual release of Dox from the particles resulted in high IC50 values (236). The uptake behavior of NPs towards the cells was expected to occur via endocytosis, while the hydrophilic free Dox was accumulated into the tumor cell via passive diffusion (237).
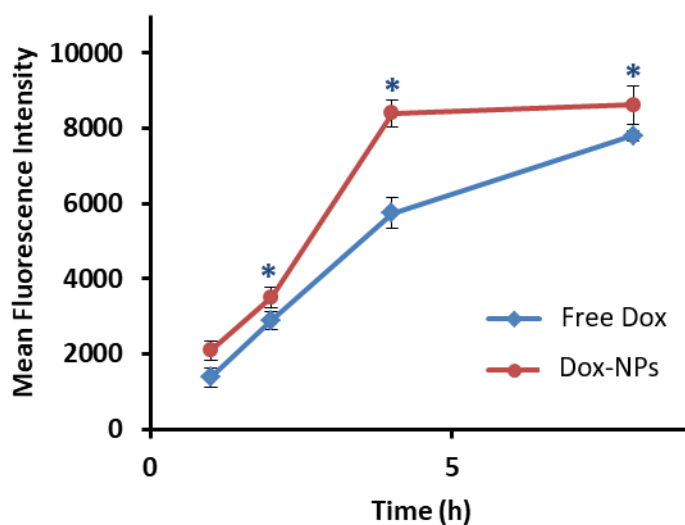
Figure 22. The cellular uptake of Dox and Dox-NPs into HT-29 cells at different time points (* Significant difference at 95% CI). The MFI was calculated from 10,000 events analyzed with the laser line of 488 nm by flow cytometer.

4.1.10 Cell death assay

To detect the death pathway of HT-29 cells, a double-staining method was performed and determined via flow cytometry. The assay detected live cells, early/late apoptotic, and necrotic cells after staining with annexin V Alexa Fluor™ 647

conjugate and SYTOX™ Green. Several dot plots are presented in Figure 23. As observed in the images, untreated control cells and those treated with blank NPs demonstrated over 90% viability and showed non-toxic activity. Cells treated with a lower concentration of free Dox did not show significant HT-29 cell death, while cytotoxicity was considerably higher once the concentration of Dox increased. This explained that an adequate concentration of Dox is required to penetrate the cell membrane and nucleus.

Meanwhile, the induction of apoptosis by Dox-NPs in HT-29 cells showed a dose-dependent character. At the concentration of 1 μM and 3 μM, 16% and 31% of apoptosis cell death occurred with Dox-NPs, while lower apoptosis cell death of free Dox was found (5% and 9%, respectively). Many factors influence cell death, including the nanocarrier, which perhaps played as a focal point in the internalization and release of drugs within the cell. Thus, there is an impact on the cells at lower concentrations. Once a higher concentration was reached (5 μM), apoptosis-mediated cell death was approximately the same (~46%) between the free Dox and Dox-NPs. It was assumed that the therapeutic cytotoxic concentration was reached towards the HT-29 cells. It is worth mentioning that induction of apoptosis is desirable for programmed cell death because it prevents the splitting of the plasma membrane and the leakage of cellular debris, leading to less inflammatory cell death (216). These findings are consistent with previous in vitro cytotoxicity studies that recognized Dox-NP as stronger in triggering apoptosis (238).
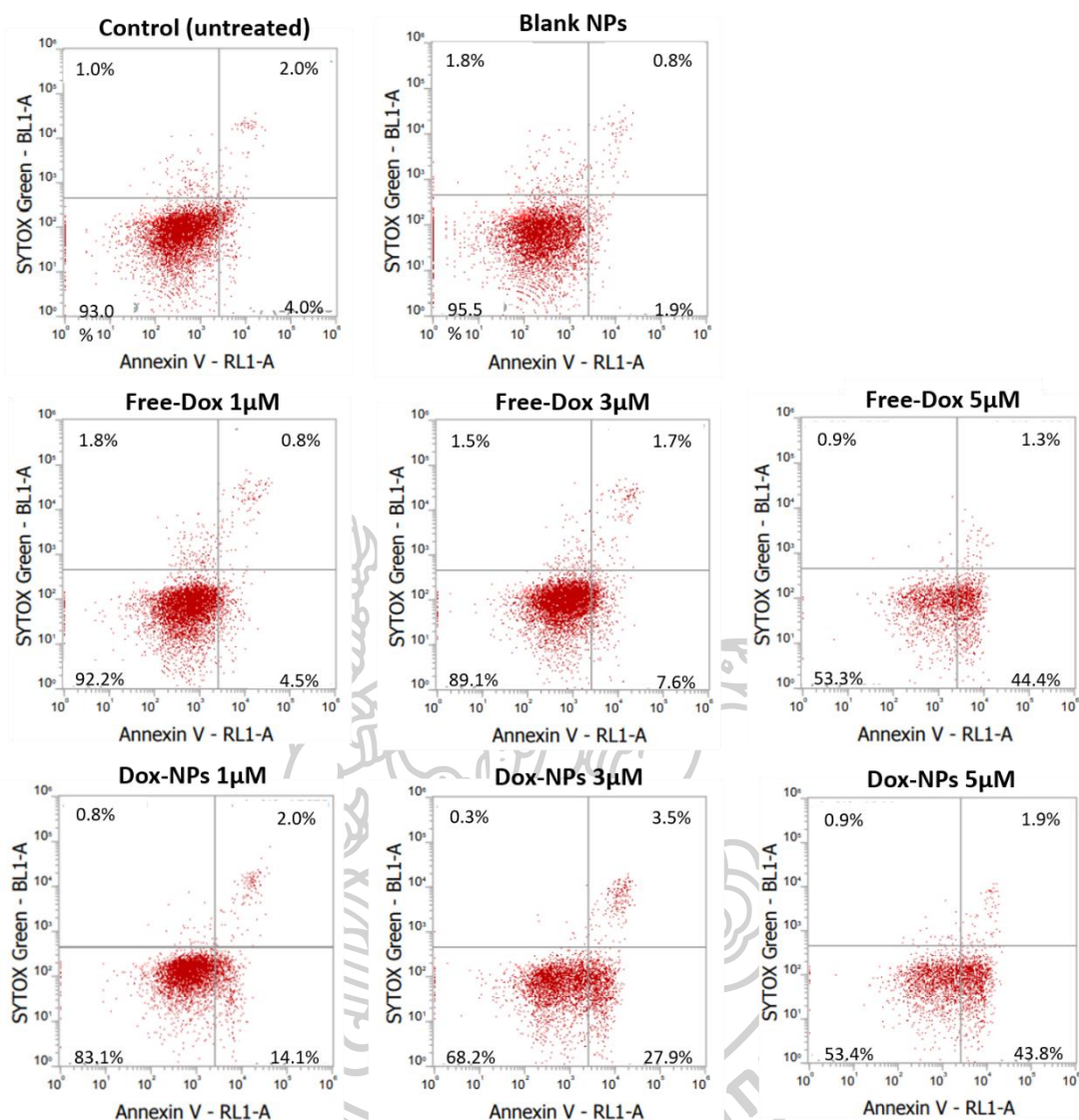
Figure 23. Apoptosis assay of HT-29 cells after treatment with different formulations including untreated control, blank NPs, free Dox (1, 3, and 5 μM), and Dox-NPs (1, 3, and 5 μM). The experiments were performed using the double staining technique of Annexin V Alexa Fluor™ conjugate and SYTOX™ Green.

4.2 Development of Dox-loaded Tras-decorated liposomes for breast cancer

4.2.1 Synthesis of CHI-IA

The CHI derivative (CHI-IA) was synthesized by attaching the amino functional groups of CHI with the carboxylic acid (-COOH) group of IA at its C-2 position. This reaction is carried out using a carbodiimide-mediated crosslinking reaction. To initiate the -COOH functional group of IA, EDAC, which contains the

carbodiimide group, was coupled. The addition of NHS then converted the reactant short-lived O-acylisourea active ester into a more stable and reactive ester form called *N*-hydroxysuccinimidyl ester. This reactive ester group was then conjugated with the amino group of CHI under pH 5, resulting in the formation of an amide functional group (217).
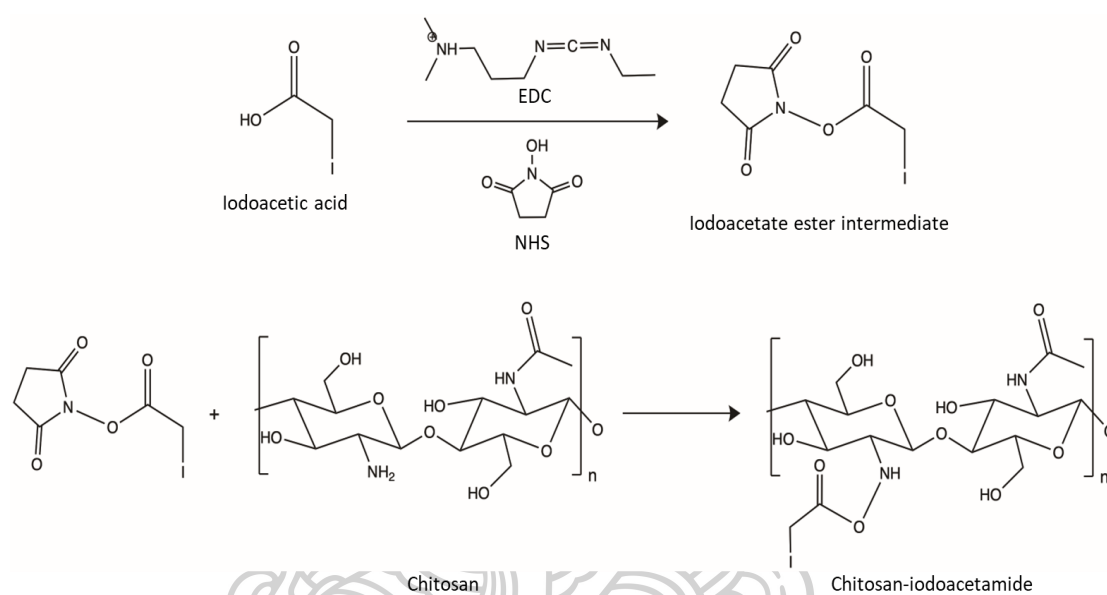
Figure 24. Synthesis pathway of CHI-IA polymer involving a two-step procedure

4.2.2 Characterization of CHI-IA

By the coupling of the carboxylic acid group (-COOH) of IA and the deacetylated amino groups of the CHI glucosamine chain, the CHI-IA derivative was successfully synthesized. The modified chemical structures of the CHI, IA, and CHI-IA structures were analyzed ATR-FTIR and ^{1}H-NMR, and the analysis findings ascertained the modification.

Figure 25. shows the ATR-FTIR spectrum of CHI-IA along with the interpretation of the spectral analyses. Both CHI and CHI-IA spectra presented a broad absorption of O-H stretching in the range of 3000 and 3500 cm^{-1}, as well as N-H stretching of amine between 3290 and 3360 cm^{-1}. The N-H bending of the amine functional group of the deacetylated pyranose ring was found at 1585 cm^{-1}, and the C=O of the secondary amide group appeared as a low to medium-intensity peak at 1590 cm^{-1}. The CH$_2$ bands in the pyranose ring were given at 2880 cm^{-1}, along with

the absorptions at 1415, 1250, and 1325 cm^{-1} (217, 239). Dissimilar to the CHI spectrum, the CHI-IA response showed a strong and new peak at 1636 cm^{-1}, which was due to the stretching of an amide bond that occurred between CHI and IA.

The ^{1}H-NMR spectra of the CHI derivative are also depicted in Figure 25. The ^{1}H-NMR spectrum of CHI showed a signal of the methyl group at the *N*-acetyl glucosamine at 2.03 ppm and signals of the pyranose ring in the range between 3.4 and 3.8 ppm (240). The iodomethylene group in the IA spectrum appeared at 3.81 ppm (217). The ^{1}H-NMR spectrum of CHI-IA showed a similar spectrum to the parent polymer. However, a peak shifting of the proton in the glucosamine ring adjacent to the substituted amino group to the downfield region (from 3.0 to 3.2 ppm) was observed (217, 239).
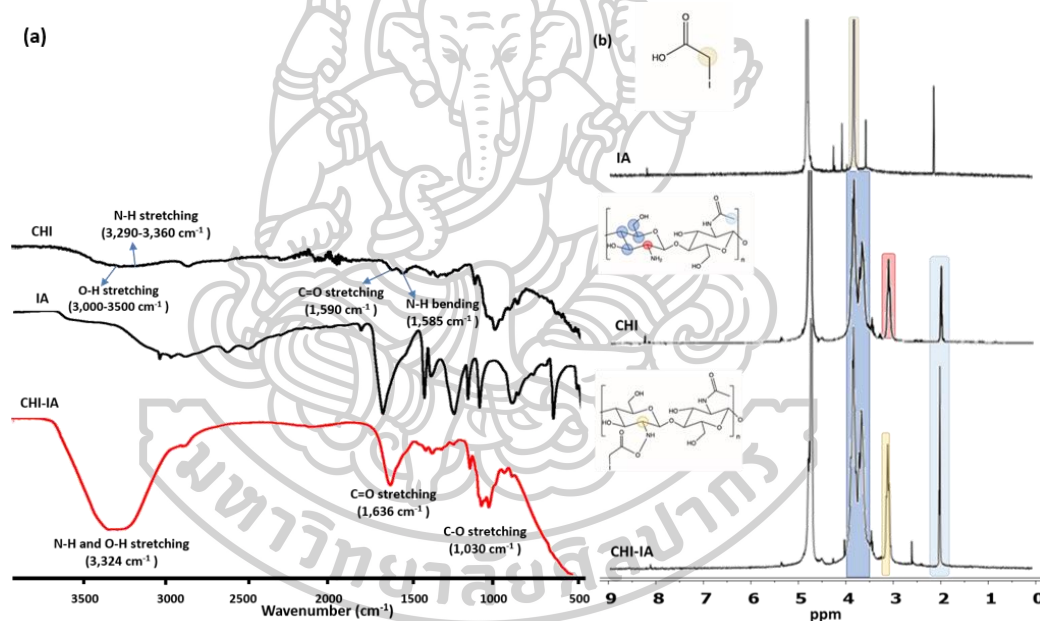
Figure 25. (a) ATR-FTIR and (b) ^{1}H-NMR spectra of CHI, IA, and the synthesized CHI-IA

4.2.3 Determination of Iodine content

The successful chemical reaction can be confirmed by the existence of amide bonds as indicated by both ATR-FTIR and ^{1}H-NMR analyses. However, the presence of grafted iodine could not be observed in either ATR-FTIR or ^{1}H-NMR spectra. Thus, to quantify the degree of substitution of iodine element in the CHI-IA derivative, ICP-MS analysis was performed. The acquired results by the ICP-MS are

expressed in Table 2. The iodine content did not show significant differences across the various ratios of CHI:IA. However, the ratio of CHI-IA (1:1) resulted in the highest percentage yield of 20%, compared to the other ratios. Therefore, this ratio (1:1) was chosen for further experiments.

Table 2. Degree of substitution of different CHI:IA ratios with the % yield.

CHI-IA	% Yield	Degree of substitution
1:1	20.0	10.9 ± 0.64
1:2	12.1	11.0 ± 0.86
1:3	6.9	9.0 ± 0.45

4.2.4 Preparation of liposomes

The anionic liposomes were prepared using the thin-film hydration method by applying different ratios of oleic acid to phosphatidylcholine (PC). Oleic acid was used as a fatty acid, single-chain amphiphiles containing only one lipid hydrocarbon tail, to get anionic liposomes to be able to attach with cationic CHI-IA. Oleic acid are generally used to prepare the anionic liposome which can give higher liposomal stability during the storage. Because the charged nanocarriers repel each other and prevent aggregation (241). Table 3. showed some experimental data, and all the anionic liposomes expressed nano-sized with negative zeta potentials. To attach with a very cationic CHI-IA derivative, it is important to choose an anionic liposome with a higher negative zeta potential. So, we selected the ratio 10:1.5 of phosphatidylcholine and oleic acid with appropriate PDI value and the highest zeta potential (-31.9 ± 1.2) for further experiments.

Table 3. Particle size, PDI, and zeta potential of the liposome formulations (*Significant difference, p<0.05)

Ratio of PC:Oleic acid	Size (nm)	PDI	Zeta Potential (mV)
10:1	65.2 ± 3.6	0.41 ± 0.01	-22.8 ± 0.3
10:1.5	64 ± 2.2	0.35 ± 0.04	-31.9 ± 1.2*
10:2	33.4 ± 0.1	0.28 ± 0.02	-17.7 ± 1.5
10:3	35 ± 1.2	0.23 ± 0.01	-22.2 ± 2.2

4.2.5 Characterization of liposomes

4.2.5.1 Particle size and polydispersity index evaluation

The findings of particle size, size distribution, and zeta potential examinations of the liposome formulations using the DLS method are presented in Table 4. According to the findings, the mean size of all liposomes was within the desirable range of 65-110 nm for targeted drug delivery through the EPR effect, which is effective for particles with size under 120 nm (242). Additionally, liposomes within this size range can evade glomerular filtration and RES, leading to prolonged drug circulation (243). A slight increase in size and PDI was observed after coating the liposomes with CHI-IA and bioconjugation with Tras due to the considerable size of the polymer and antibody surrounding the liposomes. The zeta potential, which characterizes the electrostatic repulsion force and is directly proportional to the colloidal stability of liposomal dispersions (244), showed that the liposomes made with oleic acid had an anionic surface due to the carboxylic acid group of oleic acid. After coating with CHI-IA, the negatively charged surface of the liposomes reversed to a positive charge due to the strong cationic properties of CHI-IA (245, 246), indicating that CHI-IA was favorably coated onto the liposome surface. The Tras conjugation did not affect the zeta potential of the nanocarrier since the ionizable moiety did not participate in the bioconjugation. Despite the surface charge switch and net zeta potential reduction from charge neutralization, the prepared liposome formulations showed promise as nanocarriers for cancer targeting (244). The cationic

properties of CHI-IA may improve cell membrane permeation because the anionic cell membrane attracts and permits the nanocarrier cellular uptake (242). Again, after encapsulating the Dox into coated, uncoated liposomes and Tras conjugated liposome, the particle size and PDI were increased. The anionic and cationic surface charges were slightly decreased. This may be due to the positive charge of Dox after incorporating into anionic liposome.

Table 4. Particle size, PDI, and zeta potential of the liposome formulations

Liposome	Size (nm)	PDI	Zeta Potential (mV)
CHI-IA-Lip	72.8 ± 1.1	0.3 ± 0.01	$+17.0 \pm 1.3$
Tras-CHI-IA-Lip	76.0 ± 1.5	0.5 ± 0.03	$+16.5 \pm 2.1$
Dox-Lip	90.3 ± 1.3	0.2 ± 0.06	-23.7 ± 1.9
Dox-CHI-IA-Lip	108.5 ± 3.5	0.4 ± 0.05	$+11.0 \pm 0.4$
Tras-Dox-CHI-IA-Lip	101.6 ± 2.4	0.38 ± 0.02	$+10.0 \pm 1.9$

4.2.5.2 Transmission electron microscope

The morphology of blank liposomes, CHI-IA-Lip, and Tras-CHI-IA-Lip are revealed in Figure 26. The liposomes were stained with 1% UA, which attaches to the anionic surfaces. The anionic liposome showed a dark spherical structure with a mean diameter of 30 nm. After being coated with CHI-IA, and conjugated with Tras, the background was stained for the contrasting agent that could not adhere to the cationic liposome surfaces. These liposomes also presented as a spherical shape with a slight glowing outer layer which indicated the coated CHI-IA and Tras. Moreover, the mean diameter of the CHI-IA-Lip and Tras-CHI-IA-Lip increased slightly, which were 37 and 38 nm, respectively. This finding are consistent with the results obtained from the DLS, where the particle size measured under TEM is smaller due to the measurement being in the dried state compared to the hydrodynamic diameter obtained by DLS.
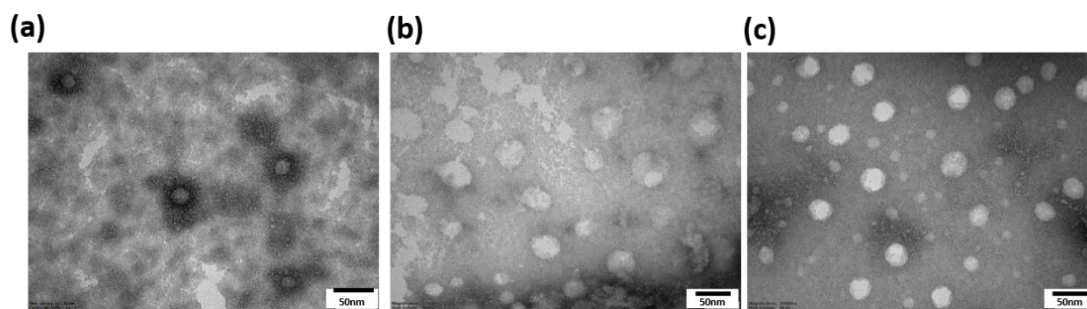
Figure 26. The morphology of (a) anionic liposomes, (b) CHI-IA-Lip, and (c) Tras-CHI-IA-Lip observed under TEM

4.2.6 Determination of Tras-conjugation efficiency to liposomes

The BCA assay was used to examine the amount of protein in the samples. CHI-IA-Lip and Tran-CHI-IA-Lip with different amounts of Tras were tested to quantify the amount of Trans conjugated on the liposome which was represented by the amount of protein found in each sample. As shown in Figure 27, the Tras-CHI-IA-Lip contained much greater protein content compared with CHI-IA-Lip ($p<0.05$) indicating that Tras was conjugated on the coated liposome. When 3 mg and 4 mg of Tras added to the liposome solutions were compared, a higher protein content was found when more Tras was added suggesting an improved conjugating efficiency. The 4-mg added Tras-CHI-IA-Lip showed 1.5-fold higher protein content compared to CHI-IA-Lip. The antibody can be conjugated with the CHI-IA-Lip via the bioconjugation mechanism between iodoacetic acid and thiol groups of the cysteine residue on the antibody. Also, pieces of the literature suggested that iodoacetamide can also react with unprotonated histidines, tyrosines, methionines, and the N-terminal amine group of the proteins which presumably play a part in the bioconjugation process (247, 248). The thioether bond created upon the conjugation was reported to be irreversible in normal conditions. The reaction is reactive among the halides especially, iodine, and thiols (249, 250). Therefore, it can be implied that the attachment of Tras on CHI-IA-Lip was possible due to the bioconjugation process between iodoacetate and the amino acid side chains in proteins.
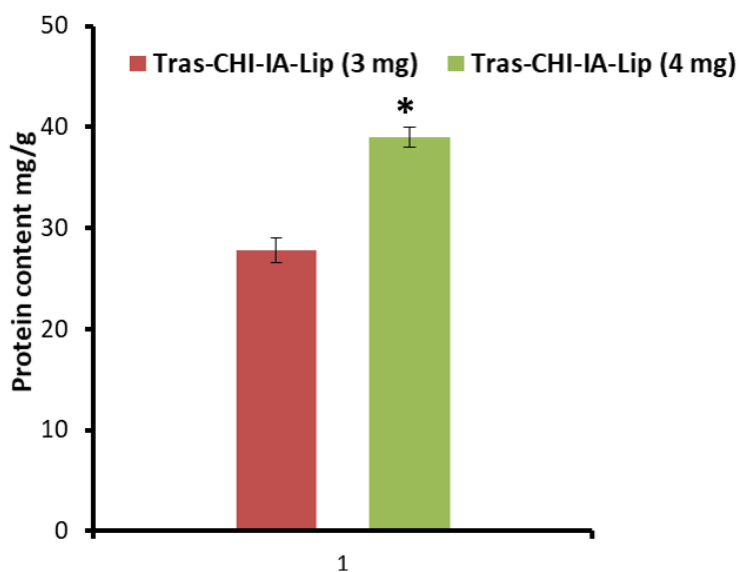
Figure 27. Verification of Tras conjugation on Tras-CHI-IA-Lip using BCA assay. (Statistical significance: *compared to Tras-CHI-IA-Lip (3 mg) at $p < 0.05$)

4.2.7 Loading of Dox and determination of drug loading content

　　%EE and LC of Dox in the liposomes were established to investigate the effect of Dox concentration on the drug loading efficiency and loading capacity. As shown in Table 5, the molar ratio Dox to liposome of 2:10 showed a significantly higher %EE (84.6%) compared to other ratios of Dox ($p<0.05$). The LC of Dox in the liposome was concentration-dependent, with the LC increasing when a higher amount of Dox was added. The maximum LC was observed at Dox:liposome ratio of 3:10, but a higher amount of Dox did not increase the LC ($p>0.05$). Therefore, the Dox:liposome ratio of 2:10 was considered the most suitable for Dox loading conditions as it resulted in the highest %EE and only slightly lower LC compared to the highest LC. This condition was employed in the preparation of Dox-CHI-IA-Lip and Tras-Dox-CHI-IA-Lip in subsequent experiments.

Table 5. %EE, LC of Dox-Lip at different Dox:Liposome ratios (*Significant difference from 1:10, p<0.05).

Dox: Liposome	%EE	LC (mg/g)
1:10	71.5 ± 11.3	11.6 ± 1.8
2:10	84.6 ± 5.2*	26.5 ± 0.7
3:10	67.9 ± 2.4	29.7 ± 1.1
4:10	50.3 ± 3.8	27.8 ± 2.2

4.2.8 In vitro release study

The drug release mechanism is crucial for achieving therapeutic outcomes in all drug delivery systems (251). When designing liposomal drug formulations, two vital parameters are the longer circulation time and slower drug leakage (252). The release profiles of Dox from the liposome preparations at pH 7.4 and pH 5.0 are shown in Figures 28(A) and 28(B), respectively. Dox solution displayed a remarkably rapid release through the dialysis bag, completing within 2-3 h in both pH conditions. In contrast, Dox-Lip, Dox-CHI-IA-Lip, and Tras-Dox-CHI-IA-Lip showed a biphasic release in both conditions. Figure 28(A) indicates that Dox-Lip released 50% of the drug before 2 h, which was faster than that from Dox-CHI-IA-Lip and Tras-Dox-CHI-IA-Lip, which reached 50% release after 2 and 4 h, respectively. The Dox-Lip showed complete drug release at 12 h, while the other liposome formulations extended the drug release to 24 h. The differences in Dox release rates could be due to the CHI-IA coating on the liposomes, which hindered Dox's ability to release through them. Additionally, the liposomal coating altered the permeability of the medium, facilitating drug migration from the vesicles (253). Moreover, the sustained release of the encapsulated Dox may be due to the drug diffusion through the lipid bilayer and the CHI-IA layer surrounding the liposome vesicles (254-256). So CHI-IA played an important role in extending Dox release by limiting the drug and medium transference (61). Moreover, the induced and faster Dox release from liposomes at low pH was

associated with the high solubility related with the protonation of Dox at acidic pH (257).
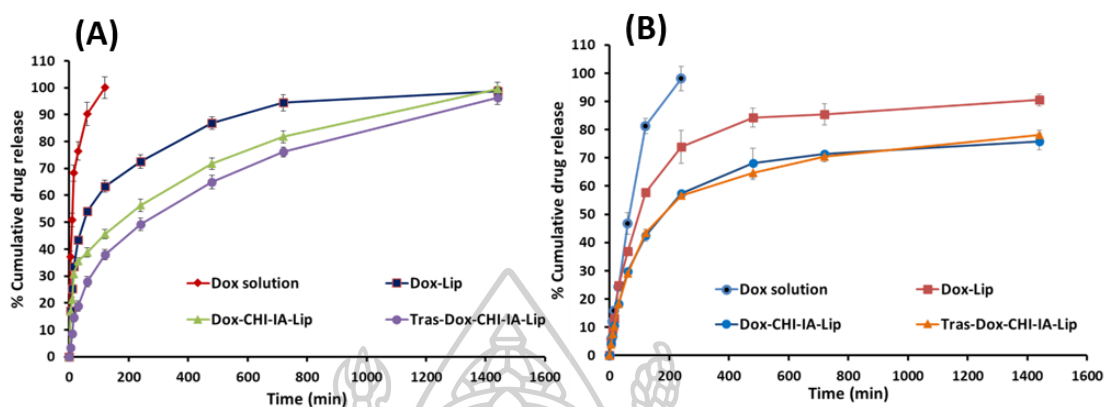
Figure 28. Cumulative drug release patterns of Dox solution, Dox-Lip, Dox-CHI-IA Lip, and Tras-Dox-CHI-IA-Lip at (A) pH 5.0 and (B) pH 7.4.

4.2.9 In vitro cytotoxicity study

To assess the biocompatibility of the liposome formulations on human fibroblast cells and cytotoxicity on the breast cancer cell line, the cellular mitochondrial metabolic activity at 24 h was measured by an MTT assay. Firstly, the biocompatibility of blank liposome was measured on HGF cell and SK-BR-3 cells. As seen in Figure 29, there were no cell death in both cell lines which confirmed that the liposome itself has no cytotoxic activity.

Figure 30 shows that the HGF cells were treated with the same conditions of liposomal formulations as the SK-BR-3 cells. Even at the lowest concentration of free Dox, the HGF cells showed approximately 20% cell death, and at the highest concentration of free Dox (50 µM), 50% cell death occurred. In contrast, for the Dox-Lip, Dox-CHI-IA-Lip and Tras-Dox-CHI-IA-Lip, the cells displayed 80% cell viability until the concentration greater than 5 µM, and cell viability displayed. This finding is consistent with previous research that Dox-loaded catechol-modified CHI/hyaluronic acid NPs showed 50% HGF cell death over 20 µg/mL of Dox (216). This may be because HGF cells proliferate at a slower rate than cancer cells (258).
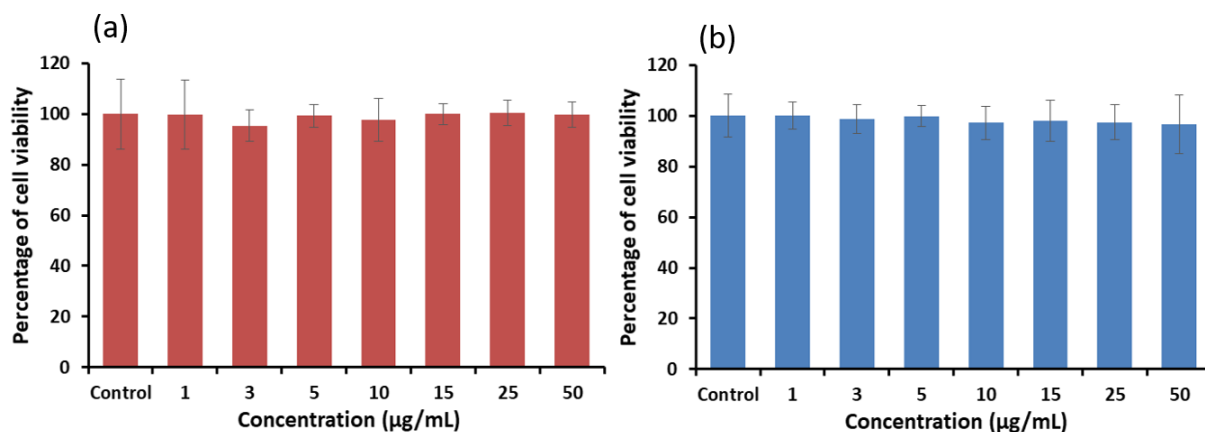
Figure 29. Biocompatibility study of blank liposomes on (a) HGF cells (b) SK-BR-3 cells after 24 h of treatment
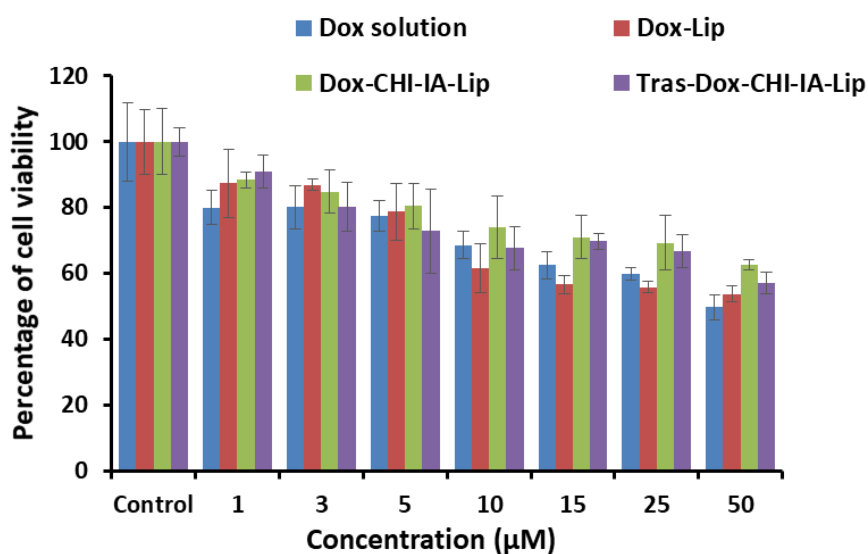
Figure 30. Biocompatibility study of Dox solution, Dox-Lip, Dox-CHI-IA-Lip, and Tras-Dox-CHI-IA-Lip on HGF cells after 24 h of treatment

To assess the cytotoxicity of the liposome formulations, the cellular mitochondrial metabolic activity was measured in SK-BR-3 breast cancer cells after 24 hours of treatment. The percentage of SK-BR-3 cell viability following treatment with liposome formulations is depicted in Figure 31. The IC_{50} value of the Dox solution was found to be 3.71 μM, while Dox-Lip, Dox-CHI-IA-Lip and Tras-Dox-

CHI-IA-Lip exhibited IC50 values of 4.26 μM, 3.53 μM, and 2.05 μM, respectively. These results indicate that Tras-Dox-CHI-IA-Lip exhibited the most potent activity compared to non-targeted liposomes and drug solution. This may be attributed to the synergistic effect of Tras and Dox, resulting in superior cell death compared to formulations without Tras. Additionally, Tras facilitated the localization and attachment of the drug-loaded nanocarrier to the SK-BR-3 cell surface by interacting with specific receptors (HER2) on the cell surface (259). Interestingly, non-targeted Dox-CHI-IA-Lip exhibited a more cytotoxic effect than Dox solution at higher drug concentrations (5-50 μM), suggesting that the drug entrapped in liposomes could be internalized by endocytosis, while hydrophilic free Dox enters cells by passive diffusion (260).
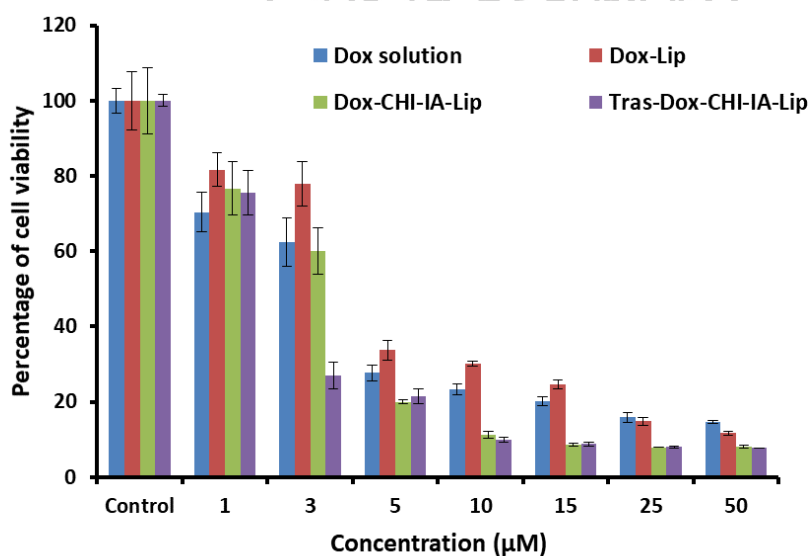
Figure 31. Percentage of SK-BR-3 cell viability (HER2-positive) after 24-h treatment with Dox solution, Dox-Lip, Dox-CHI-IA-Lip, and Tras-Dox-CHI-IA-Lip

4.2.10 Cellular uptake

Flow cytometry analysis was performed to determine the cellular uptake of each liposome formulation by SK-BR-3 cells as presented in Figure 32. Dox-Lip showed the lowest ability to enter the cell compared to the coated liposome. Tras-Dox-CHI-IA-Lip showed higher MFIs at all time points, indicating greater internalization of Dox into the cells. This was attributed to Tras, which targeted and

attached to the HER2 receptor on SK-BR-3 cells, promoting receptor-mediated endocytosis. Interestingly, the non-targeted positively charged Dox-CHI-IA-Lip initially entered the cells at a similar level as the negatively charged Dox-Lip, but showed greater cellular uptake at 4 h. This finding could be due to nonspecific endocytosis and cell adhesion via electrostatic interaction between the negative charge of the cell membrane and the positive charge of CHI-IA (261, 262). The comparison of the cellular uptake indicated that Tras-Dox-CHI-IA-Lip facilitated the entry of the targeted liposome formulation into the cells, which correlated with the potent cytotoxic effect observed. Dox-CHI-IA-Lip also presented a good potency against breast cancer cells due to its cellular adhesion mechanism. These findings supported that the targeted Dox-Lip could provide a powerful anticancer effect on HER2-positive cells.
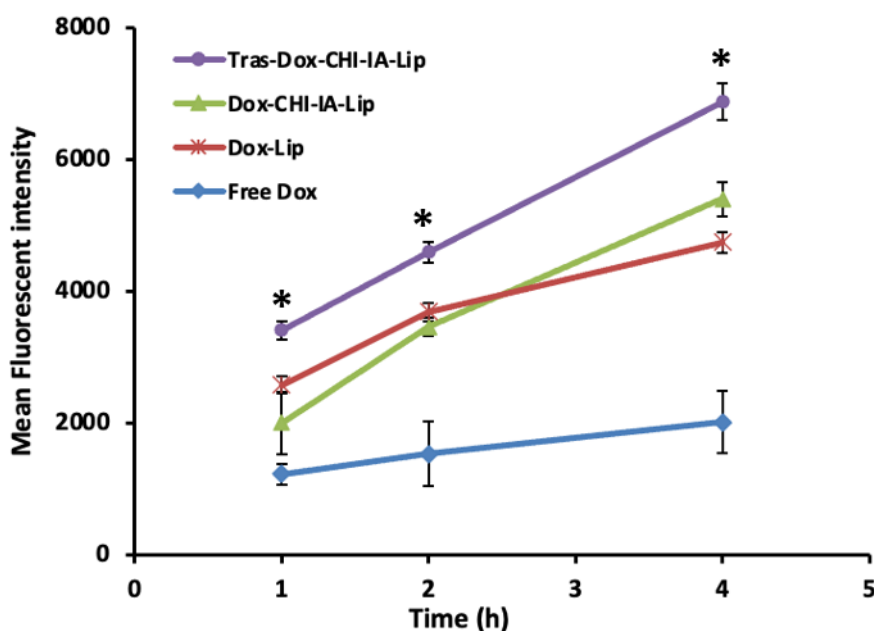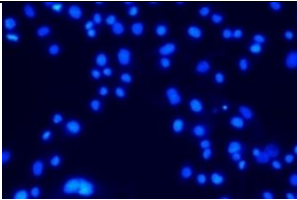
Figure 32. Cellular uptake of Dox solution, Dox-Lip, Dox-CHI-IA-Lip, and Tras-Dox-CHI-IA-Lip by SK-BR-3 cells at different time points, as measured by mean fluorescence intensity (MFI) using flow cytometry. (* Significant difference from Free Dox, Dox-Lip and Dox-CHI-IA Lip, $p < 0.05$)

4.2.11 Cell death assay

The ability to induce apoptosis is a favorable criterion for therapeutic anticancer agents, as it is a safe mechanism that does not induce inflammatory cytokines. Therefore, it is important to examine the pathway of nanocarrier-enhanced cytotoxic effect to confirm the desirability of the increased potency (263). To screen the cell death mechanism of various drug-loaded liposome formulations, Hoechst 33342 and SYTOX™ Green nucleic acid staining were used under an inverted fluorescence microscope. Normally, the apoptotic cells characterized by nuclear condensation, cell shrinkage, DNA cleavage, and plasma membrane budding (264, 265). Hoechst 33342 is a permeable nucleic acid cell dye used to identify nuclear condensation and DNA fragmentation of the nuclei of apoptotic cells. As shown in Table 6, the deep blue color of the nucleus of the HER2-positive SK-BR-3 cells can be observed. The apoptosis cell death pattern of SK-BR-3 cells shows the separation of DNA in the form of highly condensed and fragmented nuclei with brighter blue fluorescence color. The untreated cells and the cells treated with blank liposome formulations appeared oval, with very few nuclei showing bright blue or green fluorescence of dead cells, indicating that most cells were still viable. However, treatment with Dox formulations clearly induced cell death. HER2-positive SK-BR-3 cells treated with Dox-Tras-CHI-IA-Lip demonstrated much more intense bright blue/green fluorescence, confirming the increased dead cells compared to other Dox formulations. These findings indicate that the HER2-positive SK-BR-3 cells were sensitive to the treatments, and the liposome preparations induced cell death through apoptosis.

Table 6. Fluorescence images of SK-BR-3 cells stained with Hoechst 33342 and SYTOX™ Green after 24-h treatment.

	Hoechst 33342	Sytox green
Control		

Blank Liposome

Blank CHI-IA Liposome

Blank Tras-CHI-IA Liposome

Free Dox

Dox Liposome

Dox CHI-IA Liposome

Dox-Tras-CHI-IA Liposome
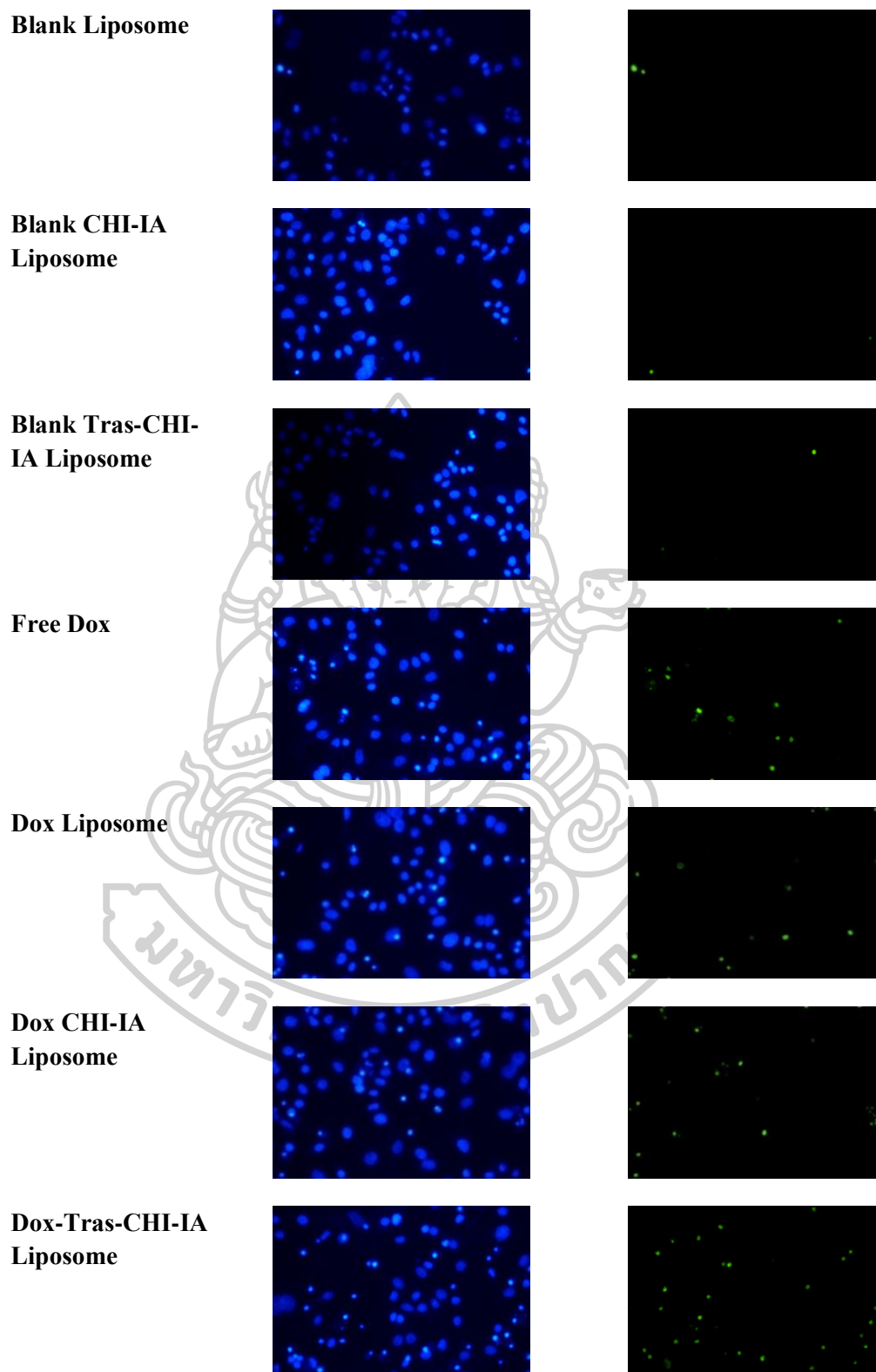
Flow cytometry assay was performed to determine the stages of cell death. The findings are displayed in Figure 33, which shows live cell, apoptotic cells, and necrosis cell after staining with annexin V Alexa Fluor™-647 conjugate and SYTOX™ Green. The untreated cells served as the control. The untreated control, blank liposomes, blank CHI-IA-Lip, and Tras-CHI-IA-Lip demonstrated 85–89% cell viability and negligible late apoptosis death. At an equivalent amount of Dox, the Dox solution induced 42% apoptotic cell death, while Dox-Lip resulted in a similar apoptotic cell death (44%). However, Dox-CHI-IA-Lip significantly increased early and late apoptosis cell death to 52%. Tras-Dox-CHI-IA-Lip, which showed the highest cytotoxic effect in other experiments, demonstrated significantly higher early and late apoptosis SK-BR-3 cell death (69%). This finding confirms Tras not only has a role in specific cell targeting but also enhances the therapeutically prominent cytotoxic activity of Dox by initiating the HER2 cascades. The cytotoxicity studies showed that conjugating Tras with Dox-CHI-IA-Lip effectively improved the anticancer effect against HER2-positive cell line SK-BR-3. This also confirmed that using targeted liposomes through Tras conjugation can enhance the anticancer activity of Dox synergistically when compared to non-targeted liposomes and Dox solution (266, 267).
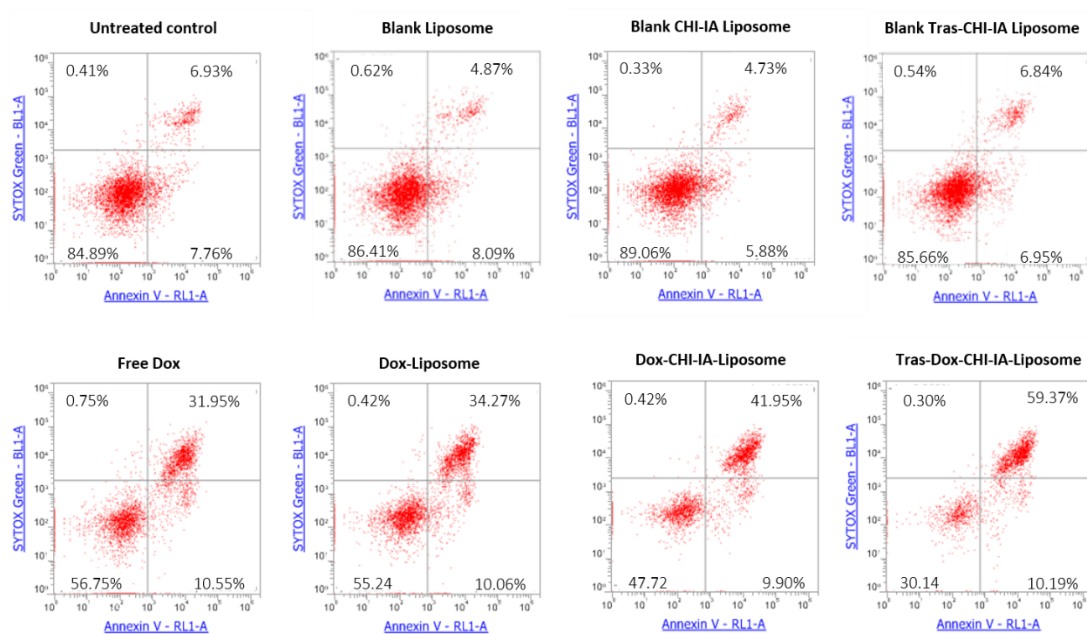
Figure 33. Flow cytometry analysis of SK-BR-3 cells treated with liposome formulations for 24 hours, showing the percentage of live cells (lower left quadrant), early and late apoptotic cells (lower and upper right quadrants, respectively), and necrotic cells (upper left quadrant), as determined by dual staining with annexin V Alexa Fluor™-647 conjugate and SYTOX™ Green.

4.3 Development of Tras-decorated CHI-Mal/Alg-Cys NPs for breast cancer

4.3.1 Synthesis of CHI-Mal

The maleimide group was conjugated onto CHI by coupling 6-maleimidohexanoic acid with CHI with the aid of EDAC and NHS as catalyst. The -COOH groups of 6-maleimidohexanoic acid were activated by these reagents and then reacted with the -NH$_2$ groups of chitosan. The obtained structure of the synthesized polymer were determined by ATR-FTIR and NMR. In the ATR-FTIR spectrum of CHI shown in Figure 34, a broad peak at 3278 cm^{-1} was observed due to the stretching of the -OH group. The bands at 2874 and 1053-1026 cm^{-1} are recognized as the C-H and C-O stretching of the saccharide pyranose ring. The peaks at 1649 and 1588 cm^{-1} were related to amide I and amide II, and these peaks shifted to 1631 and 1531 cm^{-1} after conjugation with maleimide (268). In the spectrum of CHI-Mal, the new peaks at 898 and 695 cm^{-1} were observed, which could be attributed to the vibration of =CH and C-H of the maleimide. The absorption band at 1150 cm^{-1} was due to the asymmetric C-O-C bridge stretching of CHI. The small peak at 1690 cm^{-1} was inherited from the amide of maleimide and corresponded to the C=O stretching (179).

Based on the NMR spectrum shown in Figure 35, CHI exhibited a characteristic peak at 3.1 ppm and peaks at 3.4-3.8 ppm, which are hydrogens attached to the C-2 and C-3 to C-5 of the saccharide ring. The successful conjugation of 6-maleimidohexanoic acid with CHI was confirmed by the appearance of signals at 3.5, 2.3, 2.0, 1.5, and 1.2 ppm, which correspond to the methylene protons of 6-maleimidohexanoic acid. Additionally, the characteristic peak of the maleimide ring was observed as a singlet at 6.8 ppm, indicating the success of the conjugation process (269).
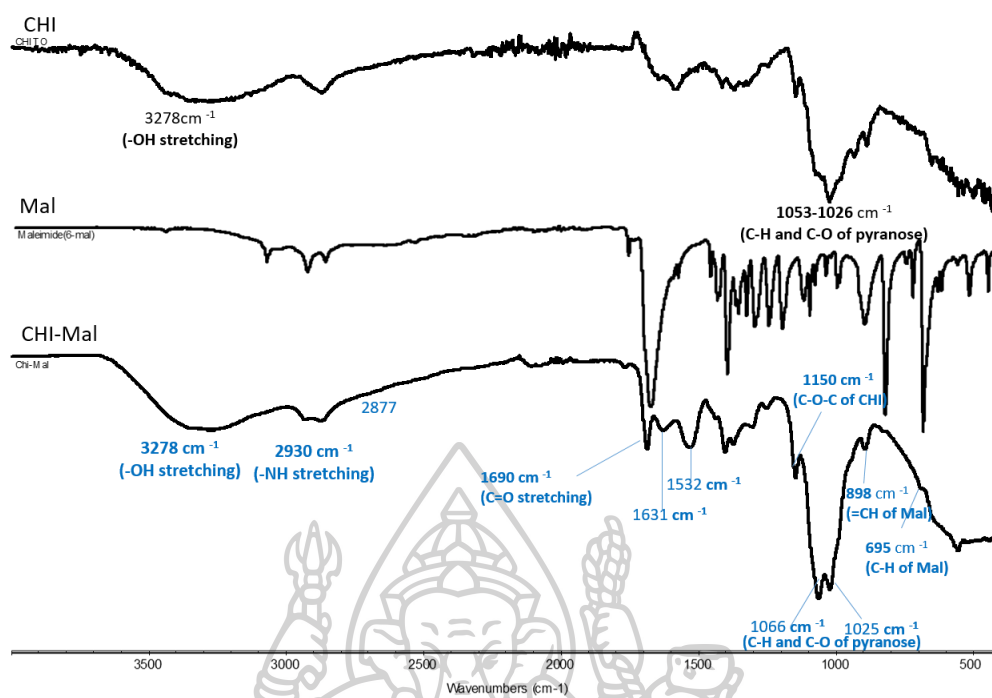
Figure 34. ATR-FTIR spectra of CHI, Mal and CHI-Mal
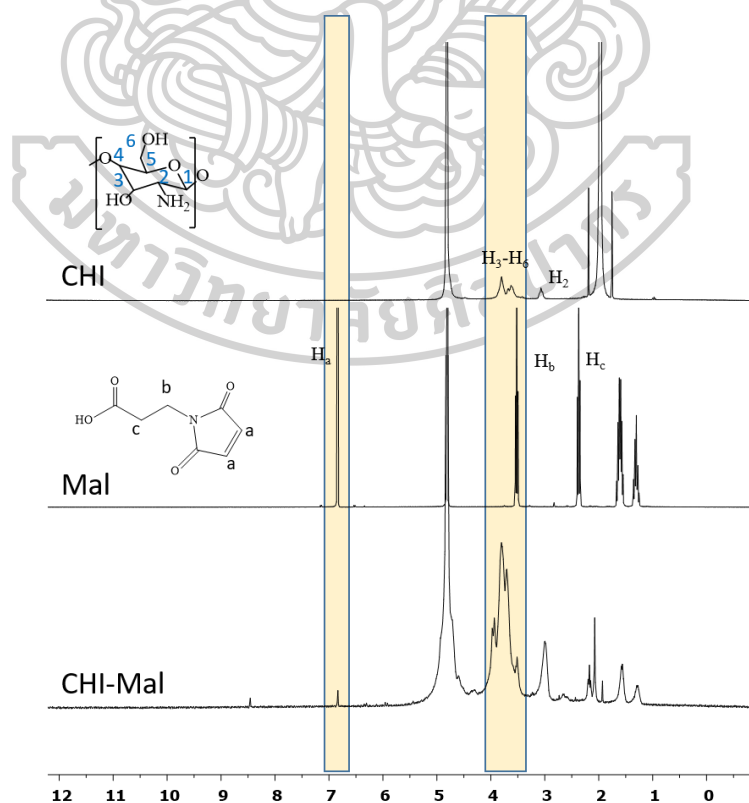
Figure 35. NMR spectra of CHI, Mal and CHI-Mal

4.3.2 Synthesis of alginate-cysteine (Alg-Cys)

Alg-Cys polymer conjugated was achieved by the formation of an amide bond between the NH_2 group of cysteine and the COOH groups of alginate. The ATR-FTIR spectrum of Alg-Cys is shown in Figure 36. The broadband at 3287 cm^{-1} and the small band at 2935 cm^{-1} represent the stretching vibration of O-H and N-H groups (270). The small band at 2767 cm^{-1} could be due to the S-H groups of cysteine. The strong peak at 1597 cm^{-1} may be due to the O-C-O carboxylate and C-OH stretching vibrations. The band at 932 cm^{-1} may be associated with the stretching vibration of the C-O of uronic acid and S-H. Additionally, the band at 882 cm^{-1} may be due to β-manuronic acid (271). The small band at 2767 cm^{-1} may be associated with the stretching vibration of the CH_2 group of cysteine. The small bands at 1291 and 1242 cm^{-1} could be related to the C-CH and O-CH stretching vibrations of the pyranose ring. Moreover, the sharp band at 1407 cm^{-1} may be responsible for the O-C-O, C-OH groups of the pyranose ring. The bands at 1000-1100 cm^{-1}, 1028 and 1080 cm^{-1} related with stretching vibration of C-C, C-H and C-O groups of the pyranose ring of alginate (272, 273).
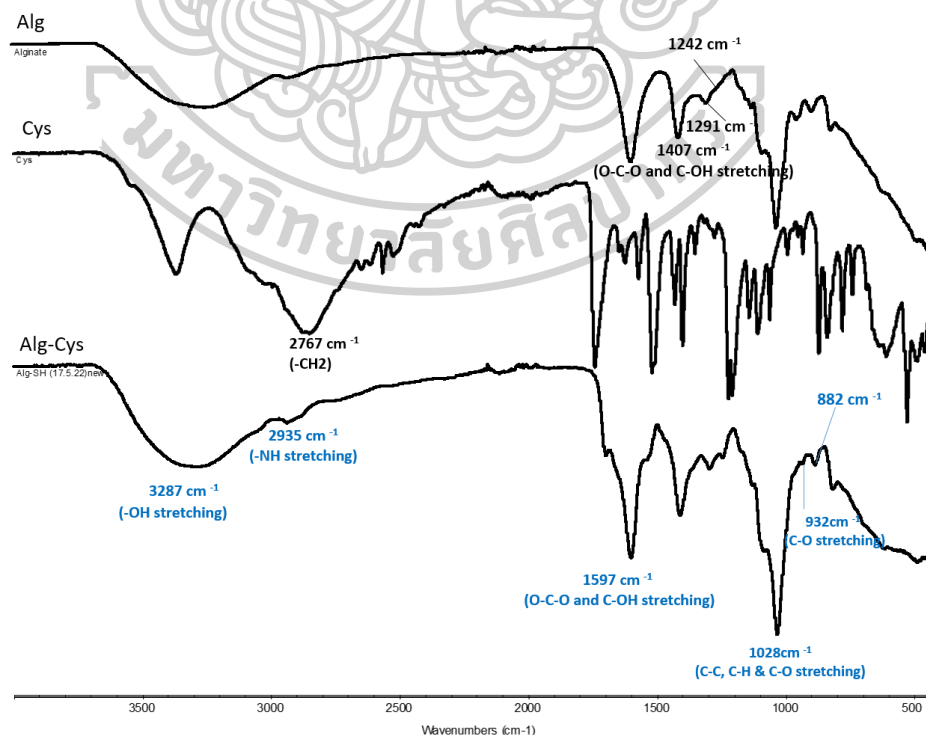
Figure 36. ATR-FTIR spectra of Alg, Cys and Alg-Cys

For the NMR characterization, the signals at 3.7-4.0 ppm were responsible for the carbon atoms contained in the pyranose ring of Alg (269). After reacting with Cys, the C-H of Cys was fused with the carbon of the pyranose ring which was 3.7 and 4.0 ppm. The peaks at 2.8, 3.0, and 3.2 of Alg-Cys are responsible for the proton of the amino acid α-carbon and carbon of the side chain of Cys that was shifted from 3.1 and 3.2 ppm of Cys. The new peak at 1.1 ppm may be responsible for the hydrogen that is attached to sulfide. It was confirmed that Cys was successfully conjugated on the CHI backbone.
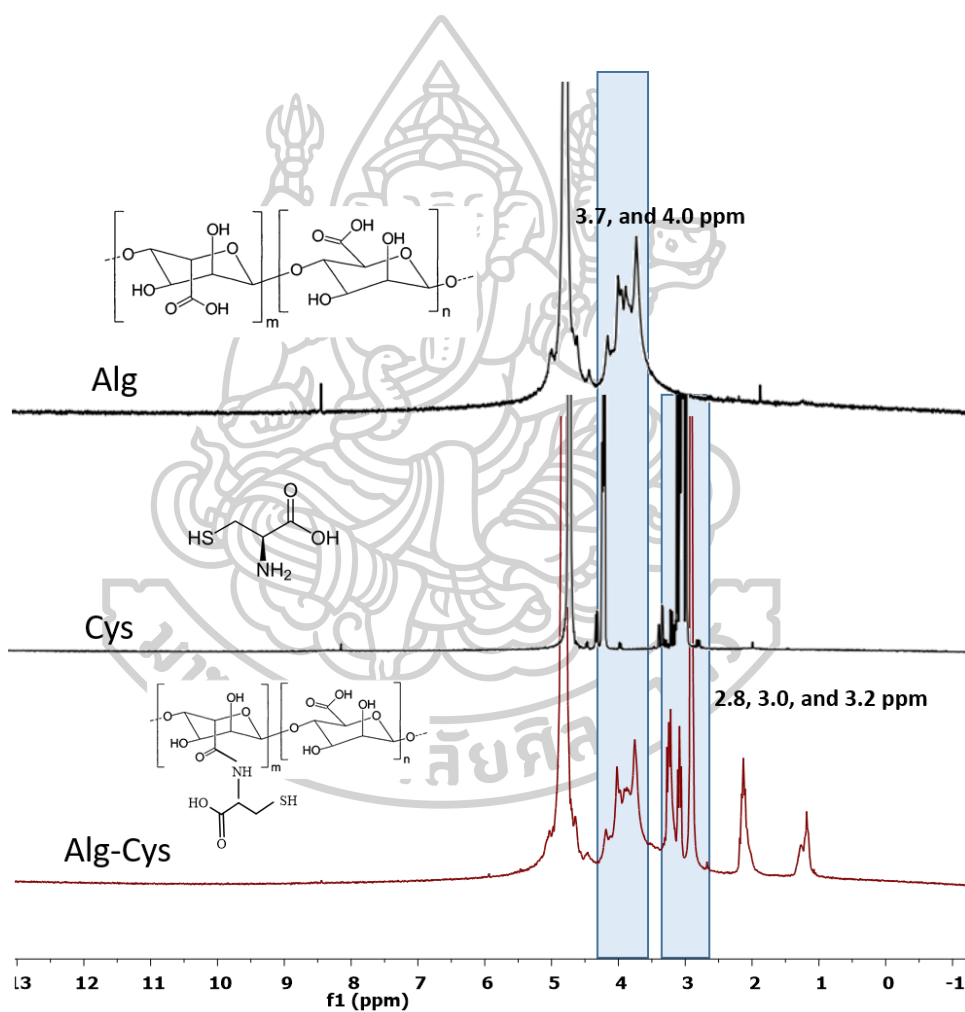
Figure 37. NMR spectra of Alg, Cys and Alg-Cys
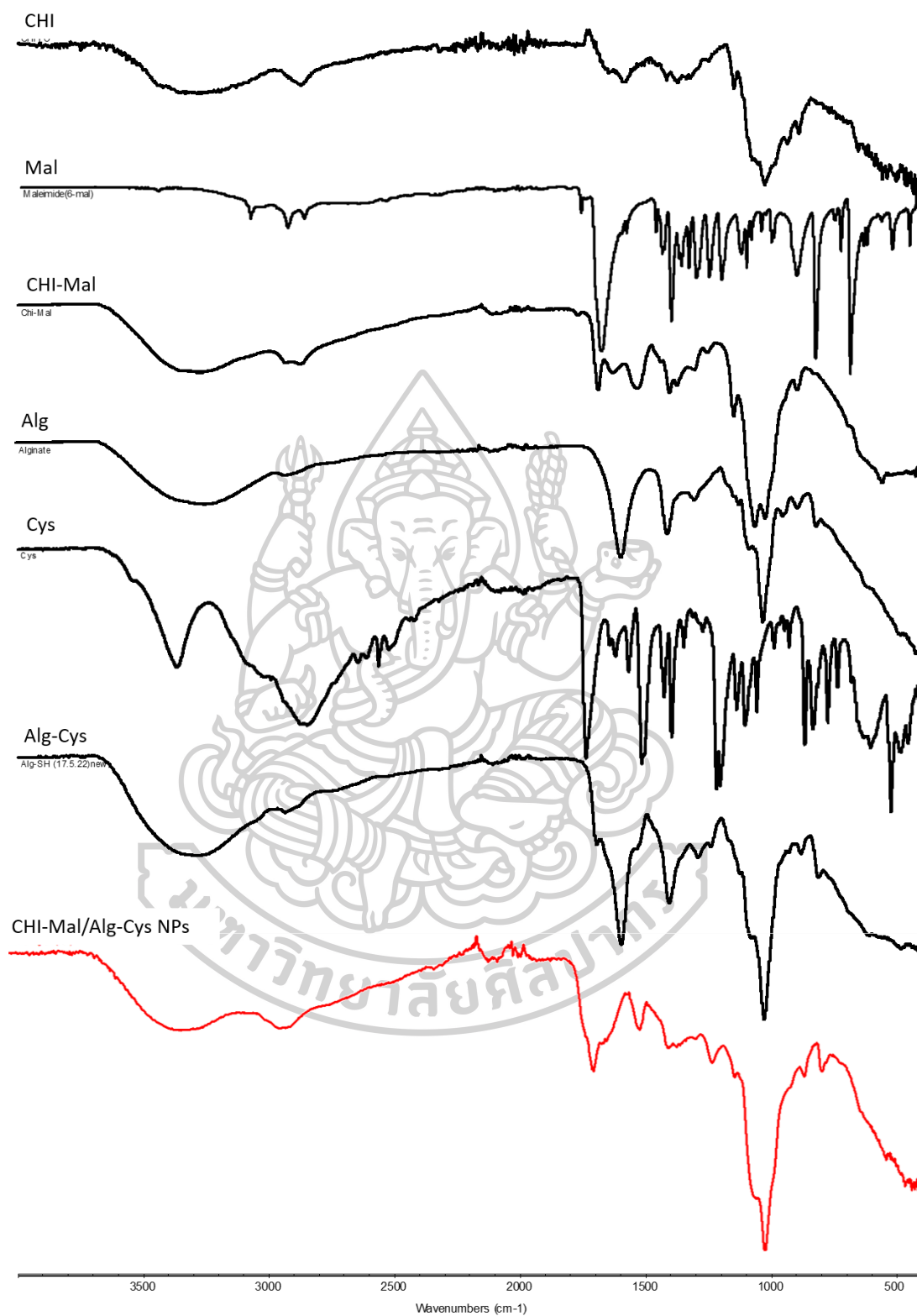
Figure 38. ATR-FTIR spectra of CHI, Mal, CHI-Mal, Alg, Cys, Alg-Cys and CHI-Mal/Alg-Cys NPs

4.3.3 Preparation and characterizations of curcumin-loaded CHI-Mal/Alg-Cys NPs

After reacting the maleimide functional groups of CHI-Mal and thiol on the Alg-Cys by click reaction, CHI-Mal/Alg-Cys NPs were obtained. The thiol-maleimide chemistry has been extensively applied in many biological reactions, such as polymer-polymer conjugation or surface functionalization of polymers. This reaction is carried out site-selective conjugation in an aqueous environment, offering the stability of reaction outcomes and does not produce any significant by-products (274). The size and superficial charge of NPs are critical considerations association with the cellular destruction of tumor cells (275). The characterization of obtained NPs by zeta sizer was shown in Table 7. The NPs show acceptable nano-size (173.7 ± 10.1 nm) with slightly positive zeta potential. This positive charge may be attributed to the excess amine group of CHI after reacting with alginate by ionic interaction. After incorporating the curcumin and conjugating with Tras, the diameter of NPs was increased to 225.6 ± 8.0 and 258.3 ± 3.4 respectively with acceptable PDI values. This increased in size was under satisfactory conditions because a size larger than 300 nm could probably undergo clearance from the blood (276). Alternately, the zeta potential showed slightly negative after conjugating curcumin and Tras. This can be assured in the attachment of Tras which contains amino acids and another reason was the negative charge of curcumin. Also, the electrostatic repulsion of incorporating drug and Tras with the NPs could be an additional reason for negative zeta potential and larger size (277).

Table 7. Mean diameter, PDI and zeta potential of CHI-Mal/Alg-Cys NPs and curcumin loaded Tras conjugated CHI-Mal/Alg-Cys NPs

NPs	Size (nm)	PDI	Zeta potential (mV)
CHI-Mal/Alg-Cys	173.7 ± 10.1	0.24 ± 0.01	+6 ± 0.1
Curcumin-CHI-Mal/Alg-Cys	225.6 ± 8.0	0.40 ± 0.00	-1.4 ± 0.4
Tras-Curcumin-CHI-Mal/Alg-Cys	258.3 ± 3.4	0.25 ± 0.02	-5.3 ± 0.5

4.3.4 Conjugation of the antibody trastuzumab to the CHI-Mal/Alg-Cys NPs

After obtaining the CHI-Mal/Alg-Cys NPs, Tras antibody was introduced directly onto the surface of particles by click chemistry. Thiol-maleimide click chemistry expects to take place by binding through thiol (-SH) groups of antibodies with maleimide of CHI-Mal/Alg-Cys NPs. The reaction was carried out by the N-terminal amino groups of antibodies (278). The content of Tras that attached to NPs was determined by BCA assay and shown in Figure 39. According to the results, 292.0 ± 4.3 µg of Tras was attached to the NPs and 236.6 ± 4.2 µg can be determined on curcumin loaded NPs. Blank NPs were used as control. It seems that the Tras can be attached more to NPs without curcumin. It may be because of the site-specific conjugation of thiol with maleimide on NPs only. Since maleimides have extensively served as a famous focal point of protein bioconjugation chemistry with thiol. They can permit precise modification with cysteine simply and rapidly. Under certain conditions, the consequently formed thioether bond is relatively stable and slowly reversible (249, 279, 280).
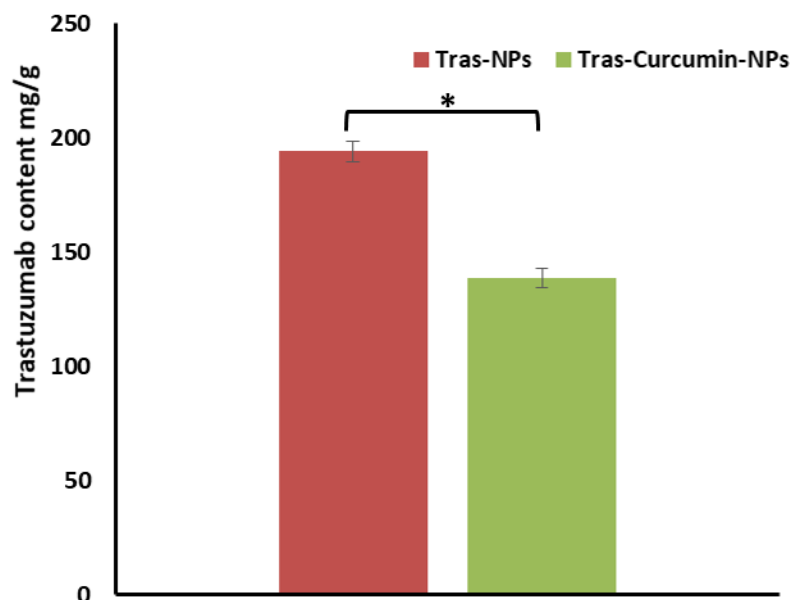
Figure 39. Quantification of Tras content in Tras-NPs and Tras-Curcumin-NPs using the BCA assay. (*Significant difference from Tras-Curcumin-NPs, $p < 0.05$).

4.3.5 Determination of %LE and LC of curcumin-loaded CHI-Mal/Alg-Cys NPs

Effective nanocarriers for breast cancer therapy should have a high drug loading capacity and be able to deliver drugs efficiently (281). In this study, different weight ratios of curcumin were loaded into the CHI-Mal/Alg-Cys NPs during the conjugation of the two polymers by ionic gelation. The loading capacity and efficiency of curcumin were presented in Table 8. The data showed that the curcumin loading capacity increased significantly with an increase in the ratio of curcumin to NPs. However, the loading efficiency decreased as the amount of curcumin was increased. The optimal weight ratio for the highest LC and loading efficiency %LE of NPs was found to be 2:15, with an LE% of 74 ± 3.2. This higher entrapment capacity and efficiency of NPs may be attributed to the incorporation of drugs during the preparation of NPs by ionic gelation rather than adsorption on (282).

Table 8. % LE and LC of curcumin-loaded CHI-Mal/Alg-Cys NPs (* Significant difference from 1:15 and 0.5:15, p < 0.05)

Curcumin:NP	LC (mg/g)	LE (%)
0.5:15	81.9 ± 7.5	92.9 ± 4.4
1:15	117.2 ± 3.9	68.6 ± 10.6
2:15	239.2* ± 18.7	74 ± 3.2

4.3.6 In vitro release study

The release mechanism of curcumin from NPs was determined using the dialysis method in PBS at pH 5.5, which mimics the tumor pH, and pH 7.4, which represents normal physiological conditions. The release profile is presented in Figure 40. The results showed sustained and steady release of curcumin in both pH conditions for up to one week. A burst release of about 13% was observed in both pH conditions at the initial 4 hours due to the release of the vicinity-related drug. At day 4, 48 ± 6.7% and 71 ± 1.3% of curcumin were released at pH 7.4 and 5.5, respectively. On day 7, approximately 57 ± 9.7% of curcumin was released at pH 7.4,

whereas $98 \pm 5.4\%$ was released at pH 5.5. The release of curcumin was faster, sustained, and complete in acidic conditions compared to neutral pH. The extended-release stage observed after the fourth day may be due to the permeation of the surrounding medium into the NPs, leading to the release of the drug (283). The fast and complete release of curcumin in acidic pH was attributed to the protonation of the unreacted amine functional group of CHI and the repulsive force between the positive charges in the acidic environment, leading to more efficient and complete release of curcumin from the swelling NPs (284, 285). Therefore, the release mechanism can be characterized as triphasic behavior, where small burst release occurred initially, followed by steady release through the diffusion of NPs until the fourth day, and finally complete release of the drug at acidic pH responsible for full degradation of NPs (286). In conclusion, the in vitro release behavior of curcumin-NPs was found to be pH-dependent.
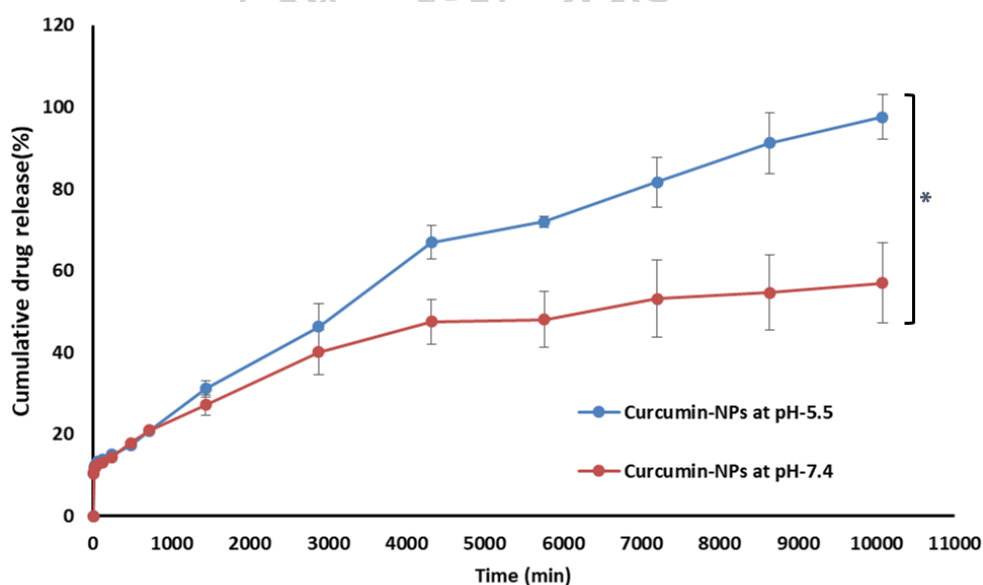
Figure 40. Cumulative release profile of curcumin from nanoparticles (Curcumin-NPs) at pH 5.5 and 7.4. Data points represent the mean $\pm$ standard deviation of three independent experiments. * denotes a significant difference from the release profile at pH 7.4 ($p < 0.05$).

4.3.7 In vitro anticancer activity

The biocompatibility of blank NPs with normal HGF cells and HER2-positive breast cancer cells was evaluated using the colorimetric MTT assay. The cell viability

after a 24-h treatment was presented in Figure 41. In both cell lines, blank NPs exhibited almost no cytotoxicity, with a viability of over 80%, indicating their non-harmful effects on healthy cells. Furthermore, as shown in Figure 42, the viability of HGF cells was over 80% after treatment with various concentrations of curcumin, Curcumin-NPs, and Tras-Curcumin-NPs.
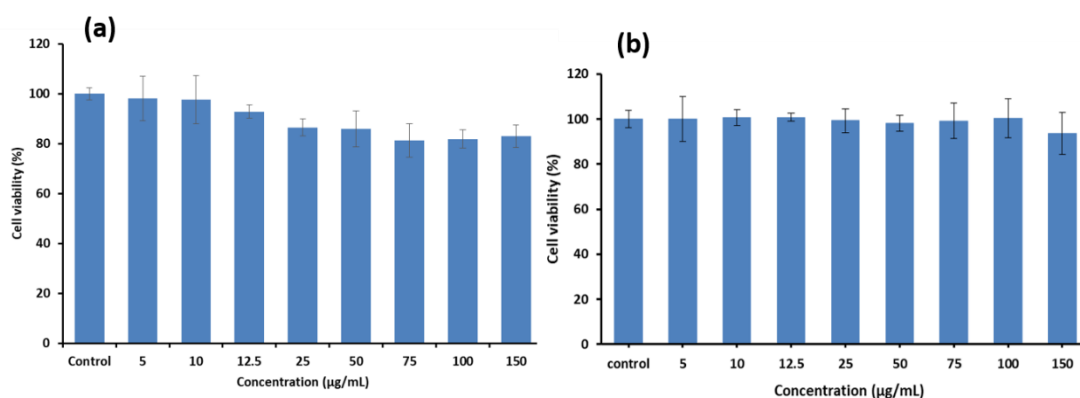
Figure 41. Biocompatibility study of blank NPs on (a) HGF cells and (b) SK-BR-3 cells

However, the viability of SK-BR-3 cells decreased with increasing concentration of free curcumin, Curcumin-NPs and Tras-Curcumin-NPs after one day of incubation. The results are shown in Figure 43. The therapeutic minimum inhibitory concentration (IC50) was determined to be 100 µM, 95.05 µM, and 33.9 µM for free curcumin, Curcumin-NPs, and Tras-Curcumin-NPs, respectively. Thus, the cytotoxicity of Tras-Curcumin-NPs is significantly stronger than that of the free drug and non-targeting NPs. The IC50 value of Curcumin-NPs was slightly higher compared to the free drug. While free curcumin induced cytotoxicity gradually with increasing concentration and terminated the toxic effect after 100 µM concentration due to its hydrophobic nature (287). The Curcumin-NPs showed significant cell-killing capacity at the concentration of 50 µM and onwards. This implied that Curcumin-NPs were internalized into the cells through the endocytosis route, although curcumin diffused into the cells rapidly (288). In contrast to curcumin and Curcumin-NPs, Tras-Curcumin-NPs showed a potent cell proliferation inhibitory effect even at a lower concentration of 12.5 µM compared to free curcumin and

Curcumin-NPs. This was due to the effective targeting of HER2 receptors on the SK-BR-3 cells by the Tras antibody, which facilitated receptor-mediated endocytosis (289). To summarize, in vitro cytotoxicity of curcumin, Curcumin-NPs, and Tras-Curcumin-NPs demonstrated a more prominent cell-killing ability in breast cancer cells compared to normal cells.
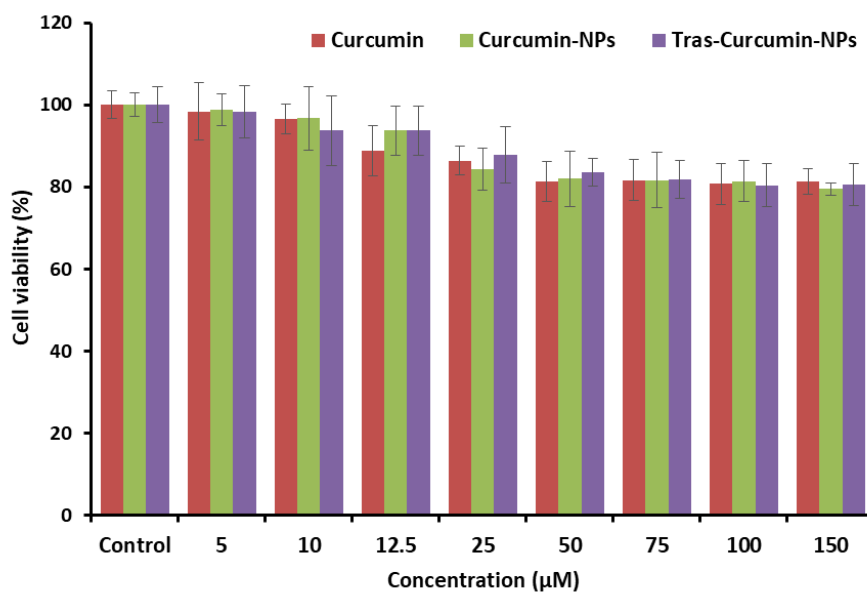
Figure 42. Cytotoxicity study of curcumin, Curcumin-NPs and Tras-Curcumin-NPs on HGF cells
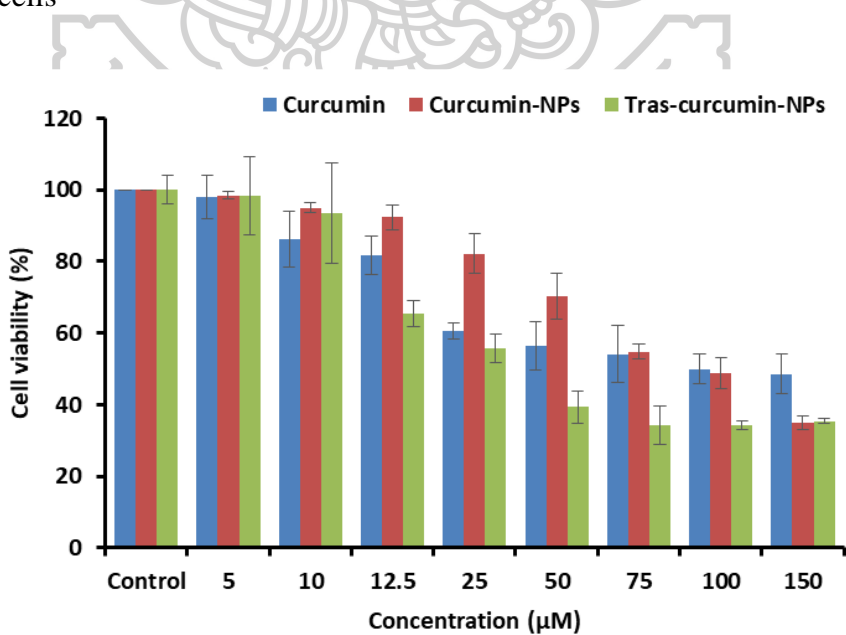
Figure 43. Cytotoxicity study of curcumin, Curcumin-NPs and Tras-Curcumin-NPs on HER2-positive SK-BR-3 cells

4.3.6 Cellular uptake study

The assessment of cellular internalization is a critical factor in evaluating the potential of an anti-cancer drug delivery system. To analyze the accumulation and internalization of NPs inside SK-BR-3 cells, flow cytometry analysis was performed. The mean fluorescence intensity of curcumin, Curcumin-NPs, and Tras-Curcumin-NPs was determined after treating with an equivalent amount of IC50 value of Curcumin, and the results are shown in Figure 44. The data revealed no significant differences in mean intensities for the first 2 h. However, as the exposure time was increased to 4 and 8 h, the uptake of Curcumin-NPs and Tras-Curcumin-NPs into the cells progressively increased, while free curcumin showed inferior fluorescence intensity. These results suggest that extended exposure of Tras-Curcumin-NPs to SK-BR-3 cells enhances cellular internalization and leads to a higher cell-killing profile. This indicates that curcumin was taken up into cells more efficiently and in a time-dependent manner when encapsulated in antibody-conjugated NPs. Furthermore, the targeted antibody on NPs strongly recognizes and interacts with the specific HER2 receptors of SK-BR-3 cells, and the receptor-antibody binding affinity could stabilize the interaction, offering greater therapeutic efficiency via receptor-facilitated transport mechanisms (290, 291).
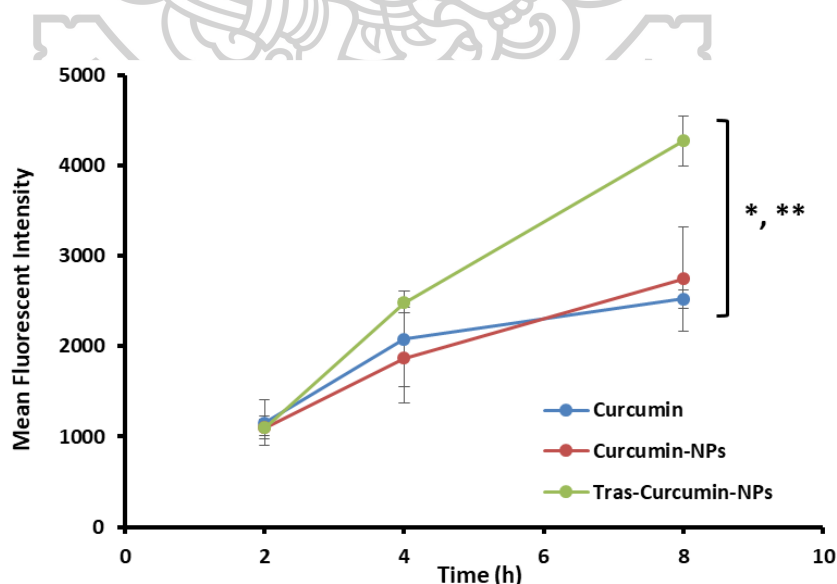
Figure 44. Determination of mean fluorescent intensity of Curcumin on HER2-positive SK-BR-3 cells by flow cytometry analysis (* Significant difference from Curcumin, ** Significant difference from Curcumin-NPs, $p < 0.05$)

4.3.7 Flow cytometry analysis

The study investigated the induction of apoptosis by curcumin, Curcumin-NPs, and Tras-Curcumin-NPs on SK-BR-3 cells using flow cytometry after 24 h of exposure time. The results of the experiment, depicting the proportion of live and apoptotic/necrotic cells, are presented in Figure 45. The data were analyzed and plotted for Annexin V and PI in a dot plot, showing viable cells, early/late apoptotic and necrotic cells in a sequence of annexin V−/PI−, annexin V+/PI−, annexin V+/PI+, and annexin V−/PI+, respectively. The overall early and late apoptotic percentages of free curcumin, Curcumin-NPs, and Tras-Curcumin-NPs were 40.89%, 49.94%, and 58.34% on SK-BR-3 cells, respectively. The formulations of curcumin showed a negligible percentage of necrotic cell death. The untreated control and blank NPs showed 82.76% and 79.48% of live cells fraction with few death portions. The findings indicated that the apoptotic cell death was significantly higher in Tras-Curcumin-NPs compared to free drug. The successful outcome of such an effect could be attributed to the synergistic effects of specific targeting antibodies and excellent modulation of apoptosis by curcumin (292). Additionally, the induced apoptosis by curcumin could also reverse the development of chemo-resistance by cancer cells (293).
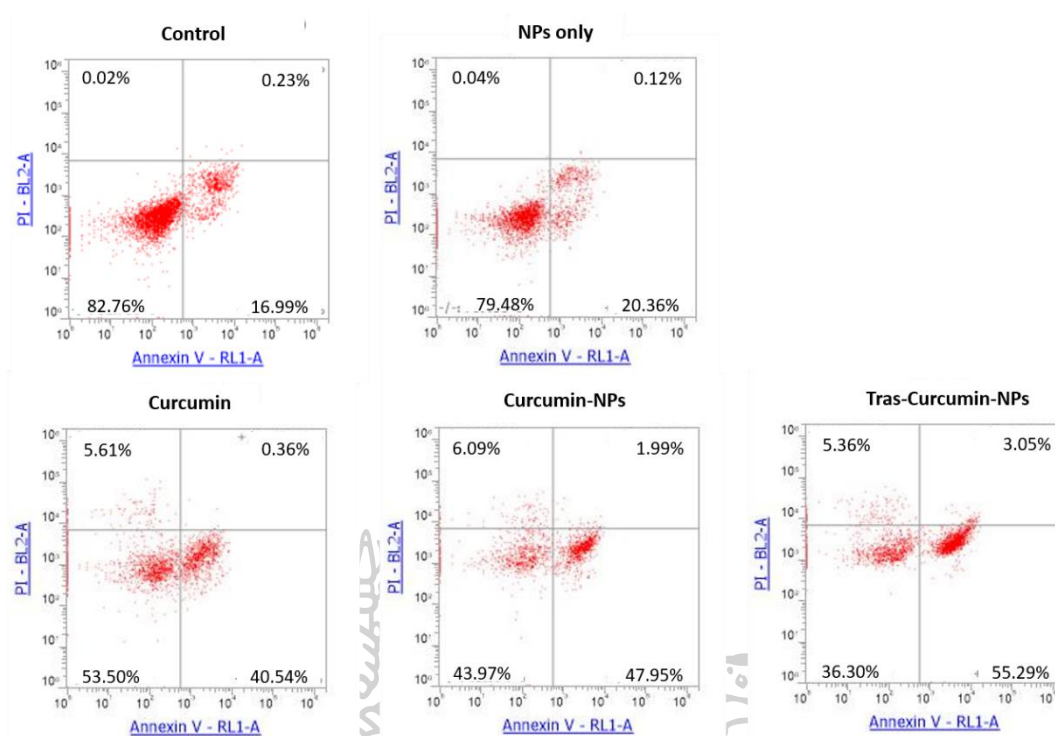
Figure 45. Apoptosis cell death study in HER2-positive SK-BR-3 cells by dual staining with Annexin V/PI after treatment with Curcumin, Curcumin-NPs and Tras-Curcumin-NPs for 24 h

CHAPTER 5

CONCLUSION

Development of Dox-loaded PEGDA/AA NPs for colorectal cancer

PEGDA/AA NPs were developed as a nanocarrier for a chemotherapeutic agent, Dox, to enable delivery into colorectal cancer cells. The NPs were spherical, monodisperse, and had a negative surface charge. Dox was encapsulated onto/into the NPs through electrostatic interactions and adsorption. The release of Dox was sustained once it was incorporated into the PEGDA/AA NPs, with the drug being released more rapidly in an acidic environment than under normal physiological conditions. The polymerized NPs were found to be non-toxic to the intestinal epithelial lining (Caco-2) cells. Additionally, Dox-NPs were capable of killing colorectal cancer cells (HT-29) with an acceptable IC50, and were internalized by the cells and acted against cancer via apoptosis which is a favorable killing mechanism that is non-inflammatory compared to free Dox. In conclusion, the polymerized PEGDA/AA NPs have potential as a carrier for the targeted delivery of chemotherapeutic agents to colon cancer cells, although in vivo experiments are still required to confirm their efficacy.

Development of Dox-loaded Tras-decorated liposomes for breast cancer

To take advantage of HER2 receptor overexpression on breast cancer cells, Tras-CHI-IA Lip was developed for the specific delivery of Dox to the breast tumor site. CHI-IA was successfully synthesized and used for liposome coating using the thin film sonication method. The liposomes were decorated with humanized antibody Tras, resulting in particles with a nano-sized range and a positive surface charge compared to non-coated liposomes. Dox loading was desirable, and the conjugation of Tras on the coated liposome was verified. The release of Dox from Tras-Dox-CHI-IA-Lip occurred in a biphasic profile. Cytotoxicity studies showed that the targeted liposome formulation was able to recognize the HER2 receptor on the breast cancer cells and effectively deliver Dox to the cancer cells. Tras-Dox-CHI-IA-Lip could possibly remain in the blood circulation and be gradually released at the breast tumor

site, where the liposome would be targeted and accumulated in the cancer cells. After reaching breast tumor cells, the active targeting paradigm occurred via ligand-receptor interaction mediated by Tras and HER2 receptors. Therefore, the bioconjugation of Tras on the positively charged CHI-IA-Lip could be an efficient active targeting nanocarrier for Dox delivery to breast cancer cells with HER2 receptor overexpression.

Development of Tras-decorated CHI-Mal/Alg-Cys NPs for breast cancer

The CHI-Mal and Alg-Cys were successfully synthesized and conjugated via the ionic gelation method to fabricate CHI-Mal/Alg-Cys NPs, which can attach to Tras antibody for breast tumor-targeted therapy. During the conjugation process, the hydrophobic herbal product curcumin was efficiently encapsulated into the NPs. Tras could conjugate onto the NPs via thiol-maleimide attachment chemistry. The resulting nano-sized NPs had a slightly positive surface charge, which became slightly negative after incorporating curcumin and Tras. In the tumor environment (pH 5), the hydrophobic curcumin can be gradually and completely released compared to normal physiological conditions. The NPs were biocompatible with normal HGF cells under both conditions, with or without curcumin and targeting antibodies, while the blank NPs were biocompatible with HER2 positive breast cancer SK-BR-3 cells. Targeted Tras-NPs exhibited potent cytotoxicities with lower IC50 values than non-targeted NPs and curcumin. Greater cellular internalization inside the SK-BR-3 cells indicated that the targeted NPs had not only therapeutic potency but also precise targeting efficiency towards breast cancer cells. Flow cytometry analysis demonstrated favorable activity of inducing apoptosis, which correlated with the previous in vitro cytotoxicity study and cellular uptake study. Therefore, the Tras-targeted CHI-Mal/Alg-Cys NPs are a potential drug carrier for breast cancer targeting therapy.

1.   Sarkar FH, Banerjee S, Li Y. Pancreatic cancer: pathogenesis, prevention and treatment. Toxicol Appl Pharmacol. 2007;224(3):326-36.

2.   Siegel RL, Miller KD, Jemal A. Cancer statistics, 2018. CA Cancer J Clin. 2018;68(1):7-30.

3.   Torre LA, Bray F, Siegel RL, Ferlay J, Lortet-Tieulent J, Jemal A. Global cancer statistics, 2012. CA Cancer J Clin. 2015;65(2):87-108.

4.   Conway K, Edmiston SN, Parrish E, Bryant C, Tse CK, Swift-Scanlan T, et al. Breast tumor DNA methylation patterns associated with smoking in the Carolina Breast Cancer Study. Breast Cancer Res Treat. 2017;163(2):349-61.

5.   Licaj I, Jacobsen BK, Selmer RM, Maskarinec G, Weiderpass E, Gram IT. Smoking and risk of ovarian cancer by histological subtypes: an analysis among 300 000 Norwegian women. Br J Cancer. 2017;116(2):270-6.

6.   Vineis P, Stewart BW. How do we judge what causes cancer? the meat controversy. International Journal of Cancer. 2016;138.

7.   Revenco T, Lapouge G, Moers V, Brohée S, Sotiropoulou PA. Low Dose Radiation Causes Skin Cancer in Mice and Has a Differential Effect on Distinct Epidermal Stem Cells. Stem Cells. 2017;35(5):1355-64.

8.   Dumalaon-Canaria JA, Hutchinson AD, Prichard I, Wilson C. What causes breast cancer? A systematic review of causal attributions among breast cancer survivors and how these compare to expert-endorsed risk factors. Cancer Causes Control. 2014;25(7):771-85.

9.   Gupta AP, Pandotra P, Sharma R, Kushwaha M, Gupta S. Chapter 8 - Marine Resource: A Promising Future for Anticancer Drugs. In: Atta ur R, editor. Studies in Natural Products Chemistry. 40: Elsevier; 2013. p. 229-325.

10.   Jemal A, Siegel R, Xu J, Ward E. Cancer statistics, 2010. CA Cancer J Clin. 2010;60(5):277-300.

11.   Peer D, Karp JM, Hong S, Farokhzad OC, Margalit R, Langer R. Nanocarriers as an emerging platform for cancer therapy. Nature Nanotechnology. 2007;2(12):751-60.

12.   Luo Y, Prestwich GD. Cancer-targeted polymeric drugs. Curr Cancer Drug Targets. 2002;2(3):209-26.

13.   Kwon GS. Polymeric micelles for delivery of poorly water-soluble compounds. Crit Rev Ther Drug Carrier Syst. 2003;20(5):357-403.

14.   Pan DC, Krishnan V, Salinas AK, Kim J, Sun T, Ravid S, et al. Hyaluronic acid-doxorubicin nanoparticles for targeted treatment of colorectal cancer. Bioeng Transl Med. 2021;6(1):e10166.

15.   Chandran SP, Natarajan SB, Chandraseharan S, Mohd Shahimi MSB. Nano drug delivery strategy of 5-fluorouracil for the treatment of colorectal cancer. Journal of Cancer Research and Practice. 2017;4(2):45-8.

16.   Gu X, Wei Y, Fan Q, Sun H, Cheng R, Zhong Z, et al. cRGD-decorated biodegradable polytyrosine nanoparticles for robust encapsulation and targeted delivery of doxorubicin to colorectal cancer in vivo. J Control Release. 2019;301:110-8.

17.   Eng C. Toxic effects and their management: daily clinical challenges in the treatment of colorectal cancer. Nat Rev Clin Oncol. 2009;6(4):207-18.

18.   Xiao H, Yan L, Dempsey EMH, Song W, Qi R, Li W, et al. Recent progress in polymer-based platinum drug delivery systems. Prog. Polym. Sci. 2018.

19.   Cisterna BA, Kamaly N, Choi WI, Tavakkoli A, Farokhzad OC, Vilos C. Targeted nanoparticles for colorectal cancer. Nanomedicine (Lond). 2016;11(18):2443-56.

20.   Binaschi M, Bigioni M, Cipollone A, Rossi C, Goso C, Maggi CA, et al. Anthracyclines: selected new developments. Curr Med Chem Anticancer Agents. 2001;1(2):113-30.

21.   Rana DK, Dhar S, Sarkar A, Bhattacharya SC. Dual Intramolecular Hydrogen Bond as a Switch for Inducing Ground and Excited State Intramolecular Double Proton Transfer in Doxorubicin: An Excitation Wavelength Dependence Study. J. Phys. Chem. 2011;115 (33):9169-79.

22.   Xiong S, Xiao GW. Reverting doxorubicin resistance in colon cancer by targeting a key signaling protein, steroid receptor coactivator. Exp Ther Med. 2018;15(4):3751-8.

23.   Cardoso F, Senkus E, Costa A, Papadopoulos E, Aapro M, André F, et al. 4th ESO-ESMO International Consensus Guidelines for Advanced Breast Cancer (ABC 4)†. Ann Oncol. 2018;29(8):1634-57.

24.   Swain SM, Miles D, Kim SB, Im YH, Im SA, Semiglazov V, et al. Pertuzumab, trastuzumab, and docetaxel for HER2-positive metastatic breast cancer (CLEOPATRA): end-of-study results from a double-blind, randomised, placebo-controlled, phase 3 study. Lancet Oncol. 2020;21(4):519-30.

25.   Cardoso F, Kyriakides S, Ohno S, Penault-Llorca F, Poortmans P, Rubio IT, et al. Early breast cancer: ESMO Clinical Practice Guidelines for diagnosis, treatment and follow-up†. Ann Oncol. 2019;30(8):1194-220.

26.   Slamon DJ, Leyland-Jones B, Shak S, Fuchs H, Paton V, Bajamonde A, et al. Use of chemotherapy plus a monoclonal antibody against HER2 for metastatic breast cancer that overexpresses HER2. N Engl J Med. 2001;344(11):783-92.

27.   Li N, Wang Z, Zhang Y, Zhang K, Xie J, Liu Y, et al. Curcumin-loaded redox-responsive mesoporous silica nanoparticles for targeted breast cancer therapy. Artif Cells Nanomed Biotechnol. 2018;46(sup2):921-35.

28.   Sung H, Ferlay J, Siegel RL, Laversanne M, Soerjomataram I, Jemal A, et al. Global Cancer Statistics 2020: GLOBOCAN Estimates of Incidence and Mortality Worldwide for 36 Cancers in 185 Countries. CA Cancer J Clin. 2021;71(3):209-49.

29.   Inotai A, Ágh T, Maris R, Erdősi D, Kovács S, Kaló Z, et al. Systematic review of real-world studies evaluating the impact of medication non-adherence to endocrine therapies on hard clinical endpoints in patients with non-metastatic breast cancer. Cancer Treat Rev. 2021;100:102264.

30.   Terret C, Russo C. Pharmacotherapeutic Management of Breast Cancer in Elderly Patients: The Promise of Novel Agents. Drugs Aging. 2018;35(2):93-115.

31.   Farghadani R, Naidu R. Curcumin as an Enhancer of Therapeutic Efficiency of Chemotherapy Drugs in Breast Cancer. Int J Mol Sci. 2022;23(4).

32.   Farghadani R, Naidu R. Curcumin: Modulator of Key Molecular Signaling Pathways in Hormone-Independent Breast Cancer. Cancers (Basel). 2021;13(14).

33.   Sen GS, Mohanty S, Hossain DMS, Bhattacharyya S, Banerjee S, Chakraborty J, et al. Curcumin enhances the efficacy of chemotherapy by tailoring p65NFκB-p300 cross-talk in favor of p53-p300 in breast cancer. J Biol Chem. 2011;286(49):42232-47.

34.   Bimonte S, Barbieri A, Palma G, Rea D, Luciano A, D'Aiuto M, et al. Dissecting the role of curcumin in tumour growth and angiogenesis in mouse model of human breast cancer. Biomed Res Int. 2015;2015:878134.

35.   Witika BA, Makoni PA, Matafwali SK, Mweetwa LL, Shandele GC, Walker RB. Enhancement of Biological and Pharmacological Properties of an Encapsulated Polyphenol: Curcumin. Molecules (Basel, Switzerland). 2021;26(14):4244.

36.   Song X, Zhang M, Dai E, Luo Y. Molecular targets of curcumin in breast cancer (Review). Mol Med Rep. 2019;19(1):23-9.

37.   Ombredane AS, Silva VRP, Andrade LR, Pinheiro WO, Simonelly M, Oliveira JV, et al. In Vivo Efficacy and Toxicity of Curcumin Nanoparticles in Breast Cancer Treatment: A Systematic Review. Front Oncol. 2021;11:612903.

38.   Gratton SEA, Ropp PA, Pohlhaus PD, Luft JC, Madden VJ, Napier ME, et al. The effect of particle design on cellular internalization pathways. Proc. Natl. Acad. Sci. 2008;105:11613 - 8.

39.   Simone EA, Dziubla TD, Muzykantov VR. Polymeric carriers: role of geometry in drug delivery. Expert Opin Drug Deliv. 2008;5(12):1283-300.

40.   Fulda S, Vucic D. Targeting IAP proteins for therapeutic intervention in cancer. Nature Reviews Drug Discovery. 2012;11(2):109-24.

41.   Abu Lila AS, Ishida T, Kiwada H. Targeting anticancer drugs to tumor vasculature using cationic liposomes. Pharm Res. 2010;27(7):1171-83.

42.   Muro S, Garnacho C, Champion JA, Leferovich J, Gajewski C, Schuchman EH, et al. Control of endothelial targeting and intracellular delivery of therapeutic enzymes by modulating the size and shape of ICAM-1-targeted carriers. Mol Ther. 2008;16(8):1450-8.

43.   Wang Y, Yang T, Wang X, Wang J, Zhang X, Zhang Q. Targeted polymeric micelle system for delivery of combretastatin A4 to tumor vasculature in vitro. Pharm Res. 2010;27(9):1861-8.

44.   Huang Z-r, Hua S-c, Yang Y-l, Fang J-y. Development and evaluation of lipid nanoparticles for camptothecin delivery: a comparison of solid lipid nanoparticles, nanostructured lipid carriers, and lipid emulsion. Acta Pharmacol. Sin. 2008;29(9):1094-102.

45.   Malam Y, Loizidou M, Seifalian AM. Liposomes and nanoparticles: nanosized vehicles for drug delivery in cancer. Trends Pharmacol Sci. 2009;30(11):592-9.

46.   Golden PL, Huwyler J, Pardridge WM. Treatment of Large Solid Tumors in Mice with Daunomycin-Loaded Sterically Stabilized Liposomes. Drug Delivery. 1998;5(3):207-12.

47.   Lammers T, Kiessling F, Hennink WE, Storm G. Drug targeting to tumors: principles, pitfalls and (pre-) clinical progress. J Control Release. 2012;161(2):175-87.

48.   Phillips MA, Gran ML, Peppas NA. Targeted Nanodelivery of Drugs and Diagnostics. Nano Today. 2010;5(2):143-59.

49.   van der Meel R, Vehmeijer LJ, Kok RJ, Storm G, van Gaal EV. Ligand-targeted particulate nanomedicines undergoing clinical evaluation: current status. Adv Drug Deliv Rev. 2013;65(10):1284-98.

50.   Korb ML, Hartman YE, Kovar J, Zinn KR, Bland KI, Rosenthal EL. Use of monoclonal antibody-IRDye800CW bioconjugates in the resection of breast cancer. J Surg Res. 2014;188(1):119-28.

51.   Yameen B, Choi WI, Vilos C, Swami A, Shi J, Farokhzad OC. Insight into nanoparticle cellular uptake and intracellular targeting. J Control Release. 2014;190:485-99.

52.   Yoo J, Park C, Yi G, Lee D, Koo H. Active Targeting Strategies Using Biological Ligands for Nanoparticle Drug Delivery Systems. Cancers (Basel). 2019;11(5).

53.   Jee J-P, Na JH, Lee S, Kim SH, Choi K, Yeo Y, et al. Cancer targeting strategies in nanomedicine: Design and application of chitosan nanoparticles. Curr. Opin. Solid State Mater Sci. 2012;16(6):333-42.

54.   Huo M, Zou A, Yao C, Zhang Y, Zhou J, Wang J, et al. Somatostatin receptor-mediated tumor-targeting drug delivery using octreotide-PEG-deoxycholic acid conjugate-modified N-deoxycholic acid-O, N-hydroxyethylation chitosan micelles. Biomaterials. 2012;33(27):6393-407.

55.   Shargh VH, Hondermarck H, Liang M. Antibody-targeted biodegradable nanoparticles for cancer therapy. Nanomedicine (Lond). 2016;11(1):63-79.

56.   Espelin CW, Leonard SC, Geretti E, Wickham TJ, Hendriks BS. Dual HER2 Targeting with Trastuzumab and Liposomal-Encapsulated Doxorubicin (MM-302) Demonstrates Synergistic Antitumor Activity in Breast and Gastric Cancer. Cancer Res. 2016;76(6):1517-27.

57.   Gennari A, Pronzato P. New understanding of the role of anthracyclines in early-stage breast cancer: patient selection considerations. Clin Breast Cancer. 2008;8 Suppl 4:S179-83.

58.   Zahmatkeshan M, Gheybi F, Rezayat SM, Jaafari MR. Improved drug delivery and therapeutic efficacy of PEgylated liposomal doxorubicin by targeting anti-HER2 peptide in murine breast tumor model. Eur J Pharm Sci. 2016;86:125-35.

59.   Su W, Wang H, Wang S, Liao Z, Kang S, Peng Y, et al. PEG/RGD-modified magnetic polymeric liposomes for controlled drug release and tumor cell targeting. Int J Pharm. 2012;426(1-2):170-81.

60.   Kumar D, Sharma-Walia N, Kapoor S, Tandon S. Antibody-Targeted Nanoparticles for Cancer Treatment. In: Saxena SK, Khurana SMP, editors. NanoBioMedicine. Singapore: Springer Singapore; 2020. p. 35-65.

61.   Ghaz-Jahanian MA, Abbaspour-Aghdam F, Anarjan N, Berenjian A, Jafarizadeh-Malmiri H. Application of chitosan-based nanocarriers in tumor-targeted drug delivery. Mol Biotechnol. 2015;57(3):201-18.

62.   Diessner J, Bruttel V, Becker K, Pawlik M, Stein R, Häusler S, et al. Targeting breast cancer stem cells with HER2-specific antibodies and natural killer cells. Am J Cancer Res. 2013;3(2):211-20.

63.   Rao JP, Geckeler KE. Polymer nanoparticles: Preparation techniques and size-control parameters. Prog. Polym. Sci. 2011;36(7):887-913.

64.   Winawer SJ. Natural history of colorectal cancer. Am. J. Med. 1999;106(1, Supplement 1):3-6.

65.   Sehgal R, Sheahan K, O'Connell PR, Hanly AM, Martin ST, Winter DC. Lynch syndrome: an updated review. Genes (Basel). 2014;5(3):497-507.

66.   Jess T, Gamborg M, Matzen P, Munkholm P, Sørensen TI. Increased risk of intestinal cancer in Crohn's disease: a meta-analysis of population-based cohort studies. Am J Gastroenterol. 2005;100(12):2724-9.

67.   Munkholm P. Review article: the incidence and prevalence of colorectal cancer in inflammatory bowel disease. Aliment Pharmacol Ther. 2003;18 Suppl 2:1-5.

68.   Eaden JA, Abrams KR, Mayberry JF. The risk of colorectal cancer in ulcerative colitis: a meta-analysis. Gut. 2001;48(4):526-35.

69.   Cheah PY. Hypotheses for the etiology of colorectal cancer--an overview. Nutr Cancer. 1990;14(1):5-13.

70.   Verma R, Bowen RL, Slater SE, Mihaimeed F, Jones JL. Pathological and epidemiological factors associated with advanced stage at diagnosis of breast cancer. Br Med Bull. 2012;103(1):129-45.

71.   Alkabban FM, Ferguson T. Breast Cancer. StatPearls. Treasure Island (FL): StatPearls PublishingCopyright © 2022, StatPearls Publishing LLC.; 2022.

72.   DeSantis C, Ma J, Bryan L, Jemal A. Breast cancer statistics, 2013. CA Cancer J Clin. 2014;64(1):52-62.

73.   Hortobagyi GN, de la Garza Salazar J, Pritchard K, Amadori D, Haidinger R, Hudis CA, et al. The global breast cancer burden: variations in epidemiology and survival. Clin Breast Cancer. 2005;6(5):391-401.

74.   Anderson WF, Chatterjee N, Ershler WB, Brawley OW. Estrogen receptor breast cancer phenotypes in the Surveillance, Epidemiology, and End Results database. Breast Cancer Res Treat. 2002;76(1):27-36.

75.   Perou CM, Sørlie T, Eisen MB, van de Rijn M, Jeffrey SS, Rees CA, et al. Molecular portraits of human breast tumours. Nature. 2000;406(6797):747-52.

76.   Hudis CA. Trastuzumab--mechanism of action and use in clinical practice. N Engl J Med. 2007;357(1):39-51.

77.   Chew HK. Adjuvant therapy for breast cancer: who should get what? West J Med. 2001;174(4):284-7.

78.   de Matteis A, Nuzzo F, D'Aiuto G, Labonia V, Landi G, Rossi E, et al. Docetaxel plus epidoxorubicin as neoadjuvant treatment in patients with large operable or locally advanced carcinoma of the breast: a single-center, phase II study. Cancer. 2002;94(4):895-901.

79.   Fisusi FA, Akala EO. Drug Combinations in Breast Cancer Therapy. Pharm Nanotechnol. 2019;7(1):3-23.

80.   Brahmachari G. Chapter 1 - Discovery and Development of Anti-Breast Cancer Agents From Natural Products: An Overview. In: Brahmachari G, editor. Discovery and Development of Anti-Breast Cancer Agents from Natural Products: Elsevier; 2021. p. 1-6.

81.   Di Marco A, Cassinelli G, Arcamone F. The discovery of daunorubicin. Cancer Treat Rep. 1981;65 Suppl 4:3-8.

82.   Verma AK, Leekha A, Kumar V, Moin I, Kumar S. Biodistribution and In-vivo Efficacy of Doxorubicin Loaded Chitosan Nanoparticles in Ehrlich Ascites Carcinoma (EAC) Bearing Balb/c Mice. J.Nanomed. Nanotechnol. 2018;09:1-6.

83.   Octavia Y, Tocchetti CG, Gabrielson KL, Janssens S, Crijns HJ, Moens AL. Doxorubicin-induced cardiomyopathy: from molecular mechanisms to therapeutic strategies. J Mol Cell Cardiol. 2012;52(6):1213-25.

84.   Tarvirdipour S, Vasheghani-Farahani E, Soleimani M, Bardania H. Functionalized magnetic dextran-spermine nanocarriers for targeted delivery of doxorubicin to breast cancer cells. Int J Pharm. 2016;501(1-2):331-41.

85.   Gewirtz DA. A critical evaluation of the mechanisms of action proposed for the antitumor effects of the anthracycline antibiotics adriamycin and daunorubicin. Biochem Pharmacol. 1999;57(7):727-41.

86.   Doroshow JH. Role of hydrogen peroxide and hydroxyl radical formation in the killing of Ehrlich tumor cells by anticancer quinones. Proc Natl Acad Sci U S A. 1986;83(12):4514-8.

87.   Carvalho C, Santos RX, Cardoso S, Correia S, Oliveira PJ, Santos MS, et al. Doxorubicin: the good, the bad and the ugly effect. Curr Med Chem. 2009;16(25):3267-85.

88.   Heidelberger C, Chaudhuri NK, Danneberg P, Mooren D, Griesbach L, Duschinsky R, et al. Fluorinated pyrimidines, a new class of tumour-inhibitory compounds. Nature. 1957;179(4561):663-6.

89.   Hurwitz H, Fehrenbacher L, Novotny W, Cartwright T, Hainsworth J, Heim W, et al. Bevacizumab plus irinotecan, fluorouracil, and leucovorin for metastatic colorectal cancer. N Engl J Med. 2004;350(23):2335-42.

90.   Cunningham D, Humblet Y, Siena S, Khayat D, Bleiberg H, Santoro A, et al. Cetuximab monotherapy and cetuximab plus irinotecan in irinotecan-refractory metastatic colorectal cancer. N Engl J Med. 2004;351(4):337-45.

91.   Peters GJ, van der Wilt CL, van Groeningen CJ, Smid K, Meijer S, Pinedo HM. Thymidylate synthase inhibition after administration of fluorouracil with or without leucovorin in colon cancer patients: implications for treatment with fluorouracil. J Clin Oncol. 1994;12(10):2035-42.

92.   Silverstein RA, González de Valdivia E, Visa N. The incorporation of 5-fluorouracil into RNA affects the ribonucleolytic activity of the exosome subunit Rrp6. Mol Cancer Res. 2011;9(3):332-40.

93.   Longley DB, Harkin DP, Johnston PG. 5-fluorouracil: mechanisms of action and clinical strategies. Nat Rev Cancer. 2003;3(5):330-8.

94.   Wani MC, Taylor HL, Wall ME, Coggon P, McPhail AT. Plant antitumor agents. VI. The isolation and structure of taxol, a novel antileukemic and antitumor agent from Taxus brevifolia. J Am Chem Soc. 1971;93(9):2325-7.

95.   Menzin AW, King SA, Aikins JK, Mikuta JJ, Rubin SC. Taxol (paclitaxel) was approved by FDA for the treatment of patients with recurrent ovarian cancer. Gynecol Oncol. 1994;54(1):103.

96.   Wang K, Zhu C, He Y, Zhang Z, Zhou W, Muhammad N, et al. Restraining Cancer Cells by Dual Metabolic Inhibition with a Mitochondrion-Targeted Platinum(II) Complex. Angew Chem Int Ed Engl. 2019;58(14):4638-43.

97.   Qi L, Luo Q, Zhang Y, Jia F, Zhao Y, Wang F. Advances in Toxicological Research of the Anticancer Drug Cisplatin. Chem Res Toxicol. 2019;32(8):1469-86.

98.   García Sar D, Montes-Bayón M, Blanco González E, Sierra Zapico LM, Sanz-Medel A. Reduction of cisplatin-induced nephrotoxicity in vivo by selenomethionine: the effect on cisplatin-DNA adducts. Chem Res Toxicol. 2011;24(6):896-904.

99.   Alderden RA, Hall MD, Hambley TW. The Discovery and Development of Cisplatin. J. Chem. Educ. 2006;83(5):728.

100.   Hu D, Yang C, Lok CN, Xing F, Lee PY, Fung YME, et al. An Antitumor Bis(N-Heterocyclic Carbene)Platinum(II) Complex That Engages Asparagine Synthetase as an Anticancer Target. Angew Chem Int Ed Engl. 2019;58(32):10914-8.

101.   Yimit A, Adebali O, Sancar A, Jiang Y. Differential damage and repair of DNA-adducts induced by anti-cancer drug cisplatin across mouse organs. Nat Commun. 2019;10(1):309.

102.   Huguenin P, Beer KT, Allal A, Rufibach K, Friedli C, Davis JB, et al. Concomitant cisplatin significantly improves locoregional control in advanced head and neck cancers treated with hyperfractionated radiotherapy. J Clin Oncol. 2004;22(23):4665-73.

103.   Alas M, Saghaeidehkordi A, Kaur K. Peptide-Drug Conjugates with Different Linkers for Cancer Therapy. J Med Chem. 2021;64(1):216-32.

104.   Chen Q, Yang Y, Lin X, Ma W, Chen G, Li W, et al. Platinum(iv) prodrugs with long lipid chains for drug delivery and overcoming cisplatin resistance. Chem Commun (Camb). 2018;54(42):5369-72.

105.   Palchoudhury S, Xu Y, Rushdi A, Bao Y. DNA Interaction of Pt-Attached Iron Oxide Nanoparticles. IEEE Trans. Magn. 2013;49:373-6.

106.   Gandioso A, Shaili E, Massaguer A, Artigas G, González-Cantó A, Woods JA, et al. An integrin-targeted photoactivatable Pt(iv) complex as a selective anticancer pro-drug: synthesis and photoactivation studies. Chem. Commun. 2015;51(44):9169-72.

107.   Kenny RG, Marmion CJ. Toward Multi-Targeted Platinum and Ruthenium Drugs-A New Paradigm in Cancer Drug Treatment Regimens? Chem Rev. 2019;119(2):1058-137.

108.   Browning RJ, Reardon PJT, Parhizkar M, Pedley RB, Edirisinghe M, Knowles JC, et al. Drug Delivery Strategies for Platinum-Based Chemotherapy. ACS Nano. 2017;11(9):8560-78.

109.   Huang X, Li Z, Yu Z, Deng X, Xin Y. Recent Advances in the Synthesis, Properties, and Biological Applications of Platinum Nanoclusters. J. Nanomater. 2019;2019:6248725.

110.   Nagahama K, Utsumi T, Kumano T, Maekawa S, Oyama N, Kawakami J. Discovery of a new function of curcumin which enhances its anticancer therapeutic potency. Sci. Rep. 2016;6(1):30962.

111.   Alibeiki F, Jafari N, Karimi M, Peeri Dogaheh H. Potent anti-cancer effects of less polar Curcumin analogues on gastric adenocarcinoma and esophageal squamous cell carcinoma cells. Sci Rep. 2017;7(1):2559.

112.   Goel A, Kunnumakkara AB, Aggarwal BB. Curcumin as "Curecumin": from kitchen to clinic. Biochem Pharmacol. 2008;75(4):787-809.

113.   Kunnumakkara AB, Bordoloi D, Padmavathi G, Monisha J, Roy NK, Prasad S, et al. Curcumin, the golden nutraceutical: multitargeting for multiple chronic diseases. Br J Pharmacol. 2017;174(11):1325-48.

114.   Anand P, Sundaram C, Jhurani S, Kunnumakkara AB, Aggarwal BB. Curcumin and cancer: an "old-age" disease with an "age-old" solution. Cancer Lett. 2008;267(1):133-64.

115.   Shen L, Liu CC, An CY, Ji HF. How does curcumin work with poor bioavailability? Clues from experimental and theoretical studies. Sci Rep. 2016;6:20872.

116.   Ohtsu H, Xiao Z, Ishida J, Nagai M, Wang HK, Itokawa H, et al. Antitumor agents. 217. Curcumin analogues as novel androgen receptor antagonists with potential as anti-prostate cancer agents. J Med Chem. 2002;45(23):5037-42.

117.   Lin TH, Izumi K, Lee SO, Lin WJ, Yeh S, Chang C. Anti-androgen receptor ASC-J9 versus anti-androgens MDV3100 (Enzalutamide) or Casodex (Bicalutamide) leads to opposite effects on prostate cancer metastasis via differential modulation of macrophage infiltration and STAT3-CCL2 signaling. Cell Death Dis. 2013;4(8):e764.

118.   Verderio P, Pandolfi L, Mazzucchelli S, Marinozzi MR, Vanna R, Gramatica F, et al. Antiproliferative effect of ASC-J9 delivered by PLGA nanoparticles against estrogen-dependent breast cancer cells. Mol Pharm. 2014;11(8):2864-75.

119.   Davis ME, Chen ZG, Shin DM. Nanoparticle therapeutics: an emerging treatment modality for cancer. Nat Rev Drug Discov. 2008;7(9):771-82.

120.   Giordano KF, Jatoi A. The cancer anorexia/weight loss syndrome: therapeutic challenges. Curr Oncol Rep. 2005;7(4):271-6.

121.   Torchilin VP. Drug targeting. Eur J Pharm Sci. 2000;11 Suppl 2:S81-91.

122.   Parveen S, Sahoo SK. Polymeric nanoparticles for cancer therapy. J Drug Target. 2008;16(2):108-23.

123.   Attia MF, Anton N, Wallyn J, Omran Z, Vandamme TF. An overview of active and passive targeting strategies to improve the nanocarriers efficiency to tumour sites. J Pharm Pharmacol. 2019;71(8):1185-98.

124.   Morales-Cruz M, Delgado Y, Castillo B, Figueroa CM, Molina AM, Torres A, et al. Smart Targeting To Improve Cancer Therapeutics. Drug Des Devel Ther. 2019;13:3753-72.

125.   Gu FX, Karnik R, Wang AZ, Alexis F, Levy-Nissenbaum E, Hong S, et al. Targeted nanoparticles for cancer therapy. Nano Today. 2007;2(3):14-21.

126.   Torchilin VP. Passive and active drug targeting: drug delivery to tumors as an example. Handb Exp Pharmacol. 2010(197):3-53.

127.   Torchilin V. Tumor delivery of macromolecular drugs based on the EPR effect. Adv Drug Deliv Rev. 2011;63(3):131-5.

128.   Honary S, Zahir F. Effect of Zeta Potential on the Properties of Nano-Drug Delivery Systems - A Review (Part 2). Trop. J. Pharm Res. 2013;12:255-64.

129.   Barenholz Y. Doxil®--the first FDA-approved nano-drug: lessons learned. J Control Release. 2012;160(2):117-34.

130.   Leserman LD, Barbet J, Kourilsky F, Weinstein JN. Targeting to cells of fluorescent liposomes covalently coupled with monoclonal antibody or protein A. Nature. 1980;288(5791):602-4.

131.   Rosenblum D, Joshi N, Tao W, Karp JM, Peer D. Progress and challenges towards targeted delivery of cancer therapeutics. Nat. Commun. 2018;9(1):1410.

132.   Deckert PM. Current constructs and targets in clinical development for antibody-based cancer therapy. Curr Drug Targets. 2009;10(2):158-75.

133.   Solomon M, Liu Y, Berezin MY, Achilefu S. Optical imaging in cancer research: basic principles, tumor detection, and therapeutic monitoring. Med Princ Pract. 2011;20(5):397-415.

134.   Raza A, Rasheed T, Nabeel F, Hayat U, Bilal M, Iqbal HMN. Endogenous and Exogenous Stimuli-Responsive Drug Delivery Systems for Programmed Site-Specific Release. Molecules. 2019;24(6).

135.   Mura S, Nicolas J, Couvreur P. Stimuli-responsive nanocarriers for drug delivery. Nat Mater. 2013;12(11):991-1003.

136.   Manchun S, Dass CR, Sriamornsak P. Targeted therapy for cancer using pH-responsive nanocarrier systems. Life Sci. 2012;90(11-12):381-7.

137.   Liu Y, Wang W, Yang J, Zhou C, Sun J. pH-sensitive polymeric micelles triggered drug release for extracellular and intracellular drug targeting delivery. Asian J. Pharm. 2013;8(3):159-67.

138.   Illum L. Nanoparticulate systems for nasal delivery of drugs: a real improvement over simple systems? J Pharm Sci. 2007;96(3):473-83.

139. Gratton SEA, Ropp PA, Pohlhaus PD, Luft JC, Madden VJ, Napier ME, et al. The effect of particle design on cellular internalization pathways. Proc. Natl. Acad. Sci. U.S.A. 2008;105(33):11613-8.

140. Larina IV, Evers BM, Ashitkov TV, Bartels C, Larin KV, Esenaliev RO. Enhancement of drug delivery in tumors by using interaction of nanoparticles with ultrasound radiation. Technol Cancer Res Treat. 2005;4(2):217-26.

141. Cho K, Wang X, Nie S, Chen ZG, Shin DM. Therapeutic nanoparticles for drug delivery in cancer. Clin Cancer Res. 2008;14(5):1310-6.

142. Jain RK. Transport of molecules in the tumor interstitium: a review. Cancer Res. 1987;47(12):3039-51.

143. Wilson B, Samanta MK, Santhi K, Kumar KP, Ramasamy M, Suresh B. Chitosan nanoparticles as a new delivery system for the anti-Alzheimer drug tacrine. Nanomedicine. 2010;6(1):144-52.

144. Lakshmanan V-K, Snima KS, Bumgardner JD, Nair SV, Jayakumar R. Chitosan-Based Nanoparticles in Cancer Therapy. In: Jayakumar R, Prabaharan M, Muzzarelli RAA, editors. Chitosan for Biomaterials I. Berlin, Heidelberg: Springer Berlin Heidelberg; 2011. p. 55-91.

145. Liu Z, Jiao Y, Wang Y, Zhou C, Zhang Z. Polysaccharides-based nanoparticles as drug delivery systems. Adv Drug Deliv Rev. 2008;60(15):1650-62.

146. Rejinold NS, Sreerekha PR, Chennazhi KP, Nair SV, Jayakumar R. Biocompatible, biodegradable and thermo-sensitive chitosan-g-poly (N-isopropylacrylamide) nanocarrier for curcumin drug delivery. Int J Biol Macromol. 2011;49(2):161-72.

147. Shukla SK, Gupta V. Utilizing nanotechnology to recuperate sorafenib for lung cancer treatment: challenges and future perspective. Ther Deliv. 2020;11(4):213-5.

148. Soppimath KS, Aminabhavi TM, Kulkarni AR, Rudzinski WE. Biodegradable polymeric nanoparticles as drug delivery devices. J Control Release. 2001;70(1-2):1-20.

149. Cano A, Ettcheto M, Chang JH, Barroso E, Espina M, Kühne BA, et al. Dual-drug loaded nanoparticles of Epigallocatechin-3-gallate (EGCG)/Ascorbic acid enhance therapeutic efficacy of EGCG in a APPswe/PS1dE9 Alzheimer's disease mice model. J Control Release. 2019;301:62-75.

150. Owens DE, 3rd, Peppas NA. Opsonization, biodistribution, and pharmacokinetics of polymeric nanoparticles. Int J Pharm. 2006;307(1):93-102.

151. Schaffazick SR, Pohlmann AR, Dalla-Costa T, Guterres SS. Freeze-drying polymeric colloidal suspensions: nanocapsules, nanospheres and nanodispersion. A comparative study. Eur J Pharm Biopharm. 2003;56(3):501-5.

152. Jain AK, Thareja S. In vitro and in vivo characterization of pharmaceutical nanocarriers used for drug delivery. Artif Cells Nanomed Biotechnol. 2019;47(1):524-39.

153. Lombardo D, Kiselev M, Caccamo MT. Smart Nanoparticles for Drug Delivery Application: Development of Versatile Nanocarrier Platforms in Biotechnology and Nanomedicine. J. Nanomater. 2019.

154. Silva AM, Alvarado HL, Abrego G, Martins-Gomes C, Garduño-Ramirez ML, García ML, et al. In Vitro Cytotoxicity of Oleanolic/Ursolic Acids-Loaded in PLGA Nanoparticles in Different Cell Lines. Pharmaceutics. 2019;11(8).

155. Carbone C, Martins-Gomes C, Pepe V, Silva AM, Musumeci T, Puglisi G, et al. Repurposing itraconazole to the benefit of skin cancer treatment: A combined azole-DDAB nanoencapsulation strategy. Colloids Surf B Biointerfaces. 2018;167:337-44.

156. Hickey JW, Santos JL, Williford JM, Mao HQ. Control of polymeric nanoparticle size to improve therapeutic delivery. J Control Release. 2015;219:536-47.

157. Chenthamara D, Subramaniam S, Ramakrishnan SG, Krishnaswamy S, Essa MM, Lin FH, et al. Therapeutic efficacy of nanoparticles and routes of administration. Biomater Res. 2019;23:20.

158.   Reis CP, Neufeld RJ, Ribeiro AJ, Veiga F. Nanoencapsulation I. Methods for preparation of drug-loaded polymeric nanoparticles. Nanomedicine. 2006;2(1):8-21.

159.   Chander A, Chiuyen P, Murali B, Santosh R, Guping T. Polymer Properties: Functionalization and Surface Modified Nanoparticles. In: Rajeev KT, Neeraj G, Rahul S, Prakash Singh B, editors. Role of Novel Drug Delivery Vehicles in Nanobiomedicine. Rijeka: IntechOpen; 2019. p. Ch. 7.

160.   Sharma N, Madan P, Lin S. Effect of process and formulation variables on the preparation of parenteral paclitaxel-loaded biodegradable polymeric nanoparticles: A co-surfactant study. Asian J. Pharm. 2016;11(3):404-16.

161.   Kumar S, Dilbaghi N, Saharan R, Bhanjana G. Nanotechnology as Emerging Tool for Enhancing Solubility of Poorly Water-Soluble Drugs. BioNanoScience. 2012;2(4):227-50.

162.   Ganachaud F, Katz JL. Nanoparticles and nanocapsules created using the Ouzo effect: spontaneous emulisification as an alternative to ultrasonic and high-shear devices. Chemphyschem. 2005;6(2):209-16.

163.   Wang Y, Li P, Truong-Dinh Tran T, Zhang J, Kong L. Manufacturing Techniques and Surface Engineering of Polymer Based Nanoparticles for Targeted Drug Delivery to Cancer. Nanomaterials (Basel). 2016;6(2).

164.   Lim K, Hamid ZAA. 10 - Polymer nanoparticle carriers in drug delivery systems: Research trend. In: Inamuddin, Asiri AM, Mohammad A, editors. Applications of Nanocomposite Materials in Drug Delivery: Woodhead Publishing; 2018. p. 217-37.

165.   Bilati U, Allémann E, Doelker E. Nanoprecipitation versus emulsion-based techniques for the encapsulation of proteins into biodegradable nanoparticles and process-related stability issues. AAPS PharmSciTech. 2005;6(4):E594-604.

166.   Thickett SC, Gilbert RG. Emulsion polymerization: State of the art in kinetics and mechanisms. Polymer. 2007;48(24):6965-91.

167.   Asua JM. Emulsion polymerization: From fundamental mechanisms to process developments. J. Polym. Sci. A Polym. Chem. 2004;42(5):1025-41.

168.   Kreuter J. On the mechanism of termination in heterogeneous polymerization. Journal of Polymer Science: Polymer Letters Edition. 1982;20(10):543-5.

169.   Hearn J, Wilkinson MC, Goodall AR, Chainey M. Kinetics of the surfactant-free emulsion polymerization of styrene:-The post nucleation stage. J. Polym.Sci. Polym. Chem. Ed. 1985;23(7):1869-83.

170.   Zhang G, Niu A, Peng S, Jiang M, Tu Y, Li M, et al. Formation of Novel Polymeric Nanoparticles. Accounts of Chemical Research. 2001;34(3):249-56.

171.   Wang AZ, Langer R, Farokhzad OC. Nanoparticle delivery of cancer drugs. Annu Rev Med. 2012;63:185-98.

172.   Laouini A, Jaafar-Maalej C, Limayem-Blouza I, Sfar S, Charcosset C, Fessi H. Preparation, Characterization and Applications of Liposomes: State of the Art. Journal of Colloid Science and Biotechnology. 2012;1:147-68.

173.   Akbarzadeh A, Rezaei-Sadabady R, Davaran S, Joo SW, Zarghami N, Hanifehpour Y, et al. Liposome: classification, preparation, and applications. Nanoscale Res. Lett. 2013;8(1):102.

174.   Riaz MK, Riaz MA, Zhang X, Lin C, Wong KH, Chen X, et al. Surface Functionalization and Targeting Strategies of Liposomes in Solid Tumor Therapy: A Review. Int J Mol Sci. 2018;19(1).

175.   Shi L, Zhang J, Zhao M, Tang S, Cheng X, Zhang W, et al. Effects of polyethylene glycol on the surface of nanoparticles for targeted drug delivery. Nanoscale. 2021;13(24):10748-64.

176.   Zhang X, Yang D, Nie J. Chitosan/polyethylene glycol diacrylate films as potential wound dressing material. Int J Biol Macromol. 2008;43(5):456-62.

177.   Bhattarai N, Gunn J, Zhang M. Chitosan-based hydrogels for controlled, localized drug delivery. Adv. Drug Deliv. Rev. 2010;62(1):83-99.

178. Strand SP, Lelu S, Reitan NK, de Lange Davies C, Artursson P, Vårum KM. Molecular design of chitosan gene delivery systems with an optimized balance between polyplex stability and polyplex unpacking. Biomaterials. 2010;31(5):975-87.

179. Sahatsapan N, Rojanarata T, Ngawhirunpat T, Opanasopit P, Tonglairoum P. 6-Maleimidohexanoic acid-grafted chitosan: A new generation mucoadhesive polymer. Carbohydr. Polym. 2018;202:258-64.

180. Duceppe N, Tabrizian M. Advances in using chitosan-based nanoparticles for in vitro and in vivo drug and gene delivery. Expert Opin Drug Deliv. 2010;7(10):1191-207.

181. Rai P, Mallidi S, Zheng X, Rahmanzadeh R, Mir Y, Elrington S, et al. Development and applications of photo-triggered theranostic agents. Adv Drug Deliv Rev. 2010;62(11):1094-124.

182. Gombotz WR, Wee SF. Protein release from alginate matrices. Adv. Drug Deliv. Rev. 2012;64:194-205.

183. Lee KY, Mooney DJ. Alginate: Properties and biomedical applications. Prog. Polym. Sci. 2012;37(1):106-26.

184. Tavakoli J, Laisak E, Gao M, Tang Y. AIEgen quantitatively monitoring the release of Ca(2+) during swelling and degradation process in alginate hydrogels. Mater Sci Eng C Mater Biol Appl. 2019;104:109951.

185. Ciofani G, Raffa V, Menciassi A, Dario P. Alginate and chitosan particles as drug delivery system for cell therapy. Biomed Microdevices. 2008;10(2):131-40.

186. Sorasitthiyanukarn FN, Muangnoi C, Ratnatilaka Na Bhuket P, Rojsitthisak P, Rojsitthisak P. Chitosan/alginate nanoparticles as a promising approach for oral delivery of curcumin diglutaric acid for cancer treatment. Mater Sci Eng C Mater Biol Appl. 2018;93:178-90.

187. Markeb AA, El-Maali NA, Sayed DM, Osama A, Abdel-Malek MA, Zaki AH, et al. Synthesis, Structural Characterization, and Preclinical Efficacy of a Novel Paclitaxel-Loaded Alginate Nanoparticle for Breast Cancer Treatment. Int J Breast Cancer. 2016;2016:7549372.

188. Scolari IR, Páez PL, Musri MM, Petiti JP, Torres A, Granero GE. Rifampicin loaded in alginate/chitosan nanoparticles as a promising pulmonary carrier against Staphylococcus aureus. Drug Deliv. and Transl. Res. 2020;10(5):1403-17.

189. Baek S, Joo SH, Toborek M. Treatment of antibiotic-resistant bacteria by encapsulation of ZnO nanoparticles in an alginate biopolymer: Insights into treatment mechanisms. J Hazard Mater. 2019;373:122-30.

190. Carter T, Mulholland P, Chester K. Antibody-targeted nanoparticles for cancer treatment. Immunotherapy. 2016;8(8):941-58.

191. Shi J, Kantoff PW, Wooster R, Farokhzad OC. Cancer nanomedicine: progress, challenges and opportunities. Nat.Rev. Cancer. 2017;17(1):20-37.

192. Jain RK, Stylianopoulos T. Delivering nanomedicine to solid tumors. Nat Rev Clin Oncol. 2010;7(11):653-64.

193. Pelaz B, Alexiou C, Alvarez-Puebla RA, Alves F, Andrews AM, Ashraf S, et al. Diverse Applications of Nanomedicine. ACS Nano. 2017;11(3):2313-81.

194. Wicki A, Witzigmann D, Balasubramanian V, Huwyler J. Nanomedicine in cancer therapy: challenges, opportunities, and clinical applications. J Control Release. 2015;200:138-57.

195. Shukla AA, Thömmes J. Recent advances in large-scale production of monoclonal antibodies and related proteins. Trends Biotechnol. 2010;28(5):253-61.

196. Flygare JA, Pillow TH, Aristoff P. Antibody-drug conjugates for the treatment of cancer. Chem Biol Drug Des. 2013;81(1):113-21.

197. Eldar-Boock A, Polyak D, Scomparin A, Satchi-Fainaro R. Nano-sized polymers and liposomes designed to deliver combination therapy for cancer. Curr Opin Biotechnol. 2013;24(4):682-9.

198.   Kamaly N, Xiao Z, Valencia PM, Radovic-Moreno AF, Farokhzad OC. Targeted polymeric therapeutic nanoparticles: design, development and clinical translation. Chem Soc Rev. 2012;41(7):2971-3010.

199.   Liébana S, Drago GA. Bioconjugation and stabilisation of biomolecules in biosensors. Essays Biochem. 2016;60(1):59-68.

200.   Tallawi M, Rosellini E, Barbani N, Cascone MG, Rai R, Saint-Pierre G, et al. Strategies for the chemical and biological functionalization of scaffolds for cardiac tissue engineering: a review. J R Soc Interface. 2015;12(108):20150254.

201.   Walkey CD, Olsen JB, Guo H, Emili A, Chan WC. Nanoparticle size and surface chemistry determine serum protein adsorption and macrophage uptake. J Am Chem Soc. 2012;134(4):2139-47.

202.   Juan A, Cimas FJ, Bravo I, Pandiella A, Ocaña A, Alonso-Moreno C. An Overview of Antibody Conjugated Polymeric Nanoparticles for Breast Cancer Therapy. Pharmaceutics. 2020;12(9):802.

203.   Chen EY, Liu WF, Megido L, Díez P, Fuentes M, Fager C, et al. Chapter 3 - Understanding and utilizing the biomolecule/nanosystems interface. In: Uskoković V, Uskoković DP, editors. Nanotechnologies in Preventive and Regenerative Medicine: Elsevier; 2018. p. 207-97.

204.   Parracino MA, Martín B, Grazú V. Chapter 9 - State-of-the-art strategies for the biofunctionalization of photoactive inorganic nanoparticles for nanomedicine. In: Prieto JP, Béjar MG, editors. Photoactive Inorganic Nanoparticles: Elsevier; 2019. p. 211-57.

205.   Saha B, Songe P, Evers TH, Prins MWJ. The influence of covalent immobilization conditions on antibody accessibility on nanoparticles. Analyst. 2017;142(22):4247-56.

206.   Yang J, Lee C-H, Park J, Seo S, Lim E-K, Song YJ, et al. Antibody conjugated magnetic PLGA nanoparticles for diagnosis and treatment of breast cancer. J.Mater.Chem. 2007;17(26):2695-9.

207.   Shen M, Rusling J, Dixit CK. Site-selective orientated immobilization of antibodies and conjugates for immunodiagnostics development. Methods. 2017;116:95-111.

208.   Agarwal P, Bertozzi CR. Site-Specific Antibody–Drug Conjugates: The Nexus of Bioorthogonal Chemistry, Protein Engineering, and Drug Development. Bioconjugate Chem. 2015;26(2):176-92.

209.   Kharkar PM, Rehmann MS, Skeens KM, Maverakis E, Kloxin AM. Thiol–ene Click Hydrogels for Therapeutic Delivery. ACS Biomater.Sci.Eng. 2016;2(2):165-79.

210.   Dovgan I, Kolodych S, Koniev O, Wagner A. 2-(Maleimidomethyl)-1,3-Dioxanes (MD): a Serum-Stable Self-hydrolysable Hydrophilic Alternative to Classical Maleimide Conjugation. Sci. Rep. 2016;6(1):30835.

211.   Markwalter CF, Kantor AG, Moore CP, Richardson KA, Wright DW. Inorganic Complexes and Metal-Based Nanomaterials for Infectious Disease Diagnostics. Chem. Rev. 2019;119(2):1456-518.

212.   Azadbakht B, Afarideh H, Ghannadi-Maragheh M, Bahrami-Samani A, Asgari M. Preparation and evaluation of APTES-PEG coated iron oxide nanoparticles conjugated to rhenium-188 labeled rituximab. Nucl Med Biol. 2017;48:26-30.

213.   Fay F, Scott CJ. Antibody-targeted nanoparticles for cancer therapy. Immunotherapy. 2011;3(3):381-94.

214.   Pornpitchanarong C, Rojanarata T, Opanasopit P, Ngawhirunpat T, Patrojanasophon P. Preactivated-thiolated polyacrylic acid/1-vinyl pyrrolidone nanoparticles as nicotine carriers for smoking cessation. RSC Advances. 2020;10:33517.

215.   Dharmalingam S, Ramamurthy S, Kumarappan C, Nadaraju S. A Simple HPLC Bioanalytical Method for the Determination of Doxorubicin Hydrochloride in Rat Plasma: Application to Pharmacokinetic Studies. Trop. J.Pharm.Res. 2014;13:409.

216.   Pornpitchanarong C, Rojanarata T, Opanasopit P, Ngawhirunpat T, Patrojanasophon P. Catechol-modified chitosan/hyaluronic acid nanoparticles as a new avenue for local delivery of doxorubicin to oral cancer cells. Colloids Surf. B. 2020;196:111279.

217.   Shen J, Nada AA, Abou-Zeid NY, Hudson SM. Synthesis of chitosan iodoacetamides via carbodiimide coupling reaction: Effect of degree of substitution on the hemostatic properties. Carbohydr. Polym. 2020;229:115522.

218.   Fonseca-Santos B, Gremião MPD, Chorilli M. A simple reversed phase high-performance liquid chromatography (HPLC) method for determination of in situ gelling curcumin-loaded liquid crystals in in vitro performance tests. Arabian J. Chem. 2017;10(7):1029-37.

219.   Pornpitchanarong C, Sahatsapan N, Rojanarata T, Opanasopit P, Ngawhirunpat T, Patrojanasophon P. Curcumin-incorporated Thiolated Chitosan/alginate Nanocarriers: Physicochemical Properties and Release Mechanism. Indian J. Pharm. Sci. 2020.

220.   Sorasitthiyanukarn FN, Muangnoi C, Rojsitthisak P, Rojsitthisak P. Chitosan oligosaccharide/alginate nanoparticles as an effective carrier for astaxanthin with improving stability, in vitro oral bioaccessibility, and bioavailability. Food Hydrocoll. 2022;124:107246.

221.   Ashjari HR, Ahmadi A, Dorraji MSS. Synthesis and employment of PEGDA for fabrication of superhydrophilic PVDF/PEGDA electrospun nanofibrous membranes by in-situ visible photopolymerization. Korean J.Chem. Eng. 2018;35(1):289-97.

222.   Mamaghani KR, Naghib SM, Zahedi A, Rahmanian M, Mozafari M. GelMa/PEGDA containing graphene oxide as an IPN hydrogel with superior mechanical performance. Mater. Today. 2018;5(7, Part 3):15790-9.

223.   Ma G, Zhang X, Han J, Song G, Nie J. Photo-polymeriable chitosan derivative prepared by Michael reaction of chitosan and polyethylene glycol diacrylate (PEGDA). Int. J. Biol. Macromol. 2009;45(5):499-503.

224.   Browe DP, Wood C, Sze MT, White KA, Scott T, Olabisi RM, et al. Characterization and optimization of actuating poly(ethylene glycol) diacrylate/acrylic acid hydrogels as artificial muscles. Polymer. 2017;117:331-41.

225.   Caster JM, Yu SK, Patel AN, Newman NJ, Lee ZJ, Warner SB, et al. Effect of particle size on the biodistribution, toxicity, and efficacy of drug-loaded polymeric nanoparticles in chemoradiotherapy. Nanomedicine. 2017;13(5):1673-83.

226.   Yu W, Liu R, Zhou Y, Gao H. Size-Tunable Strategies for a Tumor Targeted Drug Delivery System. ACS Cent. Sci. 2020;6(2):100-16.

227.   Pochapski DJ, Carvalho dos Santos C, Leite GW, Pulcinelli SH, Santilli CV. Zeta Potential and Colloidal Stability Predictions for Inorganic Nanoparticle Dispersions: Effects of Experimental Conditions and Electrokinetic Models on the Interpretation of Results. Langmuir. 2021;37(45):13379-89.

228.   Danaei M, Dehghankhold M, Ataei S, Hasanzadeh Davarani F, Javanmard R, Dokhani A, et al. Impact of Particle Size and Polydispersity Index on the Clinical Applications of Lipidic Nanocarrier Systems. Pharmaceutics. 2018;10(2).

229.   Pornpitchanarong C, Rojanarata T, Opanasopit P, Ngawhirunpat T, Patrojanasophon P. Synthesis of novel N-vinylpyrrolidone/acrylic acid nanoparticles as drug delivery carriers of cisplatin to cancer cells. Colloids Surf. B. 2020;185:110566.

230.   Mirza AZ, Shamshad H. Preparation and characterization of doxorubicin functionalized gold nanoparticles. Eur. J. Med. Chem. 2011;46(5):1857-60.

231.   Yang X, Grailer JJ, Rowland IJ, Javadi A, Hurley SA, Steeber DA, et al. Multifunctional SPIO/DOX-loaded wormlike polymer vesicles for cancer therapy and MR imaging. Biomaterials. 2010;31(34):9065-73.

232.   Muhammad F, Guo M, Qi W, Sun F, Wang A, Guo Y, et al. pH-Triggered Controlled Drug Release from Mesoporous Silica Nanoparticles via Intracelluar Dissolution of ZnO Nanolids. J. Am. Chem.Soc. 2011;133(23):8778-81.

233.   Liu G, Wang M, He H, Li J. Doxorubicin-Loaded Tumor-Targeting Peptide-Decorated Polypeptide Nanoparticles for Treating Primary Orthotopic Colon Cancer. Front Pharmacol. 2021;12:744811.

234.   Abedi F, Davaran S, Hekmati M, Akbarzadeh A, Baradaran B, Moghaddam SV. An improved method in fabrication of smart dual-responsive nanogels for controlled release of doxorubicin and curcumin in HT-29 colon cancer cells. J Nanobiotechnology. 2021;19(1):18.

235.   Norouzi M, Yathindranath V, Thliveris JA, Kopec BM, Siahaan TJ, Miller DW. Doxorubicin-loaded iron oxide nanoparticles for glioblastoma therapy: a combinational approach for enhanced delivery of nanoparticles. Sci. Rep. 2020;10(1):11292.

236.   Li F, Chen W-l, You B-g, Liu Y, Yang S-d, Yuan Z-q, et al. Enhanced Cellular Internalization and On-Demand Intracellular Release of Doxorubicin by Stepwise pH-/Reduction-Responsive Nanoparticles. ACS Appl. Mater. Interfaces. 2016;8(47):32146-58.

237.   Khaledian M, Nourbakhsh MS, Saber R, Hashemzadeh H, Darvishi MH. Preparation and Evaluation of Doxorubicin-Loaded PLA-PEG-FA Copolymer Containing Superparamagnetic Iron Oxide Nanoparticles (SPIONs) for Cancer Treatment: Combination Therapy with Hyperthermia and Chemotherapy. Int J Nanomedicine. 2020;15:6167-82.

238.   Susa M, Iyer AK, Ryu K, Hornicek FJ, Mankin H, Amiji MM, et al. Doxorubicin loaded Polymeric Nanoparticulate Delivery System to overcome drug resistance in osteosarcoma. BMC Cancer. 2009;9(1):399.

239.   Ina M, editor The Synthesis of Poly N-acetyl iodo Glucosamine and its Gelation of Blood2013.

240.   Abdelgawad AM, El-Naggar ME, Hudson SM, Rojas OJ. Fabrication and characterization of bactericidal thiol-chitosan and chitosan iodoacetamide nanofibres. Int J Biol Macromol. 2017;94(Pt A):96-105.

241.   San H, Yang ZY, Pompili VJ, Jaffe ML, Plautz GE, Xu L, et al. Safety and short-term toxicity of a novel cationic lipid formulation for human gene therapy. Hum Gene Ther. 1993;4(6):781-8.

242.   Makwana V, Karanjia J, Haselhorst T, Anoopkumar-Dukie S, Rudrawar S. Liposomal doxorubicin as targeted delivery platform: Current trends in surface functionalization. Int J Pharm. 2021;593:120117.

243.   Harashima H, Sakata K, Funato K, Kiwada H. Enhanced hepatic uptake of liposomes through complement activation depending on the size of liposomes. Pharm Res. 1994;11(3):402-6.

244.   Li Z, Paulson AT, Gill T. ENCAPSULATION OF BIOACTIVE SALMON PROTEIN HYDROLYSATES WITH CHITOSAN-COATED LIPOSOMES. J. Funct. Foods. 2015;19:733-43.

245.   Furlani F, Rossi A, Grimaudo MA, Bassi G, Giusto E, Molinari F, et al. Controlled Liposome Delivery from Chitosan-Based Thermosensitive Hydrogel for Regenerative Medicine. Int J Mol Sci. 2022;23(2).

246.   Liu W, Liu J, Liu W, Li T, Liu C. Improved physical and in vitro digestion stability of a polyelectrolyte delivery system based on layer-by-layer self-assembly alginate-chitosan-coated nanoliposomes. J Agric Food Chem. 2013;61(17):4133-44.

247.   Wang Z, Campos LA, Muñoz V. Chapter Fourteen - Single-Molecule Fluorescence Studies of Fast Protein Folding. In: Spies M, Chemla YR, editors. Methods in Enzymology. 581: Academic Press; 2016. p. 417-59.

248.   Koniev O, Wagner A. Developments and recent advancements in the field of endogenous amino acid selective bond forming reactions for bioconjugation. Chem. Soc. Rev. 2015;44(15):5495-551.

249.   Hermanson GT. Chapter 2 - Functional Targets for Bioconjugation. In: Hermanson GT, editor. Bioconjugate Techniques (Third Edition). Boston: Academic Press; 2013. p. 127-228.

250.   HalÁSz P, PolgÁR L. Negatively Charged Reactants as Probes in the Study of the Essential Mercaptide-Imidazolium Ion-Pair of Thiolenzymes. Eur. J. Biochem. 1977; 79(2): 491-4.
251.   Kong G, Anyarambhatla G, Petros WP, Braun RD, Colvin OM, Needham D, et al. Efficacy of liposomes and hyperthermia in a human tumor xenograft model: importance of triggered drug release. Cancer Res. 2000;60(24):6950-7.
252.   Gabizon AA, Shmeeda H, Zalipsky S. Pros and cons of the liposome platform in cancer drug targeting. J Liposome Res. 2006;16(3):175-83.
253.   Voinova MV, Galkin VL, Kosevich AM. Kinetics of liposome volume and permeability changes during the lipid phase transitions. J. Electroanal. Chem. Interfacial Electrochem. 1990;299(2):143-54.
254.   Alshraim MO, Sangi S, Harisa GI, Alomrani AH, Yusuf O, Badran MM. Chitosan-Coated Flexible Liposomes Magnify the Anticancer Activity and Bioavailability of Docetaxel: Impact on Composition. Molecules. 2019;24(2).
255.   Sułkowski WW, Pentak D, Nowak K, Sułkowska A. The influence of temperature, cholesterol content and pH on liposome stability. J. Mol. Struct. 2005;744-747:737-47.
256.   Sreekanth V, Medatwal N, Pal S, Kumar S, Sengupta S, Bajaj A. Molecular Self-Assembly of Bile Acid-Phospholipids Controls the Delivery of Doxorubicin and Mice Survivability. Mol Pharm. 2017;14(8):2649-59.
257.   Shibata H, Izutsu K-i, Yomota C, Okuda H, Goda Y. Investigation of factors affecting in vitro doxorubicin release from PEGylated liposomal doxorubicin for the development of in vitro release testing conditions. Drug Dev. Ind. Pharm. 2015;41(8):1376-86.
258.   Tsugeno Y, Sato F, Muragaki Y, Kato Y. Cell culture of human gingival fibroblasts, oral cancer cells and mesothelioma cells with serum-free media, STK1 and STK2. Biomed Rep. 2014;2(5):644-8.
259.   Deshpande PP, Biswas S, Torchilin VP. Current trends in the use of liposomes for tumor targeting. Nanomedicine (Lond). 2013;8(9):1509-28.
260.   Chowdhury N, Chaudhry S, Hall N, Olverson G, Zhang QJ, Mandal T, et al. Targeted Delivery of Doxorubicin Liposomes for Her-2+ Breast Cancer Treatment. AAPS PharmSciTech. 2020;21(6):202.
261.   Srinophakun P, Thanapimmetha A, Plangsri S, Vetchayakunchai S, Saisriyoot M. Application of modified chitosan membrane for microbial fuel cell: Roles of proton carrier site and positive charge. J. Clean. Prod. 2017;142:1274-82.
262.   Cai H, Liang Z, Huang W, Wen L, Chen G. Engineering PLGA nano-based systems through understanding the influence of nanoparticle properties and cell-penetrating peptides for cochlear drug delivery. Int J Pharm. 2017;532(1):55-65.
263.   Manatunga DC, de Silva RM, de Silva KMN, Malavige GN, Wijeratne DT, Williams GR, et al. Effective delivery of hydrophobic drugs to breast and liver cancer cells using a hybrid inorganic nanocarrier: A detailed investigation using cytotoxicity assays, fluorescence imaging and flow cytometry. Eur J Pharm Biopharm. 2018;128:18-26.
264.   Pistritto G, Trisciuoglio D, Ceci C, Garufi A, D'Orazi G. Apoptosis as anticancer mechanism: function and dysfunction of its modulators and targeted therapeutic strategies. Aging (Albany NY). 2016;8(4):603-19.
265.   Syed Abdul Rahman SN, Abdul Wahab N, Abd Malek SN. In Vitro Morphological Assessment of Apoptosis Induced by Antiproliferative Constituents from the Rhizomes of Curcuma zedoaria. Evid Based Complement Alternat Med. 2013;2013:257108.
266.   McCarron PA, Olwill SA, Marouf WM, Buick RJ, Walker B, Scott CJ. Antibody conjugates and therapeutic strategies. Mol Interv. 2005;5(6):368-80.
267.   Kocbek P, Obermajer N, Cegnar M, Kos J, Kristl J. Targeting cancer cells using PLGA nanoparticles surface modified with monoclonal antibody. J Control Release. 2007;120(1-2):18-26.

268. Matsumoto M, Udomsinprasert W, Laengee P, Honsawek S, Patarakul K, Chirachanchai S. A Water-Based Chitosan-Maleimide Precursor for Bioconjugation: An Example of a Rapid Pathway for an In Situ Injectable Adhesive Gel. Macromol Rapid Commun. 2016;37(19):1618-22.

269. Sahatsapan N, Rojanarata T, Ngawhirunpat T, Opanasopit P, Patrojanasophon P. Doxorubicin-loaded chitosan-alginate nanoparticles with dual mucoadhesive functionalities for intravesical chemotherapy. J. Drug Deliv. Sci. Technol. 2021;63:102481.

270. Sarker B, Papageorgiou DG, Silva R, Zehnder T, Gul-E-Noor F, Bertmer M, et al. Fabrication of alginate–gelatin crosslinked hydrogel microcapsules and evaluation of the microstructure and physico-chemical properties. J Mat Chem B. 2014;2(11):1470-82.

271. He H, Liu L, Morin EE, Liu M, Schwendeman A. Survey of Clinical Translation of Cancer Nanomedicines—Lessons Learned from Successes and Failures. Acc. Chem. Res. 2019;52(9):2445-61.

272. Mathlouthi M, Koenig JL. Vibrational Spectra of Carbohydrates. In: Tipson RS, Horton D, editors. Adv. Carbohydra. Chem. Biochem. 44: Academic Press; 1987. p. 7-89.

273. Leal D, Matsuhiro B, Rossi M, Caruso F. FT-IR spectra of alginic acid block fractions in three species of brown seaweeds. Carbohydr Res. 2008;343(2):308-16.

274. Nair DP, Podgórski M, Chatani S, Gong T, Xi W, Fenoli CR, et al. The Thiol-Michael Addition Click Reaction: A Powerful and Widely Used Tool in Materials Chemistry. Chem. Mater. 2014;26(1):724-44.

275. Corbo C, Molinaro R, Parodi A, Toledano Furman NE, Salvatore F, Tasciotti E. The impact of nanoparticle protein corona on cytotoxicity, immunotoxicity and target drug delivery. Nanomedicine (Lond). 2016;11(1):81-100.

276. Yousefpour P, Atyabi F, Vasheghani-Farahani E, Movahedi AA, Dinarvand R. Targeted delivery of doxorubicin-utilizing chitosan nanoparticles surface-functionalized with anti-Her2 trastuzumab. Int J Nanomedicine. 2011;6:1977-90.

277. Esfandiarpour-Boroujeni S, Bagheri-Khoulenjani S, Mirzadeh H, Amanpour S. Fabrication and study of curcumin loaded nanoparticles based on folate-chitosan for breast cancer therapy application. Carbohydr Polym. 2017;168:14-21.

278. Yi G, Son J, Yoo J, Park C, Koo H. Application of click chemistry in nanoparticle modification and its targeted delivery. Biomater. Res. 2018;22(1):13.

279. Baldwin AD, Kiick KL. Tunable Degradation of Maleimide–Thiol Adducts in Reducing Environments. Bioconjugate Chem. 2011;22(10):1946-53.

280. Ravasco JMJM, Faustino H, Trindade A, Gois PMP. Bioconjugation with Maleimides: A Useful Tool for Chemical Biology. Chem. Eur. J. 2019;25(1):43-59.

281. Juan A, Cimas FJ, Bravo I, Pandiella A, Ocaña A, Alonso-Moreno C. Antibody Conjugation of Nanoparticles as Therapeutics for Breast Cancer Treatment. Int J Mol Sci. 2020;21(17).

282. Alonso MJ, Losa C, Calvo P, Vila-Jato J. Approaches to improve the association of amikacin sulphate to poly(alkylcyanoacrylate) nanoparticles. Intl. J.Pharm. 1991;68(1):69-76.

283. Gomathi T, Govindarajan C, Rose HRM, Sudha PN, Imran PK, Venkatesan J, et al. Studies on drug-polymer interaction, in vitro release and cytotoxicity from chitosan particles excipient. Int J Pharm. 2014;468(1-2):214-22.

284. Prabaharan M, Reis RL, Mano JF. Carboxymethyl chitosan-graft-phosphatidylethanolamine: Amphiphilic matrices for controlled drug delivery. React. Funct. Polym. 2007;67(1):43-52.

285. Anitha A, Maya S, Deepa N, Chennazhi KP, Nair SV, Tamura H, et al. Efficient water soluble O-carboxymethyl chitosan nanocarrier for the delivery of curcumin to cancer cells. Carbohydrate Polymers. 2011;83(2):452-61.

286. Kamaly N, Yameen B, Wu J, Farokhzad OC. Degradable Controlled-Release Polymers and Polymeric Nanoparticles: Mechanisms of Controlling Drug Release. ACS Chem. Rev. 2016;116(4):2602-63.

287.   Afzali E, Eslaminejad T, Yazdi Rouholamini SE, Shahrokhi-Farjah M, Ansari M. Cytotoxicity Effects of Curcumin Loaded on Chitosan Alginate Nanospheres on the KMBC-10 Spheroids Cell Line. Int J Nanomedicine. 2021;16:579-89.

288.   Tan YL, Liu CG. Preparation and characterization of self-assembled nanoparticles based on folic acid modified carboxymethyl chitosan. J Mater Sci Mater Med. 2011;22(5):1213-20.

289.   Zhang X, Liu J, Li X, Li F, Lee RJ, Sun F, et al. Trastuzumab-Coated Nanoparticles Loaded With Docetaxel for Breast Cancer Therapy. Dose Response. 2019;17(3):1559325819872583.

290.   Vivek R, Thangam R, NipunBabu V, Rejeeth C, Sivasubramanian S, Gunasekaran P, et al. Multifunctional HER2-antibody conjugated polymeric nanocarrier-based drug delivery system for multi-drug-resistant breast cancer therapy. ACS Appl Mater Interfaces. 2014;6(9):6469-80.

291.   Kuo TT, Baker K, Yoshida M, Qiao SW, Aveson VG, Lencer WI, et al. Neonatal Fc receptor: from immunity to therapeutics. J Clin Immunol. 2010;30(6):777-89.

292.   Fulda S. Modulation of apoptosis by natural products for cancer therapy. Planta Med. 2010;76(11):1075-9.

293.   Santosh M, Liu SJ, Tsunogae T, Li JH. Paleoproterozoic ultrahigh-temperature granulites in the North China Craton: Implications for tectonic models on extreme crustal metamorphism. Precambrian Research. 2012;222-223:77-106.
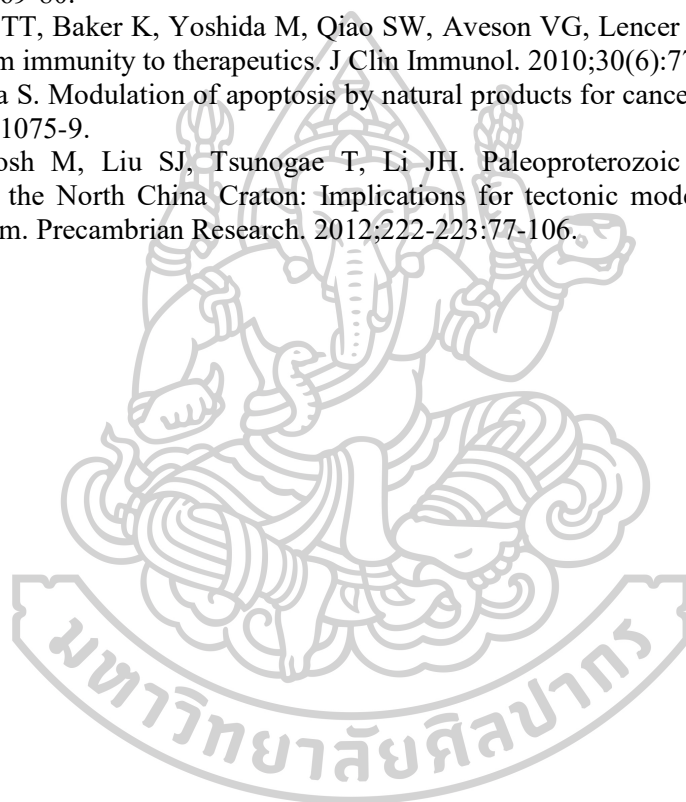
REFERENCES

VITA

NAME   Ms. Yin Yin Myat

DATE OF BIRTH   4, May, 1987

PLACE OF BIRTH   Mandalay, Myanmar

INSTITUTIONS   University of Pharmacy, Mandalay
ATTENDED
HOME ADDRESS   Mandalay

PUBLICATION   1.   Myat YY, Aung NN, Ngawhirunpat T, Rojanarata
                        T, Opanasopit P, Patrojanasophon P. Fabrication and
                        evaluation of thermally crosslinked Gantrez S-97
                        microneedle arrays. Key Engineering Materials.
                        2020;859:39-44.
                        2.   Myat YY, Ngawhirunpat T, Rojanarata T,
                        Opanasopit P, Bradley M, Patrojanasophon P, et al.
                        Synthesis of polyethylene glycol diacrylate/acrylic acid
                        nanoparticles as nanocarriers for the controlled delivery of
                        doxorubicin to colorectal cancer cells.
                        Pharmaceutics.2022;14(3).

AWARD RECEIVED   -